universität wien

MASTERARBEIT / MASTER'S THESIS

Titel der Masterarbeit / Title of the Master's Thesis

„Characterisation of the putative neurite guidance receptors *NvDscam* and *NvNeogenin* in *Nematostella vectensis*"

verfasst von / submitted by

Mark Lassnig, BSc

angestrebter akademischer Grad / in partial fulfilment of the requirements for the degree of

Master of Science (MSc)

Wien, 2022 / Vienna, 2022

Studienkennzahl lt. Studienblatt / degree programme code as it appears on the student record sheet:	UA 066 834
Studienrichtung lt. Studienblatt / degree programme as it appears on the student record sheet:	Masterstudium Molekulare Biologie UG2002
Betreut von / Supervisor:	Univ.-Prof. Dipl.-Biol. Dr. Ulrich Technau

Acknowledgements

This master thesis was performed at the Sars Center for Marine Molecular Biology, University of Bergen, and at the Department of Biological Sciences, University of Bergen from October 2020 to September 2021.

First, I want to thank Fabian Rentzsch for adopting me into his research group for this incredible year and letting me perform this super cool project! You have been a great supervisor and teacher. I am thankful for your inspiration, the master classes you have taught us master students and the education I received in terms of theoretical knowledge and scientific communication.

I want to thank Uli Technau from the Department of Neuroscience and Developmental Biology at the University of Vienna for introducing me into the world of *Nematostella*, for being my local supervisor in Vienna and for his enthusiastic inspiration.

Next, I want to speak out many thanks to Alexis Lanza for being my supervisor – although you don't want to hear it hehe – and for being my big sister in the lab. I received a lot of lab experience from you, and you taught me so much about scientific writing. I am happy that also outside the lab you have been a valuable friend and have always been there for me.

Big thanks to James who was always ready with a fancy and intelligent answer to every question. Also, thank you for your help in the lab and for being a cool friend outside the lab! Thank you, Henriette for being the smartest lab book ever! Without you many experiments would have kept failing! Thank you Natascha, Fatemeh and Eilen for all the nice conversations, the nice times, and your help in the lab!

I want to thank my fellow master students Astrid, Linda, and Susanne for being an awesome crowd, not only in the lab but also outside work as great friends!

Not to forget are very important people who I met during my year in Bergen and who made it more special as it already had been: Giulio, Blandine, Eudald and Vincenzo. Thank you for the amazing trips and time we had in Bergen (so far – there is more to come)! A thanks to all other people at Sars who I met during my stay but couldn't mention now! You made every day great!

Finally, I want to thank my family for being the most supportive people ever! Thank you for helping me out in difficult situations, advising me when times are hard, enjoying the good moments with me and being generous with advice in life! Without you, Mom, Dad and Valeria, nothing would have been possible! Special thanks to my girlfriend Jasemin, who always has been supportive, caring and kind, and helped me to get over every low I had! Thank you, Chris and Veri, for being honest, close, and supportive friends for a long time now!

Table of Contents

Summary

Although the patterns of connectivity differ between different animal nervous systems, some basic mechanisms in its development are shared. For example, axon guidance describes the extension of an axon towards and the connection to target or effector cells. Signalling molecules secreted by target tissues and receptors located in the axon tip contribute to guidance and outgrowth of the axon. The Netrin-pathway with its receptors Dcc, Neogenin, Dscam and Unc-5 has been described as a major guidance system in bilaterian model organisms.

Here, we wanted to find out if the Netrin-pathway contributes to the establishment of a nervous system outside of Bilateria. We characterised the receptors *NvDscam* and *NvNeogenin* in *Nematostella vectensis*, a sea anemone within the Cnidaria. Genome mining and a phylogenetic analysis revealed the presence of a *NvDscam*-orthologue in *N. vectensis*. In early gastrula, *NvDscam* mRNA was detected in the whole animal and at higher levels in scattered ectodermal cells, *NvNeogenin* mRNA in the endoderm and ectodermal cells. Furthermore, co-expression of *NvDscam* and *NvNeogenin* with *NvSoxB(2)* was discovered. Next, a transgenic reporter construct expressing membrane bound GFP under regulation of a putative promoter for *NvNeogenin* was generated. F0 animals injected with this construct showed a mGFP-signal in neurites along the body column. Using CRISPR/Cas9, F1 heterozygous mutant lines for *NvDscam* and *NvNeogenin* were established, both causing a truncated version of the protein, if translated. In addition, RNA-interference targeted against *NvDscam* and *NvNeogenin* was developed.

Overall, the spatio-temporal expression patterns, establishment of a transgenic reporter construct, mutant lines and RNA-interference will likely serve as important tools to investigate the role of *NvDscam* and *NvNeogenin* in neurite guidance in *N. vectensis*.

Zusammenfassung

Trotz unterschiedlicher Nervensysteme in allen Tierarten liegen ähnliche Mechanismen der Neuroentwicklung zu Grunde, wie z. B. die axonale Wegfindung. Diese beschreibt das Aussenden eines Axons von einem Neuron und den Kontaktaufbau zu Ziel- und Effektor-Zellen. Liganden, die von Zielgeweben sekretiert werden, und Rezeptoren am Axonfortsatz tragen zur Wegfindung und Aussendung des Axons bei. In bilateralen Modelorganismen wurde unter anderem der Netrin-Signalweg mit den Rezeptoren Dcc, Neogenin, Dscam und Unc-5 in der axonalen Wegfindung identifiziert.

In dieser Arbeit wollten wir herausfinden, ob der Netrin-Signalweg auch außerhalb der Bilateria zur Entwicklung des Nervensystems beiträgt. Hier beschrieben wir die beiden Rezeptoren *NvDscam* und *NvNeogenin* in der Seeanemone *Nematostella vectensis* aus dem Stamm der Cnidaria (Nesseltiere). Eine phylogenetische Analyse von Dscam-Proteinsequenzen zeigte das Vorhandensein eines *NvDscam*-Orthologs in *N. vectensis*. In der frühen Gastrula wurde *NvDscam*-mRNA im ganzen Tier und in einzelnen, ektodermalen Zellen exprimiert, *NvNeogenin*-mRNA im Entoderm und in ektodermalen Zellen. Außerdem wurde herausgefunden, dass *NvDscam* und *NvNeogenin* in Gastrula-Stadien mit *NvSoxB(2)* co-exprimiert sind, welches unter anderem ein Marker für Vorläufer von Nerven- und Drüsenzellen ist. Ebenfalls wurde ein transgenes Reporterkonstrukt entwickelt, welches ein Membran-gebundenes GFP unter Regulierung des möglichen *NvNeogenin*-Promoters exprimiert. Schon im F0-Tier konnten lange $mGFP^+$ Neuriten entlang der Körpersäule ausgemacht werden. Weiters wurden heterozygote F1 Mutanten-Linien mithilfe von CRISPR/Cas9 etabliert, welche ein verkürztes *NvDscam* oder *NvNeogenin* translatieren würden. Ebenso wurde RNA-Interferenz entwickelt, um *NvDscam*- und *NvNeogenin*-mRNAs zu degradieren.

Zusammengefasst tragen die zeitlichen und räumlichen mRNA-Expressions-Muster, Etablierung eines transgenen Reporterkonstrukts, Mutanten-Linien und RNA-Interferenz dazu bei, die Rollen von *NvDscam* und *NvNeogenin* in der axonalen Wegfindung zukünftig zu studieren.

Abstract

The patterns of connectivity differ between the nervous systems of all species, however some basic mechanisms for the establishment of this connectivity are shared between many bilaterian species. In one of these mechanisms, axon guidance, the developing neuron sends out an axon, which will connect to target neurons or effector cells, therefore building up a network. Molecules secreted from target tissues and receptors present on the axon tip contribute to the guidance and outgrowth of axons. The Netrin guidance pathway has been shown to be a major guidance system in bilaterian model organisms, for example in the midline crossing of commissural neurons in the mouse embryonic spinal cord. Amongst others, Netrin binds to Deleted in colorectal cancer (Dcc), its homologue Neogenin, Down syndrome cell adhesion molecule (Dscam) and Uncoordinated-5 (Unc-5).

In this study, we wanted to elucidate whether the Netrin signalling system is involved in the formation of the nervous system outside of the bilaterian clade. Here, we characterised the receptors *NvDscam* and *NvNeogenin* in the sea anemone *Nematostella vectensis*, an anthozoan in the cnidarian phylum. Genome mining and a phylogenetic analysis revealed the presence of a *NvDscam*-orthologue in *N. vectensis*. Using *in-situ* hybridisation (ISH), it was found that *NvDscam* is expressed in the whole animal and at higher levels in scattered ectodermal cells. At planula stages the expression is seen in the oral pole and afterwards in the tips of developing tentacles. With double fluorescence ISH (dFISH), *NvDscam* was shown to be partially co-expressed with *NvSoxB(2)* in the ectoderm at gastrula stages, a marker also for neural and gland cell progenitors. *NvNeogenin* expression was first detected with ISH at early gastrula stage in the endoderm and in ectodermal single cells. At late gastrula and early planula, it is seen in the pharynx, endoderm and aboral pole. In later planula stages and tentacle bud stage it is only detected in the oral and aboral endoderm and in endodermal single cells. Also, dFISH revealed co-expression of *NvNeogenin* with *NvSoxB(2)* in endodermal cells during gastrulation and in the aboral ectoderm at planula stage. Furthermore, a transgenic reporter construct, *NvNeogenin::mGFP*, expressing membrane-bound GFP under regulation of a putative promoter for *NvNeogenin* was generated. F0 animals injected with this construct showed a GFP-signal in neurites along the body column. Using CRISPR/Cas9, F1 heterozygous mutant lines for *NvDscam* and *NvNeogenin* were established, both causing a truncated version of the protein, if translated. In addition, RNA-interference based on short hairpin RNAs targeted against *NvDscam* and *NvNeogenin* was developed.

Overall, the spatio-temporal expression patterns, establishment of a transgenic reporter construct, mutant lines and RNA-interference will likely serve as important tools to investigate the role of *NvDscam* and *NvNeogenin* in neurite guidance in *N. vectensis*.

Selected abbreviations

cDNA	complementary desoxyribonucleic acid
DB	Dcc binding
Dcc	Deleted in colorectal cancer
DD	Death domain
DNC	Dorsal nerve cord
Dpf	Days post fertilisation
Dscam	Down syndrome cell adhesion molecule
EGF	Epidermal growth factor
FNIII	Fibronectin Type III
gDNA	genomic desoxyribonucleic acid
Hpf	Hours post fertilisation
IG	Immunoglobulin
NTR	Netrin C-terminal region
Rgm	Repulsive guidance molecule
Robo	Roundabout
Sema	Semaphorin
sgRNA	single guide ribonucleic acid
Shh	Sonic hedgehog
shRNA	short hairpin ribonucleic acid
TSP-1	Thrombospondin type I
Unc-5	Uncoordinated-5
UPA	Unc-5/PIDD/Ankyrin domain
VNC	Ventral nerve cord
WT	Wild type

1. Introduction

1.1 Diversity of nervous systems

In almost all animals, Ctenophora, Cnidaria, and Bilateria, there is a highly complex structure called the nervous system that functions to integrate sensory information (afferent stimuli) and respond with actions (efferent stimuli). Despite having a conserved function, however, the nervous system is structurally different between phyla (**Figure 1**). In non-bilaterian animals such as Ctenophora and Cnidaria, the nervous system takes the form of a diffuse nerve net (**Figure 1A**). In many Bilateria, however, the nervous system is centralised. For instance, in Planaria (**Figure 1B**), accumulations of neurons called ganglia positioned anteriorly serve as a central hub from which a pair of nerve cords extend longitudinally, mediating afferent sensory and efferent stimuli. In the arthropod head, a cerebral ganglion can be found from which a ventral nerve cord extends to the posterior end (**Figure 1C**). In other animals like Cephalopoda and Vertebrata, a more complex structure called the brain serves as the centralised hub around which the nervous system is based (**Figure 1D & E**). The brain harbours an extensive number of neurons and neural networks. Although nervous systems vary

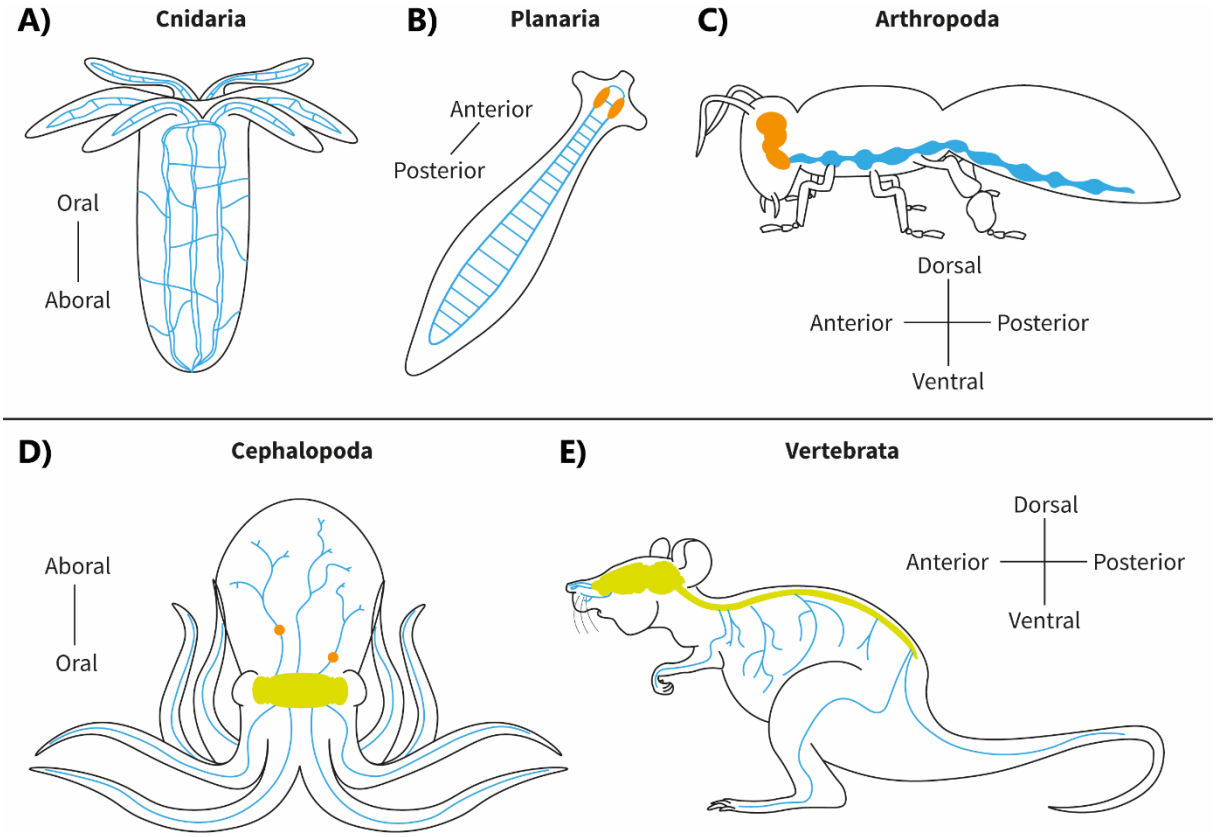

Figure 1.1: **Diversity of nervous systems amongst animals.** Here representatives of various phyla are shown to depict the structural diversity of the nervous system. **B-E** depict Bilaterian taxa with a centralised nervous system. **A)** Cnidaria possess a nerve net (blue), without centralised structures like ganglia or brains. **B)** Planaria harbour two ganglia (orange) on the anterior site from which nerve cords (blue) are extending to the posterior site. **C)** In the head of Arthropoda, a cerebral ganglion (orange) can be found from which a ventral nerve cord extends to the posterior end. **D)** Cephalopoda contain a brain (green) with nerve cords (blue) extending to the distal parts of the animal. Also, ganglia (orange) can be found in the tissue. **E)** In Vertebrata the central nervous system consists of a brain and a spinal cord (green) which is the origin for nerves (blue) expanding to the rest of the animal. Also, ganglia can be found in vertebrates (not shown). **A-D** adapted from (Rye et al., 2016) and **E** from (Montgomery et al., 2016).

between animals a few steps in nervous system development are conserved. Early during nervous system formation, it starts with neurons extending their axons into their surroundings to connect to target or effector cells. Neurons can then send stimuli via their axons and establish a neural network. This process during neurodevelopment is termed axon guidance, or more generally neurite guidance, which will be described in more detail in the next section.

1.2 Axon guidance in bilaterian model organisms

The majority of work on axon guidance has been performed in bilaterian organisms, like the mouse embryo (Chédotal, 2019), but also in *Caenorhabditis elegans* (Chisholm et al., 2016) and *Drosophila melanogaster* (Howard et al., 2019). Many genes and signaling pathways are involved in axon guidance and shared between those animals, some are highlighted below.

In the developing spinal cord of mouse embryos (**Figure 1.2A**), commissural neurons residing in the dorsal spinal cord extend their axons ventrally, make a turn, then cross the midline to the other side. This process is guided by various molecules, including Netrin, Draxin, Slits, and Semaphorins, as well as Shh and Wnts (Chédotal, 2019; Stoeckli, 2018). Netrin-1 is expressed in the ventricular zone and floor plate of the spinal cord, and functions mainly to guide axons ventrally towards the floorplate. Dorsally at the roof plate, repellent guidance cues like Draxin direct the axon to the ventral side. At the floor plate, the axon encounters a mixture of cues: attractants like Netrin-1, VegfA and repellents like Slits, Semaphorins. Futhermore, changes on the receptor level happen as well (Chédotal, 2019). Before reaching the midline the axon expresses receptors like Dcc binding to Netrin-1 (Fazeli et al., 1997; Keino-Masu et al., 1996) or Robo-3 binding to Netrin-1 via Dcc (Zelina et al., 2014) and once within the floor plate the axon switches its receptor repertoire, for example to Robo-1 or Robo-2 both mediating repulsive binding to Slits (Tong et al., 2019), and Plexin-A1 mediating repulsive binding to Sema-3B (Negishi et al., 2005). Furthermore the receptors Boc, Patched and Smoothened are involved in modulating axon guidance in response to Shh. The receptors Frizzled and Ryk respond to Wnt (Chédotal, 2019). Not all neurons cross the midline. Those that stay on the side of the spinal cord are termed ipsilateral neurons (Williams et al., 2003). Netrin-1 ablation from the floor plate has shown to impair the crossing of corticospinal axons, but not to fully abrogate it (Pourchet et al., 2021), whereas on hindbrain and spinal commissural neurons the depletion has little effects (Varadarajan et al., 2017). Here, Netrin-1 derived from the ventricular zone is essential for axon guidance towards the midline (Varadarajan et al., 2017), which can also act on corticospinal neurons (Pourchet et al., 2021). Like the results seen following *Netrin-1* ablation, the knock-out of the Netrin receptor *Dcc* causes impaired axon guidance (Fazeli et al., 1997).

Similar guidance molecules can be found in the nematode *C. elegans*. The nervous system consists of an anterior nerve ring extending neurites longitudinally towards the posterior end, forming two

longitudinal tracts on the ventral (ventral nerve cord, VNC) and on the dorsal side (dorsal nerve cord, DNC) (**Figure 1.2B**). Those two nerve cords contain the majority of axons. The body wall also contains five smaller longitudinal tracts on each side. Interestingly, the VNC is split into two tracts (left and right) whereby the right VNC harbours about fifty axons and the left VNC only four to five (Hutter, 2019). Axons in the left VNC cross the midline towards the right VNC and continue to grow to the posterior end. Little is known about longitudinal axon outgrowth. Mutations in *Unc-6* (*Netrin*) leads to defects in midline crossing of various motor- and interneurons. Mild defects are seen in mutants of orthologues of *Wnt*, *Hedgehog*, *Collagen* and *Ephrins*. Gradients of Unc-6 (ventral-dorsal) and Slit-1 (dorsal-ventral) contribute to circumferential axon outgrowth and these genes are essential for axon guidance. Dorsal neurons expressing the Unc-6 receptor Unc-40 (Dcc orthologue) grow towards the ventral side. Expression of Unc-5 or a combination of Unc-5 and Unc-40 on ventral neurons leads to repulsive

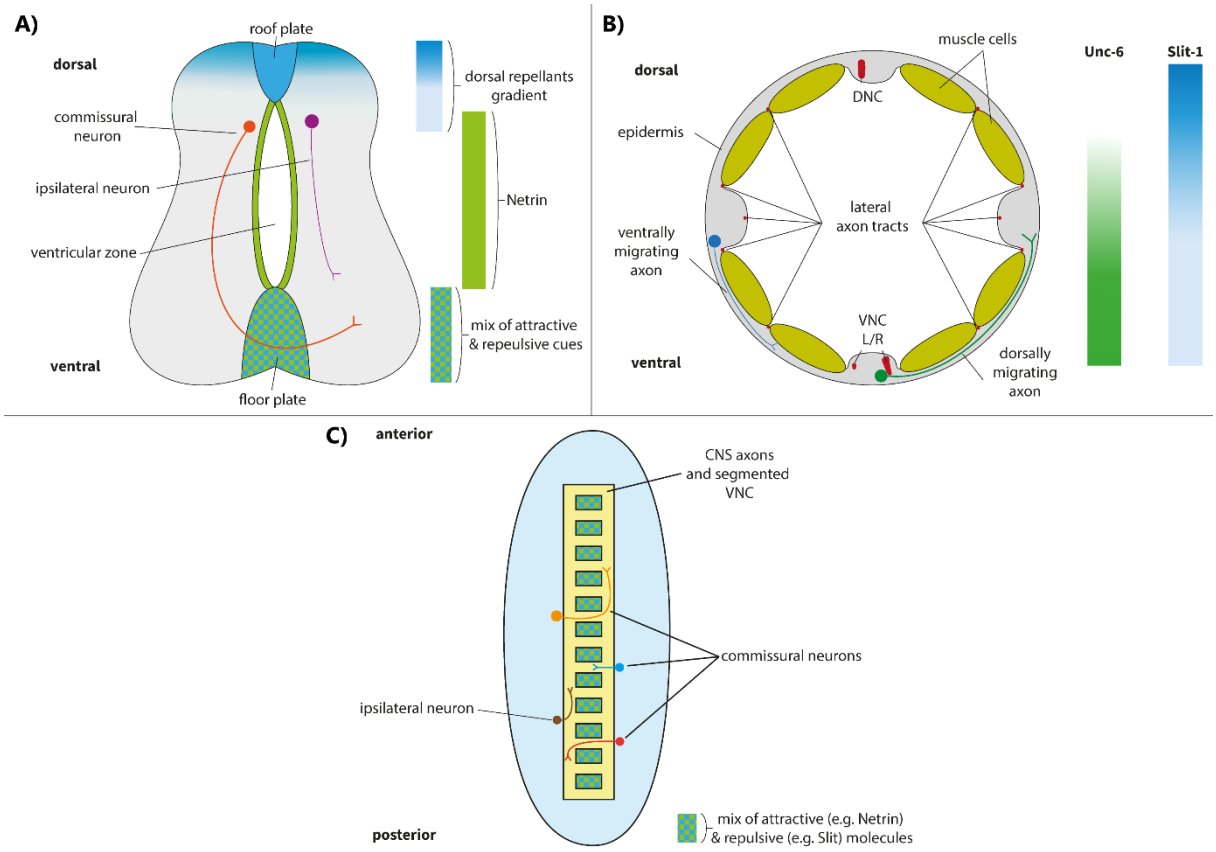

Figure 1.2: Axon guidance in bilaterian model systems. A) In the mouse embryo commissural neurons in the dorsal spinal cord extend their axon towards the floor plate, which crosses the midline and binds to the target cells on the other side. This mechanism is guided by repulsive molecules from the roof plate and dorsal spinal cord. The essential attractant promoting axon growth is Netrin expressed at the ventricular zone. A mix of attractive and repulsive cues in the floor plate allow through dynamic expression of receptors the crossing of the axon. **B)** In the nematode *C. elegans* neurons are growing along the dorso-ventral and anterior-posterior axis. During longitudinal outgrowth, axons from the left ventral nerve cord (VNC) cross the midline to the right VNC, which causes the asymmetry in axon abundance in the two VNCs. In the dorsal nerve cord (DNC) midline crossing cannot be observed. A ventral-dorsal Unc-6/Netrin gradient allows growth of axons expressing the Netrin receptor Unc-40/Dcc towards the ventral side. The dorsal-ventral gradient of Slit-1 leads to repulsion of the axon expressing the Slit-receptor Sax-3 towards the ventral side. Furthermore, Netrin can lead to repulsion of axons expressing Unc-5 or Unc-5 plus Unc-40/Dcc in dorsally migrating axons. **C)** In the *Drosophila melanogaster* embryo, the ventral nerve cord is segmented like the body. Midline crossing can also be observed. Cells in the middle express the major attractant Netrin and repellent Slit. Commissural neurons grow towards the midline expressing the Netrin receptor Frazzled/Dcc and leave the midline on the other side expressing the Slit receptor Robo. Ipsilateral neurons do not cross the midline. Figures adapted from (Chédotal, 2019; Chisholm et al., 2016; Howard et al., 2019).

response to Unc-6, thus axons grow dorsally. Slit-1 acts on the receptor Sax-3 and promotes axon growth from the dorsal to the ventral side. Similiar to longitudinal axon growth, orthologues of Wnt, hedgehog and ephrins affect circumfenterial axon outgrowth only mildly (Chisholm et al., 2016; Hutter, 2019). Although mice and *C. elegans* possess differently structured nervous systems, it can be seen that basic mechanisms like midline crossing in both animals depend mostly on Netrin signalling.

Midline crossing is also well-studied in fly embryos. The *Drosophila* nervous system is centralised in a brain anteriorly and the ventral nerve cord that is segmented along the body, with each segment able to make its own guidance decisions (**Figure 1.2C**). Glia cells in the midline express both Netrin-A and B, which bind to their receptor Frazzled (Dcc orthologue) and Dscam to promote midline crossing of incoming commisural axons. Commisural axons then exit the midline in response to the repulsive molecule, Slit, which acts upon Robo (Roundabout), a receptor located on the axon. The abundance of Robo-1 on the neuron surface is under indirect control of Frazzled (Howard et al., 2019).

In addition to well-studied model organisms, Netrin-signalling is also attributed to nervous system development in the sea urchin *Hemicentrotus pulcherrimus,* which displays bilateral symmetry at larval stages. In the pluteus larva, both Netrin and its receptor, Unc-5, are essential for serotonergic axon projections (Abe et al., 2013).

Netrin is also known to function outside of axon guidance. For instance, in *Xenopus laevis*, Netrin-1 is involved in the proper closure of the neural tube after the neural tube has folded in from the neuroectoderm (Kee et al., 2013). In addition to nervous system development, various other functions for Netrin have been described. For example, in lung morphogenesis, Netrin regulates lung epithelial branching with its receptors, Dcc and Unc-5 (Liu et al., 2004). During pancreatic development, Netrin is involved in epithelial cell adhesion and migration by binding to integrins (Yebra et al., 2003). Lastly, in developing mammary glands, Netrin-1 and its receptor Neogenin connect luminal epithelial cells with adjacent cap cells (Srinivasan et al., 2003).

Altogether, there exist many similarities in the mechanisms for nervous system development across Bilateria. In particular, the Netrin-signalling pathway, which will be the focus in this study, is conserved and appears to be essential for axon guidance.

1.3 Netrin signalling

Netrin signalling can evoke an attractive or a repulsive response from the Netrin-source. The response depends on the receptors, which are associated with the cytoskeleton via their intracellular domains, or their combination (Sun et al., 2011). Attraction results from Netrin binding to the receptors Dcc, its homologue Neogenin and Dscam. Dcc/Neogenin binds to Netrin as a homodimer, mediated by the intracellular domains, whereas Dscam binds Netrin as a monomer. Dscam can also dimerise with Dcc and mediate attraction (Ly et al., 2008). The role of Dscam in axon guidance has previously been debated (Ly et al., 2008; Palmesino et al., 2012), however, it was recently found to be essential in the guidance of GABAergic neurons into the Substantia Nigra mediated by Netrin (Brignani et al., 2020). A repulsive response to the Netrin source is mainly achieved by the receptor Unc-5, either alone when Netrin concentrations are high, or together with Dcc when Netrin concentrations are low. Unc-5 can also dimerise with Dscam to mediate axon repulsion in response to Netrin (Purohit et al., 2012). Furthermore, Neogenin was shown to be involved in axon repulsion and suppression of axon outgrowth by binding to Rgm (Repulsive guidance molecule) (Isaksen et al., 2020; Wilson & Key, 2006, 2007), suggesting a role of Rgm in Netrin signalling.

The domain architectures of Netrin and its receptors are depicted in **Figure 1.3**, as reviewed by (Meijers et al., 2020; Sun et al., 2011). The Netrin ligand harbours a laminin IV domain, three EGF repeats that make up the V domain, and a C-terminal Netrin-like domain (NTR) (**Figure 1.3**). The receptors are single-pass transmembrane proteins, and they belong to the Immunoglobulin (IG) superfamily. The receptor Dcc/Neogenin contains 4 IG and 5 Fibronectin type III (FNIII) domains on the extracellular side. The Netrin ligand is thought to bind to the last 3 FNIII domains. The intracellular peptide consists

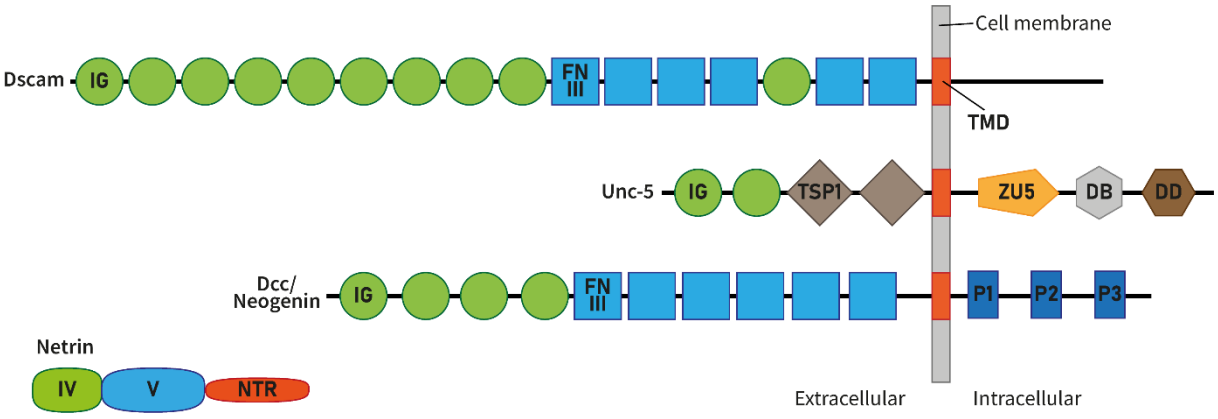

Figure 1.3 Domain structure of Netrin and its receptors Dcc/Neogenin, Unc-5 and Dscam. Netrin contains a Laminin IV domain, three EGF repeats that summarise as the V domain, and the Netrin C-terminal region (NTR). The receptors shown here belong to the Immunoglobulin (IG) superfamily. Dcc and its paralogue Neogenin have 4 IG domains and 6 Fibronectin type III (FNIII) domains on the extracellular side. Intracellularly they have the P1-3 motives. Unc-5 shows only 2 IG and 2 Thrombospondin type I (TSP1) domains extracellularly. On the intracellular side it has the 3 domains Zona occludens-5 (ZU5), Dcc binding domain (DB) and a Death domain (DD). The large Dscam harbours 10 IG and 6 FNIII domains extracellularly, whereby the 10th IG domain is located between the 4th and 5th FNIII domain. The intracellular part is not well studied yet. Figure adapted from (Meijers et al., 2020).

of the P1-3 motifs and upon Netrin binding they mediate homodimerization for chemoattraction or heterodimerisation with Unc-5 for chemorepulsion.

Aside from the attractant, Netrin, Dcc is also known to bind to a repulsive molecule called Draxin (Ahmed et al., 2011). The Unc-5 receptor has 2 IG and 2 Thrombospondin type I (TSP) domains extracellularly. It binds Netrin with the 2 IG domains. Intracellularly, it harbours a Zona occludens-5 (ZU-5), a Dcc binding (DB) domain, and a death domain. Binding of Netrin to Unc-5 leads leads to axon repulsion. The Dscam receptor molecule consists of 10 IG and 6 FNIII domains on the extracellular part, the IG domain 10 lying between the 4th and 5th FNIII domain. Netrin was found to bind the Dscam IG domains 7 through 9. Dscam also has an intracellular domain, but downstream signalling has not yet been resolved. Dscam is a prominent protein in *Drosophila melanogaster* in which up to 38.016 splice variants can be formed. In *Drosophila*, Dscam is known to be involved in cell identity, dendritic self-avoidance, and neural wiring (Schmucker et al., 2000). This diversity in function has not yet been observed outside insects.

In this study, we investigate whether Netrin-signalling and its role in neurite guidance exists in non-bilaterian animals. By studying the Cnidaria, the sister taxon of Bilateria, we attempt to decipher the degree to which axon guidance is evolutionarily conserved.

1.4 Cnidaria

The Cnidaria and Bilateria both emerged from a common ancestor more than 600 million years ago (Zhang & Shu, 2021). Cnidaria is divided into two clades, Medusozoa and Anthozoa. Medusozoa contains the Hydrozoa as a sister group to Cubozoa, Scyphozoa and Staurozoa, and Myxozoa as a sister group to those four (Kayal et al., 2018). They have a life cycle that includes a planula, polyp and medusa stage. Anthozoa, on the other hand, contain the subclasses Octocorallia and Hexacorallia, and differ from the Medusozoa as they do not have a medusa stage. Octocorallia includes soft corals or sea pens, and Hexacorallia includes the well-known reef-building stony corals, Scleractinia, or the sea anemones, Actiniaria.

Other key features of Cnidaria are that they are diploblastic animals meaning that they have two germ layers; ectoderm and endoderm, but not mesoderm, and that they have a single opening that functions as the mouth/anus. The mouth/anus is surrounded by tentacles at polyp stage, and it defines the oral pole of the animal. On the opposite end of the animal there exists a foot in what is defined as the aboral pole. In cnidarians, the oral-aboral axis is the only axis of symmetry, whereas Bilateria possess two axes of symmetry (anterior-posterior, dorso-ventral). Despite Cnidaria sharing many developmental features there are exceptions in the class Anthozoa, which differ from other cnidarians in the following points. Anthozoa lack a medusa stage and remain sessile after larval development. In

addition to the oral-aboral axis they contain a so-called "directive axis," which is orthogonal to the oral-aboral axis and manifests in internal structures (Genikhovich & Technau, 2017). Furthermore, anthozoans have endodermal infolds, which form structures called mesenteries that contain parietal and retractor muscles as well as gonadal tissue (Steinmetz, et al., 2017).

Most knowledge about anthozoan development is derived from the model organism *Nematostella vectensis*, the starlet sea anemone (Layden, et al., 2016a; Hand & Uhlinger, 1992; Putnam, et al., 2007). The fertilised egg (**Figure 1.4A**) develops over cleavage stages to a blastula stage (**Figure 1.4B**), building up the blastoderm surrounding the blastocoel. At gastrulation, part of the ectoderm folds in and grows inside into the blastocoel (**Figure 1.4C**). This initial point of invagination will become the future mouth. At planula stage (**Figure 1.4D**), the larvae are ciliated, enabling locomotion, and have an apical tuft on the aboral pole which serves as the settling point as a juvenile. After planula the animal starts developing tentacles (**Figure 1.4E**) and at the primary polyp stage the basic body plan is established (**Figure 1.4F**). Post settling, the animal remains sessile for the rest of its life. After four to five months, they become mature and can be induced for spawning (Hand & Uhlinger, 1992).

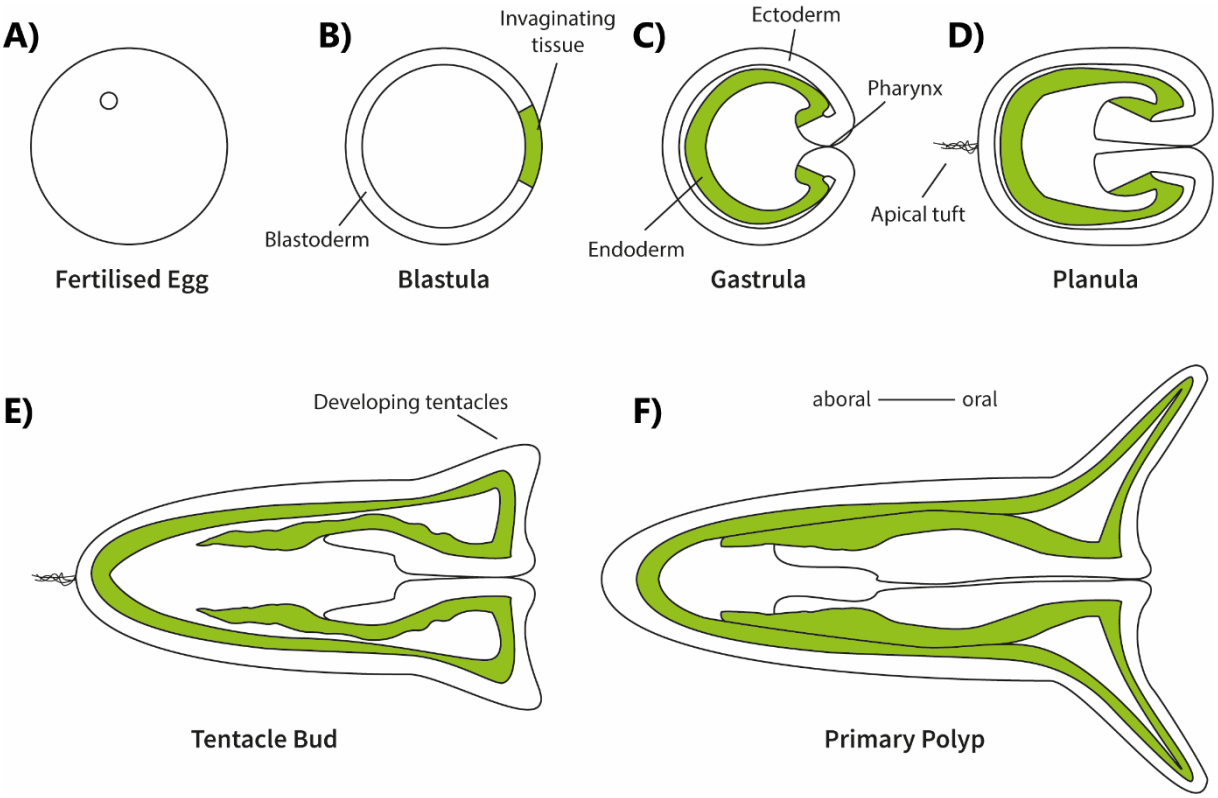

Figure 1.4: Embryonic development of *Nematostella vectensis*. Shown here are the developmental stages of *N. vectensis*. From the fertilised egg (**A**) the blastula stage arises (**B**), which has one cell layer, the blastoderm. In a small region the blastoderm (green) starts infolding during gastrulation which gives rise to the pharynx and the two germ layers endoderm (green) and ectoderm (white) in the gastrula stage (**C**). The distinct larva of the Anthozoa is the planula larva (**D**), containing an apical tuft organ on the aboral pole. The planula larva can move through the water column with cilia attached to the ectoderm (not shown). After planula the tentacles embark on developing at tentacle bud stage (**E**). Eventually at the primary polyp stadium (**F**) the first tentacles have grown out and the body plan remains from this point on, but it will develop more tentacles. Figure adapted from (Botman et al., 2015)

1.5 Neurogenesis in *Nematostella vectensis* and other cnidarians

Cnidarian polyps do not possess a centralised nervous system but rather a nerve net. Three major types of nerve cells can be distinguished: sensory neurons, ganglion cells and cnidocytes (stinging cells). Moreover, it is not clear whether a distinction of the neural processes into dendrites or axons exists. So, dendrites and axons are summarised as neurites and the term neurite guidance describes the outgrowth of neurites and the connecting of neurites to target cells. The cnidocyte is one of the most distinct morphological features in Cnidaria. There are subtypes which can penetrate or entangle prey. The cells consist of a cnidocil, a cilium detecting the presence of prey and the cnidocyst, a post-Golgi organelle consisting of a tightly coiled-up tubule, which is packed in a capsule under enormous osmotic pressure. In an explosive manner it can be expelled upon cnidocil stimulation (David et al., 2008).

In hydrozoans neural cells originate from a specific multipotent progenitor cell population, so-called interstitial stem cells (i-cells) (Bode et al., 1987; David, 2012; Denker et al., 2008; Gahan et al., 2016; Galliot et al., 2009). On the other hand, in *N. vectensis* neurogenesis starts at blastula stage with progenitor cells expressing *NvSoxB(2)*$^{+}$, which give rise to neural cells and gland/secretory cells (Tournière et al., n.d.). **Figure 1.5** gives an overview about the location of neural genes within the developing larva. At early gastrula the achaete-scute gene *NvAshA* starts being expressed under control of *NvSoxB(2)* (Richards & Rentzsch, 2014, 2015). The abundance of progenitor cells and the regulation of proneural genes is not only under control of Notch and MAPK signalling but also under that of *NvAth-like, NvAshA* and *NvSoxB(2)* (Layden et al., 2016; Richards & Rentzsch, 2015). Various differentiated neural populations derive from *NvSoxB(2)*$^{+}$ progenitors, like *NvNcol3*$^{+}$ cnidocytes (Richards & Rentzsch, 2014), *NvFoxQ2d*$^{+}$ sensory cells (Busengdal & Rentzsch, 2017), *NvLWamide*$^{+}$

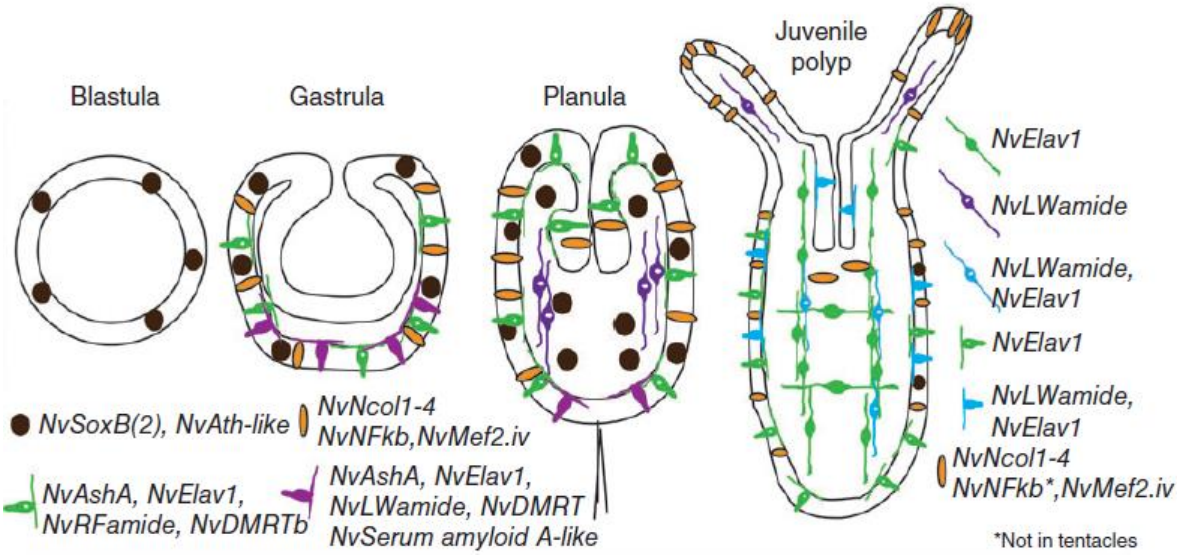

Figure 1.5: Overview of neurogenesis and germ layer localisation of known neuronal genes in *N. vectensis*. Time of development is depicted from left to right with the oral side facing up. Black cells are progenitor cells, orange cells resemble nematocytes, elongated bipolar neurons represent sensory cells in the endoderm and ectoderm. Figure adapted from (Rentzsch et al., 2017).

ganglion cells (Stone et al., 2020) or NvRPamide expressing sensory cells in the apical organ (Zang & Nakanishi, 2020). Under control of *NvSoxB(2)* and *NvAth-like* (Richards & Rentzsch, 2014, 2015) expression of *NvElav1* – encoding an RNA binding protein – starts at gastrulation in the ectoderm and in the endoderm of the early planula. Transplantation experiments using the *NvElav1::mOrange* transgenic reporter line revealed that ecto- as well as endoderm have neurogenic potential. *NvElav1*::mOrange positive cells give rise to sensory neurons and ganglion cells in the ectoderm. They form a basi-epithelial network of neurites in the ecto- and endoderm. Interestingly, ectodermal *NvElav1*::mOrange^{+} neurons grow processes towards the aboral pole at early-planula stage. However, at mid-planula newly born *NvElav1*::mOrange^{+} neurons grow neurites transversally. This process can also be seen in neurons stained for the neuropeptide NvGLWamide (Nakanishi et al., 2012).

Overall, *N. vectensis* harbours a diversity of neuronal populations. The development of the nerve net starts from neurons generated throughout the entire tissue. Important questions arise like how do cells extend their neurites and connect to their target cells? Which mechanisms are underlying these processes and which genes are necessary for neurites to be guided through the tissue? Neurite outgrowth in aboral direction in the sea anemone can be observed (Nakanishi et al., 2012), thus it seems fair to ask the question if axon guidance, a mechanism observed in Bilateria, is evolutionary conserved in the earlier branching Cnidaria.

In this thesis we focussed on one of the ligand-receptor systems described above in the examples for axon guidance in bilaterians. We are aiming at characterising the NvNetrin system and if neurite guidance in *N. vectensis* comparable to other model organisms exists. Already, an orthologue of the guidance molecule *Netrin* (*NvNetrin*) has been described in *N. vectensis* (Leclère & Rentzsch, 2012; Matus et al., 2006). An *in-situ* hybridisation – labelling a specific mRNA and resolving the spatio-temporal expression pattern during embryonic development – revealed an asymmetric expression of *NvNetrin* in the endoderm at planula stage. Also, it is found in the apical tuft at the aboral pole (Matus et al., 2006), in which direction the *NvElav1*::mOrange neurons temporarily project (Nakanishi et al., 2012). However, a charactarisation of NvNetrin receptors is lacking in *N. vectensis* and thus serves as the basis for this study.

Thus, the observation of a broad neurogenic potential, neurite outgrowth and expression of *NvNetrin* make *Nematostella vectensis* a suited model to study neurite guidance outside of Bilateria. This study aims to characterise the possible NvNetrin receptors *NvDscam* and *NvNeogenin* in *N. vectensis*. It should be clear that this thesis is about putative NvNetrin receptors, because it has not been studied yet, if the receptors found in *N. vectensis* interact with NvNetrin. The receptors were first described with a phylogenetic analysis (for *NvDscam*) and *in-situ* hybridisations. The phylogenetic analysis confirmed that the *N. vectensis* genome encodes a *NvDscam* orthologue. mRNA staining of *NvDscam*

and *NvNeogenin* revealed an expression pattern like that of known neural genes during gastrulation, but also points at a broader expression outside of the nervous system. Also, co-expression with the progenitor marker *NvSoxB(2)* is found, which also gives rise to neurons. Furthermore, a transgenic reporter construct for *NvNeogenin*-expressing cells was established. As well, mutant lines for functional analysis of *NvDscam* and *NvNeogenin* were developed, which was achieved by CRISPR/Cas9-mediated mutagenesis. For further functional analysis RNA interference based on short-hairpin-RNAs targeted against *NvDscam* and *NvNeogenin* was set up.

1.6 Aims of the study

In this thesis we aimed to answer three basic questions about the putative NvNetrin receptors *NvDscam, NvNeogenin* and *NvUnc-5*.

- Are the receptors present in the genome of *Nematostella vectensis*?
- Where in the animal are the genes expressed?
- What are the functions of the genes?

We addressed the first question by a phylogenetic analysis of *NvDscam* and analysis of RNA-sequencing data for the three genes. Phylogenies of *NvNeogenin* and *NvUnc-5* have already been performed (Leclère & Rentzsch, 2012).

The next step involved the assessment of the spatio-temporal expression pattern of the genes' mRNA with *in-situ* hybridisations (ISHs), and with fluorescence double ISH to identify potential co-expression with known neural genes. The establishment of transgenic reporter lines driving mGFP expression under control of the putative *NvDscam* or *NvNeogenin* promoter would give a clearer signal than *in-situ* hybridisations, more insights into cell morphology and the lines can be crossed to other transgenic reporter lines for further characterisation of $mGFP^+$ cells.

Thirdly, the establishment of gene knockouts and knockdowns allows for future functional studies. This was addressed by creating mutant lines using the CRISPRS/Cas9 system and establishing RNA-interference.

Taken together, this study aims at a basic characterisation of the NvNetrin receptors, and the tools created in this thesis will help to study the roles of NvNetrin receptors in neurite guidance in *N. vectensis* in future experiments.

2. Materials

2.1 Chemicals

Chemical	Abbreviation	Company	Catalogue number
4-(1,1,3,3-Tetramethylbutyl)phenyl-polyethylene glycol	Triton-X-100	Sigma Aldrich	9002-93-1
4`,6-diamidino-2-phenylindole	DAPI	Thermo Fisher	62248
Acetic anhydride	$(CH_3CO)_2O$	Sigma Aldrich	45830
Agarose	$[C_{12}H_{18}O_9]_n$	Life Technologies	16500500
Bovine serum albumin	BSA	Sigma Aldrich	A4503
Chloroform	$CHCl_3$	Merck	02487
Citric acid	$C_6H_8O_7$	Sigma Aldrich	C0579
Di-sodium -hydrogen-phosphate – dihydrate	Na_2HPO_4 x 2 H_2O	Merck	1.06580.1000
Ethanol absolute	C_2H_6O / EtOH	Sigma Aldrich	1.00983
Ethylenediaminetetraacetic acid	$C_{10}H_{16}N_2O_8$ / EDTA	Thermo Fisher	F9260G
Formaldehyde (37%)	CH_2O	Sigma Aldrich	252549
Formamide (deionised)	CH_3NO	Sigma Aldrich	F9037 / 47671
Gluteraldehyde	$C_5H_8O_2$	Sigma Aldrich	G7651
Glycerol	$C_3H_8O_3$	Sigma Aldrich	49781
Glycine	$C_2H_5NO_2$	Sigma Aldrich	50046
Hydrogen peroxide	H_2O_2	Merck	K50794709911
L-Cysteine	$C_3H_7NO_2S$	Sigma Aldrich	W326305
Lithium chloride	LiCl	Thermo Fisher	9480G
Magnesium chloride	$MgCl_2$	Sigma Aldrich	208337
Maleic acid	$C_4H_4O_4$ / MA	Sigma Aldrich	M0375
Methanol	CH_3OH / MeOH	Sigma Aldrich	32213
Milli-Q water	H_2O	Merck	ZR0Q008WW
Nuclease-free water	H_2O	Invitrogen	AM9937
Polyethylene glycol sorbitan monolaurate	Tween®-20	Sigma Adlrich	P9416-100ML
Potassium chloride	KCl	Sigma Adlrich	P9541
Sodium chloride	NaCl	Sigma Aldrich	S7653
Sodium citrate tribasic dehydrate	Na-citrate	Sigma Aldrich	71402
Sodium dodecyl sulfate (20%)	$NaC_{12}H_{25}SO_4$ / SDS	Sigma Aldrich	05030
Sodium-di-hydrogen-phoshpate – monohydrate	NaH_2PO_4 x H_2O	Merck	1.06346.1000
Triethanolamine	$C_6H_{15}NO_3$ / TEA	Sigma Aldrich	90279
Tris-EDTA buffer solution		Fluka Analytical	93283-100ML

2.2 Buffers and Solutions

10x Phosphate buffered saline (PBS)	
NaH_2PO_4 x H_2O	18.6 mM
Na_2HPO_4 x 2 H_2O	84.1 mM
NaCl	1.75 M

PTw
1x PBS
0.1% (v/v) Tween-20

PTx
1x PBS
0.2% (v/v) Triton-x-100

PTx-BSA
1x PBS
0.1% (w/v) BSA
0.2% (v/v) Triton-X-100

20x SSC pH 7.0	
NaCl	3 M
NaCitrate	340 mM

2x SSCT
10% (v/v) 20x SSC
0.1% (v/v) Tween-20

0.1x SSCT
0.5% (v/v) 20x SSC
0.1% (v/v) Tween-20

NTMT	
NaCl	100 mM
Tris-HCl pH 9.5	100 mM
$MgCl_2$	50 mM
Tween-20	0.1% (v/v)

5x Maleic Acid Buffer (MAB) pH 7.5	
Maleic acid	0.50 M
NaCl	0.75 M

Hybridisation Buffer (-)	
Formamide	50% (v/v)
20x SSC	5x
SDS	1% (v/v)
Tween-20	0.1% (v/v)
Citric acid	9.25 mM

Hybridisation Buffer (+)	
Hybridisation Buffer (-)	
Heparin	50 µg/ml
Deoxyribonucleic acid, single stranded from salmon testes	100 µg/ml

10x TN	**TNTw**	**TNTx**	**TNB**
Tris-HCl pH 7.5 1M	10% (v/v) 10x TN	10% (v/v) 10x TN	10% (v/v)
NaCl 1.5 M	0.1% Tween-20	0.2% Triton-X-100	0.5% TSA Blocking Reagent

Extraction Buffer	
Tris-HCl pH 8	10 mM
EDTA	1 mM
NaCl	25 mM
Proteinase K	200 µg/µl

LB Agar plates	
26.25 g	LB Broth with agar
40 µg/ml	X-Gal in DMSO
100 µg/ml	Ampicillin
750 ml	Milli-Q H_2O

2.3 Kits and ready-to-use reagents

Name	Company	Catalogue number
Ampicillin	Merck	A9518
AmpliScribe™ T7-Flash™ Transcription Kit	Lucigen	ASF3257
Boehringer Blocking solution (BBS)	Sigma Aldrich	11096176001
Boehringer Blocking solution (BBS)	Sigma Aldrich	11096176001
Cas9	PNA Bio	CP01
Cut Smart Buffer	BioLabs	B72045
Deoxyribonucleic acid, single stranded from salmon testes	Sigma Aldrich	D9156
Dextran, Alexa Fluor™ 568	Invitrogen	D22912
Dextrane, Alexa Fluor™ 488	Invitrogen	D22910
DIG RNA labelling mix (10X)	Merck	11277073910
DNA Gel Loading Dye (6X)	Thermo Scientific™	R0611
DNP-labelled uridine	PerkinElmer	NEL555001EA
dNTP mix	Thermo Scientific	R0191
EnGen® sgRNA synthesis kit, S. Pyogenes	New England BioLabs	ES3322
Eva Green	Biotium	31000
ExTaq® DNA Polymerase	TaKaRa	RR001A
GeneRuler 100 bp Plus DNA Ladder	Thermo Scientific™	SM0321
GeneRuler DNA Ladder Mix	Thermo Fisher	SM0331
Gibson Assembly® Master Mix – Assembly	NEB	E2611
GoTaq® G2 Flexi DNA Polymerase	Promega	M7801
I-SceI Restriction enzyme	BioLabs	RO6945
LB	Merck	L3022
LB Broth with agar	Sigma Aldrich	L2897
MEGAscript™ SP6 Transcription Kit	Invitrogen	AM1330
MEGAscript™ T7 Transcription Kit	Invitrogen	AM1334
Natural Goat serum	Merck	G9023
NBT/BCIP stock solution	Merck	11681451001
Nucleospin® Gel and PCR clean up	Macherey-Nagel	REF 740609.250
pGEM®-T easy vector	Promega	A1360
Prolong Gold (with DAPI)	ThermoFisher	P36931
Proteinase K	Sigma Aldrich	P2308
PureYield™ Plasmid Miniprep System	Promega	A1222
Q5® High-Fidelity DNA polymerase	NEB	M0491S
QuantiTect® SYBR Green PCR kit (200)	Qiagen	204143
Random hexamer primers (50 µM)	Invitrogen	N8080127
Ribonuclease H	Invitrogen	18021014
RNA Clean & Concentrator Kit	Zymo Research	R1017
RNAqueous™ Total RNA Isolation Kit	Invitrogen	AM1912
RNase-OUT™ Recombinant Ribonuclease Inhibitor (40 U/µl)	Invitrogen	10777019
RNeasy® Micro Kit (50)	Qiagen	74004
SOC medium	Invitrogen	15544034
SuperScript™ III Reverse Transcriptase	Invitrogen	18080-044
SYBR Safe® DNA gel stain	Life technologies	S33102
Trizol™ LS Reagent	Ambion	10296010
TSA® Blocking Reagent	Perkin Elmer	FP1012
TSA® Plus Cyanine 3	Akoya Biosciences	NEL744001KT

TSA® Plus fluorescein	Akoya Biosciences	NEL741001KT
TURBO DNA-free™ Kit	Invitrogen	AM1907
X-Gal	Thermo Fisher	R0404

2.4 Antibodies

Antibody	Company	Catalogue number
AlexaFluor™ goat anti rabbit IgG	Invitrogen	A1108
Anti-GFP antibody, rabbit	Abcam	Ab290
Anti-DNP-HRP	Akoya Biosciences	FP1129
Anti-DIG-POD, Fab-fragments	Merck	11207733910
Anti-DIG-AP, Fab-fragments	Merck	11093274910

2.5 Instruments

Instrument	Company	Use
C1000 Thermocycler CFX96™ Real-Time System	BioRad	qPCR, melt curves
Centrifuge 5418	Eppendorf	Centrifuge, room temperature
Centrifuge 5418 R	Eppendorf	Centrifuge, 4°C
ChemiDoc XRS+	BioRad	Gel imaging
Eclipse TE2000-U	Nikon	Injection into zygotes
FemtoJet 4i + CellTram Vario	Eppendorf	Injection into zygotes
FV3000 Confocal Laser Scanning Microscope	Olympus	FISH imaging
Mastercycler Nexus GSX1	Eppendorf	PCR
NanoDrop™ One/OneC Microvolume UV-Vis Spectrophotometer	Thermo Scientific	DNA/RNA concentration and purity measurement
Nikon eclipse E800 compound microscope + Nikon Digital Sight DSU3 camera	Nikon Corporation	ISH imaging
SMZ18 + DS-Qi2 Camera	Nikon	Stereomicroscope
Thermo mixer C	Eppendorf	Heating block

2.6 Software and websites

Software name	Purpose	Developer/Comapny
CFX Manager 3.1	qPCR/melt curve	BioRad
Fiji – ImageJ	Image processing	(Schindelin et al., 2012)
FV31S-SW	Confocal microscopy	Olympus
Illustrator 25.0.1	Image processing	Adobe
ImageLab 5.1	Gel imaging	BioRad
NIS-Elements 5.11	Stereomicroscope imaging, colorimetric ISH imaging	Nikon
Photoshop 21.1.0	Image processing	Adobe
Prism 9.2.0	Data visualisation and statistics	GraphPad
SnapGene 5.2	Sequence analysis	GSL Biotech LLC

Website name	Purpose	Link
BioLabs Tm Calculator	Primer annealing temperature	https://tmcalculator.neb.com/#!/main
CHOPCHOP	sgRNA design	https://chopchop.cbu.uib.no/
CRISP-ID V1.1	Sequence analysis	http://crispid.gbiomed.kuleuven.be/
InvivoGen siRNA Wizard Software	shRNA design	https://www.invivogen.com/sirnawizard/index.php
IQ-TREE web server	Phylogenetic analysis	http://iqtree.cibiv.univie.ac.at/
iTOL	Phylogenetic tree	https://itol.embl.de/
Jpred 4	Secondary structure prediction	http://www.compbio.dundee.ac.uk/jpred/
MAFFT-7	Multiple sequence alignment	https://mafft.cbrc.jp/alignment/server/
NCBI	Database for sequences	https://www.ncbi.nlm.nih.gov/
Primer3web	Primer design	https://primer3.ut.ee/
Promega Tm Calculator	Primer annealing temperature	https://no.promega.com/resources/tools/biomath/tm-calculator/
SMART	Protein domain prediction	http://smart.embl-heidelberg.de/
Vienna Genome Browser	*Nematostella vectensis* genome (Putnam, et al., 2007)	http://genomebeta-evo.zoo.univie.ac.at/

2.7 Primers and Oligonucleotides

Primers were designed using Primer3 (https://primer3.ut.ee/), ordered and synthesised at Merck KGaA, Darmstadt, Germany.

Sequence 5´-3´	Use	Annealing temperature (DNA polymerase)
CTACGGTTTGCAGATGAGCC	F. NvDscam *in situ* probe	55°C (ExTaq™)
AGTGATTGGGCGTTCTGGTA	R. NvDscam *in situ* probe	
CTTCCCACTCAACCACAAGC	F. Robo2 *in situ* probe	61°C (Q5®)
TGTATTGGACTGAAGCCCGT	R. Robo2 *in situ* probe	
TTTTTTTTTTTTTTTTTTTT	Oligo-dT-20, cDNA synthesis	-
ATTTAGGTGACACTATAG	SP6, sequencing	-
TAATACGACTCACTATAGGG	T7, sequencing	-
GTAAAACGACGGCCAG	F. M13, plasmid PCR	55°C (GoTaq®)
CAGGAAACAGCTATGAC	R. M13, plasmid PCR	
AGCATTCCCCACATACTTTTACT	F. NvDscam promoter	64°C (Q5®)
GGGGCGAAAATCAGGTCAAA	R. NvDscam promoter	
ACCGATACCGTTATGATCAACAG	F. NvNeogenin promoter	64°C (Q5®)
CACGAGTGATTTCAGGACTTCA	R. NvNeogenin promoter	
ATGGTCAGCAAAGGAGAGGAACTC	F. CB1043, transgenic vector backbone	65°C (Q5®)
GGCCGGCCTTAATTAAATTACCCTG	R. CB1043, transgenic vector backbone	

TTTGACCTGATTTTCGCCCC ATGGTCAGCAAAGGAGAGGAACTC	NvDscam-CB1043 linker, Gibson assembly	65°C (Q5®)
AGTAAAAGTATGTGGGGAATGCT GGCCGGCCTTAATTAAATTACCCTG	CB1043-NvDscam linker, Gibson assembly	
TGAAGTCCTGAAATCACTCGTG ATGGTCAGCAAAGGAGAGGAACTC	NvNeogenin-CB1043 linker, Gibson assembly	65°C (Q5®)
CTGTTGATCATAACGGTATCGGT GGCCGGCCTTAATTAAATTACCCTG	CB1043-NvNeogenin linker, Gibson assembly	
ATATTCGGTGGTTGCTTGCG	F. NvDscam::mGFP Colony PCR	64°C (GoTaq®)
ACACGCCGTCAAATTTCCTT	F. NvNeogenin::mGFP Colony PCR	
GTTGCTTCATGTGGTCAGGG	R. NvDscam::mGFP / R. NvNeogenin::mGFP Colony PCR	
TTCTAATACGACTCACTATAGCGGGAACACTACACATGCG GTTTTAGAGCTAGA	NvDscam-Ex7, sgRNA oligo	-
TTCTAATACGACTCACTATAGAGCAATTACAGCAAAACCCG GTTTTAGAGCTAGA	NvDscam-Ex21, sgRNA oligo	-
TTCTAATACGACTCACTATAGTCACTCGTGTGGCCTGTGAT GTTTTAGAGCTAGA	NvNeogenin-Ex1.2, sgRNA oligo	-
TTCTAATACGACTCACTATAGATATAAAGACATCCTATCAC GTTTTAGAGCTAGA	NvNeogenin-Ex1.3, sgRNA oligo	-
TTCTAATACGACTCACTATAGTCAAAGGGAGGGTGACACGG GTTTTAGAGCTAGA	NvNeogenin-Ex11, sgRNA oligo	-
TTCTAATACGACTCACTATAGCTGTGCAAGAAGCGATCCG GTTTTAGAGCTAGA	NvNeogenin-Ex15, sgRNA oligo	-
CCTCGGATCACGCCATTCAT	F. NvDscam-Ex7, melt curve	60°C (Q5®)
GTGTAACATCACGTGGTTGA	R. NvDscam-Ex7, melt curve	
GTCTGGCTGCTAGGGGAC	F. NvDscam-Ex21, melt curve	60°C (Q5®)
CTGACCCTAGAGACGCCAC	R. NvDscam-Ex21, melt curve	
TCTGAGGTGAGTTTCGGTGG	F. NvDscam-Ex21, sequencing	65°C (Q5®)
ACCGAGTTTCTGAGACGCAT	R. NvDscam-Ex21, sequencing	
TGCCCTGTATTTGGACCTTT	F. NvNeogenin-Ex1, melt curve	60°C (Q5®)
TTACGTCTCTCTTCTCTTCACG	R. NvNeognein-Ex1, melt curve	
CGTGTGAATCAGCCCTATCTC	F. NvNeogenin-Ex11, melt curve	60°C (Q5®)
ATCCTTCATGTCCAGTGGCA	R. NvNeogenin-Ex11, melt curve	
GCCATCATCATCATTAGTGTTGT	F. NvNeogenin-Ex15, melt curve	60°C (Q5®)
GGAGGTTTAGTATAGTGCTTGGA	R. NvNeogenin-Ex15, melt curve	

ACTTCCAGCAATGCCCTGTA	F. NvNeogenin-Ex1, sequencing	65°C (Q5®)
TGTGGTTGGTTTCTCGGGTA	R. NvNeognein-Ex1, melt curve	
CGGTGCTTCTGAGGTCAAAG	F. NvNeogenin-Ex11, sequencing	65°C (Q5®)
CAAACCTCCTGAGACGGGTA	R. NvNeogenin-Ex11, sequencing	
TGCTGAATTGCTTGCTTACTGT	F. NvNeogenin-Ex15, sequencing	65°C (Q5®)
ACCCCGTTATAAAGGCACCT	R. NvNeogenin-Ex15, sequencing	
TAATACGACTCACTATAGAGACTGGACCCTAGTAT TTCAAGAGAAATACTAGGGTCCAGTCTCTT	F. shNvDscam-1, shRNA forward oligo	-
AAGAGACTGGACCCTAGTATTTCTCTTGAA ATACTAGGGTCCAGTCTCTATAGTGAGTCGTATTA	R. shNvDscam-1, shRNA reverse oligo	-
TAATACGACTCACTATAGACAGACTATCCCGTATGA TCAAGAGATCATACGGGATAGTCTGTCTT	F. shNvDscam-2, shRNA forward oligo	-
AAGACAGACTATCCCGTATGATCTCTTGA TCATACGGGATAGTCTGTCTATAGTGAGTCGTATTA	R. shNvDscam-2, shRNA reverse oligo	-
TAATACGACTCACTATAGCTGAAGGGACCATATCAA TCAAGAGATTGATATGGTCCCTTCAGCTT	F. shNvDscam-3, shRNA forward oligo	-
AAGCTGAAGGGACCATATCAATCTCTTGA TTGATATGGTCCCTTCAGCTATAGTGAGTCGTATTA	R. shNvDscam-3, shRNA reverse oligo	-
TAATACGACTCACTATAGGATGGGAGTGAAATAGCA TCAAGAGATGCTATTTCACTCCCATCCTT	F. shNvNeogenin-1, shRNA forward oligo	-
AAGGATGGGAGTGAAATAGCATCTCTTGA TGCTATTTCACTCCCATCCTATAGTGAGTCGTATTA	R. shNvNeogenin-1, shRNA reverse oligo	-
TAATACGACTCACTATAGCCCAACACCAAGTATGAA TCAAGAGATTCATACTTGGTGTTGGGCTT	F. shNvNeogenin-2, shRNA forward oligo	-
AAGCCCAACACCAAGTATGAATCTCTTGA TTCATACTTGGTGTTGGGCTATAGTGAGTCGTATTA	R. shNvNeogenin-2, shRNA reverse oligo	-
TAATACGACTCACTATAGACGTAAACGGCCACAAGTT TCAAGAGAACTTGTGGCCGTTTACGTCTT	F. shGFP, shRNA forward oligo	-
AAGACGTAAACGGCCACAAGTTCTCTTGA AACTTGTGGCCGTTTACGTCTATAGTGAGTCGTATTA	R. shGFP, shRNA reverse oligo	-
GGCGAATGGTTCACTGGTTT	F. NvDscam-qPCR	60°C (Q5®)
AACGCGCCAAATCTGTTCTT	R. NvDscam-qPCR	
GGCATTCTCTTCCTGATTCCATA	F. NvNeogenin-qPCR	60°C (Q5®)
AGGCAGTAATGTCACTTTGCT	R. NvNeogenin-qPCR	
TTACGGAGCTCTGGCTTTCCTTTC	F. NvRiboprotein-qPCR	60°C (Q5®)
TGCCGTTAAGGGTATCAAAGGACG	R. NvRiboprotein-qPCR	

3. Methods

3.1 Animals

Adult *Nematostella vectensis* anemones were kept in *Nematostella*-medium (NM; 1/3 filtered sea water) at 18°C. They were induced for spawning as previously described (Genikhovich & Technau, 2009; Fritzenwanker & Technau, 2002), fertilised for 45 min and the jelly surrounding the eggs was dissolved with 3% L-Cystein in NM (pH 7.4 – 7.6) for 15 min at 70 rotations per minute (rpm) shaking horizontally, followed by 7 washes in NM. Embryos were kept in NM at 21°C and raised to adulthood with daily feeding and washing routines. After two to three months, when animals approached sexual maturity, animals were moved to 18°C. Besides wild type (WT) animals, for this master thesis the following lines were used: *NvElav1::NTR-Cerulean* (Richards & Rentzsch, 2014) and *NvElav1::mOrange* (Nakanishi, et al., 2012).

3.2 Animal fixation

For colorimetric as well as double fluorescence *in situ* hybridisation embryos at 12 hours post fertilisation (hpf) (blastula), 20 hpf (early gastrula), 30 hpf (late gastrula), 48 hpf (early planula), 72 hpf (mid planula), 96 hpf (late planula), 120 hpf (early tentacle bud), 144 hpf (late tentacle bud) and 168 hpf (primary polyp) were used for fixation. Prior to fixation, animals older than 48 hpf in a petri dish with ~25 ml NM were treated with 1 ml of 1M $MgCl_2$ for relaxation and stopping of movement. They were transferred to 1.5 ml tubes on ice and treated with 1 ml cold 3.7% formaldehyde and 0.25% glutaraldehyde in NM for 90 sec. Then, animals were kept for 1 h in 1 ml 3.7% formaldehyde in PTw at 4°C and rotated at 5 rpm. This was followed by 4 washes with 1 ml of ice cold PTw, once with 1 ml PBS and once again with 1 ml Milli-Q H_2O. Fixed animals were stored in methanol at -20°C.

3.3 *In-situ*-hybridisation-probe synthesis

3.3.1 RNA isolation

Total RNA was isolated from 120 hpf old animals using the RNAqueous Kit (Invitrogen). All centrifugation steps for RNA isolation with the kit were 13.000 rpm for 1 min at 4°C. In one 1.5 ml tube 500 µl Lysis Buffer was added to approximately 200 animals. The tube was vortexed until the solution was homogenised. An equal volume of 64% ethanol was added, the sample mixed by pipetting and the lysate was transferred to a Filter Cartridge in a Collection Tube which was centrifuged. Then 3 washes followed: once with 700 µl Wash Solution #1 and twice with 500 µl Wash Solution #2/3, each in combination with centrifugation. To remove remaining ethanol the tube was centrifuged drily. The Elution Buffer was heated to 70°C, 40 µl were added to the column, which was incubated at room temperature for 1 min and then centrifuged. The elution step was repeated with 10 µl of Elution Buffer.

3.3.2 DNase treatment

Afterwards, 0.1x volume of 10X TURBO DNase Buffer (Invitrogen) and 1 µl of TURBO DNase (Invitrogen) were added to the eluted RNA and incubated for 25 min at 37°C. The Inactivation Reagent (Invitrogen) was vortexed and 0.1x volume was added to the DNase treated RNA. The tube was kept at room temperature for 3 min and mixed by inverting, followed by centrifugation for 1.5 min at 10.000g. The supernatant containing RNA was transferred to a new tube, which was assessed for purity and concentration by NanoDrop-One and degradation by gel electrophoresis.

3.3.3 cDNA synthesis

For cDNA Synthesis the SuperScript™ III Reverse Transcriptase kit was used (Invitrogen). Therefore, 5 µg of RNA were mixed with 1 µl of Random Hexamer Primers (Invitrogen), 1 µl of dNTP Mix (Thermo Scientific) and nuclease-free water (Invitrogen) up to 13 µl. The mixture was incubated at 65°C for 5 min and then on ice for 1 min, followed by a quick centrifugation. Next, 4 µl 5x First Strand Buffer, 1 µl 0.1 M DTT, 1 µl RNaseOUT™ Recombinant RNase Inhibitor (40 U/µl, Invitrogen) and 1 µl of SuperScript™ III Reverse Transcriptase (300 U/µl) were added. The contents were mixed by pipetting and the tube incubated at 25°C for 5 min. For reverse transcription the mixture was incubated at 55°C for 60 min and for inactivation it was set to 70°C for 15 min. Removal of remaining RNA was achieved by adding 1 µl of Ribonuclease H (2 U/µl, Invitrogen) and incubation at 37°C for 20 min.

3.3.4 Polymerase Chain Reaction (PCR)

Primers were designed in Primer3web using default values. Amplicon length for *in situ* hybridisation (ISH) probes were around 1000-1200 base pairs (bp). Primers are shown in section ***2.7 Primers and Oligonucleotides***. Sequences were amplified in a PCR using ExTaq DNA Polymerase (TaKaRa). One reaction was set up as following: 10 ng cDNA were mixed with 2.5 µl 10x Reaction Buffer, 2 µl 2.5 mM dNTPs, 0.5 µl 10 µM forward, 0.5 µl 10 µM reverse primer and 0.2 µl ExTaq DNA Polymerase; nuclease free water (Invitrogen) was added to a total of 25 µl. The thermocycler protocol started with 3 min activation at 94°C, followed by 40 cycles of denaturation at 94°C for 30 sec, primer annealing according to the temperature in section *Primers and Oligonucleotides* for 30 sec and elongation at 72°C for 1 min/kb. The PCR ended with 3 min at 72°C of final elongation and holding at 4°C. Amplicon lengths were checked on a 1% agarose gel.

3.3.5 Ligation and Transformation

The amplicon was cloned into the pGEM-T Easy Vector (Promega) by mixing 3.5 µl of the PCR reaction with 0.5 µl of pGEM-T Easy Vector, 1 µl of T4 Ligase and 5 µl of 2x Reaction Buffer. The mixture was incubated at 4°C overnight (o/n). For transformation, competent *E. coli* were thawed on ice and 4 µl of ligation mix were added to 100 µl of bacteria. After resting on ice for 30 min the bacteria were heat-shocked in a 42°C water bath for 45 sec and then allowed to rest on ice for 5 min. 300 µl SOC medium

(Invitrogen) was added, and the tube incubated at 37°C and 120 rpm for 1 hour. Afterwards, 100 µl of the bacterial culture were plated onto LB-agar plates with X-Gal (Thermofisher) and Ampicillin (Merck) which were incubated for 16 hours at 37°C.

To control the insertion of the amplicon into the vector, colony PCR with GoTaq® Flexi (Promega) was performed as following: 5.0 µl 5x GoTaq® Buffer, 2.5 µl 25 mM $MgCl_2$, 0.5 µl 10 mM dNTPs, 0.5 µl M13 forward primer, 0.5 µl M13 reverse primer, 0.125 µl GoTaq® Flexi and 15.875 µl nuclease-free water (Invitrogen). 8 white colonies were randomly picked and incubated in the reaction mix for 5 min. The temperature protocol in the thermocycler started with 5 min initial denaturation at 95°C, 35 cycles of denaturation at 95°C for 30 sec, primer annealing at 55°C for 30 sec and elongation at 72°C for 1 min/kb; final elongation at 72°C was done for 5 min and holding at 4°C. Amplicon lengths were checked on a 1% agarose gel and colonies which carried the appropriate insert were picked and inoculated in 5 ml of LB medium with ampicillin. The tubes were incubated at 37°C and 120 rpm for 18 hours.

3.3.6 Plasmid DNA extraction

Bacterial plasmids were extracted using the PureYield™ Plasmid Miniprep System (Promega). All centrifugations were performed at room temperature and maximum speed. The bacterial culture was spun down in a 2 ml Eppendorf tube and resuspended in 600 µl Milli-Q H_2O. 100 µl Cell Lysis Buffer were added and the tube inverted for 10 times. Then, 350 µl cold Neutralisation Buffer were added and the tube inverted for 10 times. The mixture was centrifuged for 3 min, the supernatant transferred to the provided column which was centrifuged again for 30 sec. The flow-through was discarded, 200 µl Endotoxin Removal Buffer added and centrifuged for 30 sec, followed by addition of 400 µl Column Wash Solution and centrifugation for 30 sec. The flow-through was discarded and the column was centrifuged for 1 min to remove remaining ethanol. The Elution Buffer was heated to 65°C, 30 µl added to the column which was incubated for 2 min at room temperature and centrifuged for 1 min. Concentrations were determined with NanoDrop-One and the plasmids were sent for sequencing to GENEWIZ®, Leipzig, Germany. The mix for sequencing contained 30 – 100 ng plasmid, 2.5 µl 10 µM T7 or SP6 primer and nuclease-free water in a total reaction of 10 µl.

3.3.7 Probe Synthesis

Sequencing results revealed the orientation of the fragment within the vector. Next, the antisense RNA probe had to be synthesised. Therefore, the M13 fragment was amplified from the vector, containing the probe fragment flanked by an SP6 and a T7 promoter site. The PCR was performed using ExTaq Polymerase (TaKaRa) and M13 forward and reverse primers (see protocol above in section *Polymerase Chain Reaction*). The PCR product was purified with the Nucleospin® Gel and PCR Clean Up kit (Macherey & Nagel) and concentrations measured with NanoDrop-One. Afterwards, it was used as a template to synthesise the RNA probe using either the SP6 or T7 MEGAscript kit (Invitrogen),

depending on the antisense orientation of the fragment. The protocol was as following: 1 µg M13 PCR template, 1 µl Polymerase Mix, 1 µl 10x Reaction Buffer, 1 µl DIG RNA Labelling Mix (Merck)/1 µl DNP-labelled uridine (Perkin Elmer) and filled up to 10 µl with nuclease-free water (Invitrogen). This mix was incubated at 37°C for 5 hours. To remove remaining DNA 1 µl of TURBO DNase (Invitrogen) was added and incubated at 37°C for 20 min. RNA was precipitated with 15 µl of 7.5 M LiCl and 15 µl of nuclease-free H_2O, incubated at -20°C overnight. Next, RNA was spun down at 4°C and 13.000 rpm for 30 min. The pellet was washed with 500 µl 70% ethanol and again spun down at 4°C and 13.000 rpm for 7 min. Ethanol was removed and the pellet was air-dried for 20 min at room temperature. RNA was dissolved in 20 µl of nuclease-free water (Invitrogen), its concentration measured with NanoDrop-One and then dissolved with 1 volume of deionised formamide. In addition, RNA purity was checked with gel-electrophoresis. The RNA probes were stored at -80°C.

3.4 Whole mount *in-situ*-hybridisation (ISH)

Fixed animals were rehydrated in a 75%/50%/25% series of methanol in PTw in 5 min washes, followed by 3 washes for 5 min in PTw. Animals older than 12 hpf were transferred to baskets and treated with 10 µg/ml Proteinase K (Sigma Aldrich) in PTw for 5 min. The enzyme got inactivated by 2 washes with 4 mg/ml glycine in PTw for 5 min each. Animals younger than 12 hpf were added at the second glycine wash. Next, animals were washed in 1% triethanolamine in PTw, 0.25% acetic anhydride in 1% triethanolamine in PTw and 0.5% acetic anhydride in 1% triethanolamine in Ptw, each for 5 min. This was followed by three 5 min washes in Ptw, refixation in 3.7% formaldehyde in PTw for 30 min and 5 Ptw washes for 5 min. Refixation and the 5 PTw washes were performed on a horizontal shaker at 30 rpm. Baskets were transferred into an Eppendorf tube rack containing 300 µl Hybridisation Buffer (+) for pre-hybridisation. The tube rack was sealed with plastic and aluminium foil, sealed in a plastic bag, and incubated in a 60°C water bath overnight for 18 hours. RNA probes were diluted to 0.4 – 2 ng/µl in 300 µl Hybridisation Buffer (+), denatured at 95°C for 5 min (+) and added to the tubes, resulting in a total volume of 600 µl with 0.2 – 1 ng/µl RNA probe. The rack was incubated in the 60°C water bath for 70 hours.

After hybridisation, baskets were washed in Hybridisation Buffer (-) for 5 min followed by a 75%/50%/25% gradient of Hybridisation Buffer (-) in 2x SSCT, each for 30 min and at 60°C. Afterwards, 60°C washes in 2x SSCT for 30 min, 0.2x SSCT for 20 min and twice 0.1x SSCT for 20 min were carried out. On the horizontal shaker (30 rpm) at room temperature baskets were washed in a 75%/50%/25% gradient with 0.1x SSCT in PTw, each for 10 min, followed by 2 5 min PTw washes.

For blocking, animals were washed in 0.05% Blocking Solution (Sigma Aldrich) in 1x MAB/Ptw (50/50 v/v) for 5 min and blocked in 0.05% Blocking Solution in 1x MAB for 2 hours. Primary antibody

incubation was performed with anti-DIG-AP (Merck) diluted 1:4000 in 0.05% Blocking Solution in 1x MAB overnight at 4°C.

Next day, animals were washed 10 times with PTx-BSA for 15 min each. Then, 3 times with NTMT. First for 1 min, then twice for 10 min. Animals were kept in NTMT overnight at 4°C. NTMT was exchanged with staining solution (NBT/BCIP (Merck) 1:50 in NTMT), the staining was developed and monitored at a stereomicroscope. When the staining was deemed sufficient, the reaction was stopped with NTMT washes. Background was removed with an ethanol gradient (25%/50%/75%) and incubation in 100% ethanol until staining was satisfying.

Animals were mounted onto glass slides and imaged on a Nikon eclipse E800 compound microscope. Pictures were taken using the Nikon Digital Sight DSU3 camera and the NIS-Elements 5.11 software.

3.5 Double fluorescence *in-situ*-hybridisation (dFISH)

dFISH allows the visualisation and localisation of two different mRNAs in one animal. This is based on two types of RNA probes: DIG- and DNP-labelled probes. This allows detection with different antibodies and staining with different fluorophores.

Fixed animals were bleached in 2% H_2O_2 in methanol. Next steps until blocking were performed according to the whole mount *in-situ*-hybridisation. For blocking, animals were washed 4 times for 5 min in TNTw and incubated for 1 hour in TNB at room temperature. Then1:100 anti-DIG-POD (Merck) in TNB was added and the samples incubated at 4°C overnight. 10 15min washes with TNTx followed and samples were stained with 1:50 Cyanine 3 in 1x Amplification Solution (Akoya Biosciences) for 40 min. All further steps were carried out in the dark. Next, animals were washed twice with TNTw and once with PTw for 5 min each. Enzyme activity was stopped with 0.1 M glycine in H_2O with 0.1% Tween, pH 2, for 10 min. 3 washes with TNTw for 5 min followed and samples were incubated with 0.5% TNB for 1 hour at room temperature. The second antibody – 1:100 anti-DNP-HRP (Akoya Biosciences) in TNB – was added and samples incubated at 4°C overnight. Afterwards, 10 washes for 15 min with TNTx followed and the second staining was developed with 1:50 Fluorescein in 1x Amplification Solution (Akoya Biosciences) for 40 min. Animals were washed twice with TNTx and once with PTx for 5 min each. Nuclear staining was performed for 30 min with 1:1000 DAPI (Thermo Fisher) in PTx. Samples were washed twice with PTx for 10 min and mounted in ProLong Gold with DAPI onto glass slides. Images were taken on an Olympus FV3000 Confocal Laser Scanning Microscope with the FV31S-SW software.

3.6 Fluorescence *in situ* hybridisation + antibody staining

In this study fluorescence *in situ* hybridisation (FISH) of one gene was combined with an antibody staining in *NvElav1::NTR-Cerulean* animals. The fluorescent protein was fused to a cytoplasmic nitroreductase and its expression is driven by the *NvElav1* promoter (Richards & Rentzsch, 2014). Thus, it can be found out whether *NvElav1::NTR-Cerulean*$^{+}$ cells express the genes of interest (GOI).

FISH was performed according to the protocol above until the first blocking for the first antibody was completed. Then, samples were incubated with 1:100 anti-DIG-POD (Merck) + 1:250 rabbit anti-GFP (Abcam) in TNB over night at 4°C. The next day, animals were washed 10 times for 15 min in TNTx. The staining for the RNA probes was developed with 1:50 Cyanine 3 in 1x Amplification Solution (Akoya Biosciences) for 40 min, followed by 2 wases with TNTw and 1 wash with PBT for 5 min each. Enzyme activity was stopped with 0.1 M glycine in H_2O with 0.1% Tween, pH 2, for 10 min. 3 washes with TNT for 5 min each followed.

Afterwards, three 5 min and three 30 min washes with PTx-BSA were performed and samples were blocked for 30 min in 5% Natural Goat Serum (NGS) in PTx-BSA. The goat-anti-rabbit secondary antibody was added 1:200 in PBTx-BSA-NGS and incubated over night at 4°C. Then, animals were washed 5 times for 5 min and 3 times for 30 min in PTx-BSA. Nuclear staining was performed with 1:100 DAPI in PBTx. Two final washes with PTx for 10 min were performed and samples mounted in ProLong Gold with DAPI. Images were taken on an Olympus FV3000 Confocal Laser Scanning Microscope with the FV31S-SW software.

3.7 Synthesis and injection of transgenesis vectors

In this work one type of transgenesis vector was produced: A vector containing the promoter region of the gene of interest (GOI) driving the expression of membrane-targeted Green Fluorescent Protein (mGFP). Regulatory sequences were identified based on the histone modifications H3K36me3, H3K27Ac, H3K4me3, H3K4me2 and p300-ChIP-seq data (Schwaiger, et al., 2014) and their DNA sequences extracted from http://genomebeta-evo.zoo.univie.ac.at/index.html.

3.7.1 Polymerase Chain Reaction

Putative regulatory regions were amplified from whole genomic DNA (gDNA) in a PCR using Q5® Polymerase (NEB, 2 U/ml). As well the backbone for the transgenesis vector was amplified from an existing vector. The reaction was set up as following: 5 µl of 5x Q5® Reaction Buffer, 0.5 µl 10 mM dNTPs, 0.5 µl of each 10 µM forward and reverse primer, 0.25 µl of Q5® DNA polymerase, 1 µl of gDNA and 17.25 µl nuclease-free H_2O. The temperature protocol was initial denaturation at 98°C for 1 min; 40 cycles of denaturation at 98°C for 10 sec, primer annealing at the temperature according to section *Primers and Oligonucleotides* for 30 sec, elongation at 72°C for 1 min/ kb; final elongation at 72°C for

2 min and hold at 4°C. Reactions were carried out in 8 replicates increasing the amount of the amplicon and therefore concentration after purification.

3.7.2 Purification of gel excised fragments

Finished PCR reactions were pooled, loaded onto a 0.8% agarose gel, excised, and purified with the Nucleospin PCR and Gel Clean Up Kit (Macherey & Nagel). All centrifugation steps were performed at 11.000 g at room temperature. 200 µl of NT1 Buffer were added to 100 mg of excised gel and incubated at 55°C for 10 min, vortexed every 2-3 min, until the gel piece was dissolved. The mixture was added to the provided silica membranes, centrifuged for 30 sec and the flow-through discarded. Then, 2 rounds of washing followed, adding 400 µl of NT3 Buffer and centrifugating for 30 sec. To remove remaining ethanol, a dry centrifugation for 1 min was carried out. The spin column was transferred to a 1.5 ml Eppendorf tube and 20 µl Elution Buffer added which was heated to 70°C. The tube was incubated at 70°C for 5 min, centrifuged for 1 min at 100 g, then for 1 min at 11.000 g. This was repeated with 10 µl Elution Buffer. Afterwards, concentrations and purity were measured with Nanodrop-One.

3.7.3 Gibson Assembly® Ligation

After vector backbones and putative promoter regions were purified, they were ligated using the Gibson Assembly® method (Gibson et al., 2009). It is based on three enzymes: a 5' exonuclease that generates long overhangs, so insert and backbone can hybridize; a polymerase fills the gaps again; a ligase is conjugating the fragments.

Therefore, for each assembly three reactions were performed: insert and backbone were mixed in a 1:1 and 3:1 molar ratio, and as a negative control the backbone alone was used, which should not be ligated together in the reaction. 5 µl 2x Gibson Assembly® Master Mix (NEB) were added and nuclease-free water (Invitrogen) to a total of 10 µl. Tubes were incubated at 50°C for 30 min and 3 µl added to 66 µl of competent bacterial cells. Transformation was performed as described in section Ligation and Transformation, instead that for 66 µl of bacteria 200 µl of SOC medium (Invitrogen) were added. All further steps from Colony PCR, Miniprep to Sequencing were performed as described above.

3.7.4 Injection of transgenesis plasmids into *N. vectensis* zygotes

Freshly laid eggs from *N. vectensis* were fertilised at 18°C to prolong the time until eggs start dividing. The jelly was removed at room temperature as described above (see section ***3.1 Animals***). The injection set-up consisted of a Nikon Eclipse TE2000-U inverted fluorescence microscope, a holding capillary attached to CellTram Vario oilpump and an injection needle connected to an Eppendorf FemtoJet 4i. Capillary and needle were under control of micromanipulators.

Prior to injecting, plasmids had to be digested with the I-SceI restriction enzyme (5 U/µl, NEB) in the following reaction: 1 µl of restriction enzyme, 1 µl of 10x Cut Smart Buffer (NEB), 200 ng plasmid, 5 µl of dextran MW10.000 coupled to Alexa 568 (Invitrogen), filled up to 10 µl with nuclease-free water (Invitrogen). The reaction was incubated at 37°C for 30 min prior to injection. Approximately 500-600 animals were injected per plasmid. As a control, un-injected WT animals were kept. Afterwards, the remaining injection mix was loaded onto a 1% agarose gel to ensure correct digestion.

3.8 Synthesis and injection of sgRNAs for CRISPR/Cas9 mediated mutagenesis

3.8.1 sgRNA design

Genomic regions of the GOIs were extracted from the Vienna Genome Browser and via the Chop Chop website multiple sgRNAs were suggested. Oligonucleotides with a length of 20 nt were picked according to their efficiency and abundance of mismatches. The 3' NGG was removed as well a 5' G was added if necessary. A T7 promoter sequence (TTCTAATACGACTCACTATA) was added to the 5' end and a 14 nt long overlapping sequence (GTTTTAGAGCTAGA) to the 3' end.

3.8.2 Synthesis of sgRNAs

Using the EnGen® sgRNA Synthesis Kit (NEB) sgRNAs were synthesised as following: 1 µl nuclease free water, 5 µl EnGen® 2x sgRNA Reaction Mix, *S. pyogenes*, 2.5 µl of the 1 µM target specific oligo, 0.5 µl of 0.1 M DTT and 1 µl of EnGen® sgRNA Enzyme Mix – 10 µl in total. This reaction was incubated at 37°C for at least 1 h. Then, 15 µl nuclease-free water (Invitrogen) and 1 µl DNase I was added and incubated at 37°C for 15 min. 26 µl of 7.5 M LiCl were added and the mix was incubated at -20°C for at least 1 h. The precipitated RNA was spun down at 4°C for 15 min at 13.000 rpm, the pellet washed with 500 µl 70% ethanol and again centrifuged for 7 min with the same settings. Ethanol was removed and the pellet allowed to dry for 20 min. It was dissolved in 10 µl nuclease-free water (Invitrogen) and concentrations were measured with Nanodrop. sgRNAs were stored at -80°C.

3.8.3 Injection of sgRNAs

Eggs were prepared and the same injection setup was used as described above in section ***3.7.4. Injection of transgenesis plasmids into N. vectensis zygotes***.

One injection mix contained 450 ng of sgRNA, 1.8 µl Cas9 protein in xx, 1µl of Dextran Alexa 488 in 1.1 M KCl. The injection mix was activated at 37°C for 5 min prior to injection. Approximately 300 animals were injected per sgRNA. As a control, un-injected WT were kept.

3.9 shRNA synthesis

3.9.1 shRNA design

Open reading frames were extracted from the Vienna Genome Browser and pasted into the InvivoGen siRNA website. Motif size was set to 19 nt, everything else was set with default values. From the resulting list 3 sites were chosen, in the middle of the coding sequence and close to the 3'- and 5'-end. Sense and antisense sequences were extracted and a T7 promoter added to the 5' end. Primers for qPCR were synthesised as well, generating a fragment of about 100 nt containing the shRNA target site.

3.9.2 Synthesis of shRNAs

2 µl of each sense and antisense oligos (100 µM) were mixed with 16 µl nuclease-free water and heated to 98°C on a Thermo Mixer C (Eppendorf) for 2 min. The heating was turned off and the samples allowed to cool down to 37°C. shRNAs were transcribed using the AmpliScribe T7 kit (Lucigen) in the following reaction: 2.75 µl of the oligo mix, 1 µl of each NTP (ATP, UTP, CTP, GTP), 1 µl of T7 polymerase, 1 µl of 10x Reaction Buffer, 1µl of 0.1 M DTT and 0.25 µl of Riboguard, an RNase inhibitor. The mix was incubated at 37°C for 5 hours. Next, 0.5 µl of RNase-free DNase was added and again incubated at 37°C for 30 min. 39 µl of nuclease-free water (Invitrogen) was added and RNA was extracted with the RNA Clean and Concentrator kit (Zymo Research).

All following centrifugations were carried out at room temperature for 30 sec at 16.000 g, unless indicated otherwise. 2x volume of RNA binding buffer were added and mixed by pipetting. An equal volume of absolute ethanol was added and the solution was mixed by pipetting. The content was transferred to a Zymo-Spin™ IICR Column3 in a Collection Tube and got centrifuged. The flow-through was discarded, 400 µl of RNA Prep Buffer were added to the column, spun down and the flow-through discarded. The same followed with 700 µl of RNA Wash Buffer. Using 400 µl RNA Wash Buffer the second time, it got spun down for 1 min. One round of dry centrifugation followed. The column was transferred to a 1.5 ml Eppendorf tube and incubated for 5 min with 25 µl DNase-/RNase-free Water. RNA was eluted for 1 min at full speed. Finally, concentrations were measured with NanoDrop-One and shRNAs were stored at -80°C.

3.9.3 Injection of shRNAs

Eggs were prepared and the same injection setup was used as described above in section ***3.7.4 Injection of transgenesis plasmids into N. vectensis zygotes***.

The injection mix contained 900 ng of shRNA, 2 µl of Dextrane, Alexa 488 in 1.1 M KCl, filled up to 4 µl with nuclease-free water (Invitrogen). shRNAs could be directly injected. As a control, a scrambled

shRNA for GFP was used. Approximately 250 animals were injected per shRNA. Animals were kept for 24 hpf and their RNA was extracted.

3.10 gDNA extraction

To test the efficiency of sgRNAs, gDNA of injected animals was extracted and analysed with melt curves. Animals injected with sgRNAs were raised for 2 weeks. From 300 injected animals 8 polyps were taken to test the sgRNA. First, genomic DNA had to be extracted. Therefore, individuals were put into PCR tubes, 200 µl of absolute ethanol added, vortexed and incubated for 5 min at room temperature. Animals were spun down shortly and almost the whole ethanol removed. Tubes were put into a 55°C heat block for 45 min with the lid open, thus ethanol can fully evaporate. Proteinase K (Sigma Aldrich) was added to the Extraction Buffer with a final concentration of 50 ng/µl. 50 µl of this was added to one individual and it was incubated in the thermocycler at 60°C for 1 h digestion and at 75°C for 15 min proteinase K inactivation. The debris was spun down, and the supernatant could be used for further experiments.

3.11 Melt curve analysis

In a melt curve analysis, a fragment containing the sgRNA target site was amplified from gDNA. First, a PCR containing EvaGreen, a double-stranded DNA binding fluorophore, was carried out. After the PCR, a temperature gradient protocol to generate melt curves was set up. During the temperature gradient in the thermocycler DNA denatures and becomes single-stranded thereby releasing the fluorophore and causing its fluorescence to cease, what is captured with a detector and a melt curve is generated. Mutants carrying point mutations, insertions or deletions have a different melt curve, since those modifications cause different base pairs with different binding affinities, and longer or shorter sequences, respectively, in comparison to WT DNA.

Melt curve PCR was performed in the Mastercycler Nexus GSX1 (Eppendorf) and mixed as following: 1 µl of gDNA was added to 14 µl Q5 reaction mix (NEB), which contained 3 µl of 5x Q5 Reaction Buffer, 0.375 µl 10 mM dNTPs, 0.5 µl of each forward and reverse primer, 0.125 µl of Q5 Polymerase, 0.75 µl EvaGreen (Biotium) and 8.75 µl of nuclease-free water (Invitrogen). The temperature protocol was initial denaturation at 98°C for 1 min; 40 cycles of 10 sec denaturation at 98°C, 30 sec primer annealing at 60°C and 30 sec elongation at 72°C; 2 min final elongation at 72°C; hold on 4°C.

Tubes were transferred to the C1000 Thermocycler (BioRad) in which the melt curve protocol was performed. It started at 95°C for 3 min, followed by 0.5°C/10 sec increments from 65°C to 95°C, detecting fluorescence every 10 sec.

3.12 RNA isolation and qRT-PCR protocol

At 24 hpf RNA from shRNA-injected animals was isolated and converted to cDNA for qPCR in the following process: Animals were transferred to 1.5 ml Eppendorf tubes (roughly 250 animals per tube). The NM was removed and exchanged with 500 µl TRIzol™ LS Reagent (Ambion). The tube was vortexed until the solution was clear, and all embryos dissolved. On ice, 135 µl chloroform was added, the tube inverted for 3 min and incubated on ice for 7 min. The sample was centrifuged at 4°C, full speed and 15 min. This resulted in three layers, the lower organic layer containing protein and DNA, an intermediate layer rich in lipids and an upper aqueous layer containing RNA. The aqueous layer was transferred to a new tube and mixed with 1x volume of absolute ethanol, which was mixed by pipetting.

The following reagents, columns and tubes were provided by the RNeasy Micro Kit (Qiagen). All centrifugations were performed at room temperature, 30 sec and 8000 g. The mixture was loaded onto a RNeasy MiniElute spin column in a collection tube and centrifuged. Then, 350 µl RW1 buffer was added and centrifuged. 10 µl of DNase (supplied) were mixed with buffer RDD, added, and incubated for 15 min on ice. Again, 350 µl buffer RW1 were added and centrifuged. Columns were put into a new collection tube, 500 µl buffer RPE were added and centrifuged. Next, 500 µl 80% EtOH were added, and it was centrifuged for 2 min at 8000 g. Columns were placed into a new collection tube and centrifuged for 5 min at full speed with an open lid, to allow for EtOH-evaporation. Columns were put into 1.5 ml collection tubes, 14 µl of RNase free water were added and incubated for 5 min. To elute, it was centrifuged for 1 min at 100 g and then 1 min at full speed. RNA concentration and purity were measured with NanoDrop-One and it was ready for reverse transcription. The RNA was stored at -80°C.

cDNA synthesis was performed as described above in the section *cDNA synthesis*. 500 ng of total RNA were used, and Ribonuclease H incubation was omitted. After the reaction, WT cDNA samples from the animals were serially diluted 1:10, 1:100 and 1:1000 and cDNAs from shRNA injected animals were diluted 1:10 for qPCR analysis in a 96-well plate. Each cDNA sample was analyzed in technical duplicates. As a negative control no cDNA was added. The qPCR mix contained 10 µl of QuantiTect® SYBR Green PCR mix (Qiagen), 1 µl of each 10 µM forward and reverse primer, 1 µl of cDNA and 7 µl of nuclease-free water (Invitrogen). The thermocycler protocol was set as: 15 min enzyme activation and initial denaturation at 95°C; 40 cycles of 15 sec denaturation at 94°C, 30 sec primer annealing at 60°C, 30 sec elongation at 72°C and plate read. Afterwards, a melt curve was generated, initiated by 10 sec at 95°C and an increase from 65°C to 95°C by 0.5°C/5 sec.

The obtained ΔCT values were corrected as previously described (Kubista & Sindelka, 2007). Fold-change was calculated relative to Riboprotein mRNA expression with the $2^{-\Delta\Delta C_T}$ method (Livak & Schmittgen, 2001).

3.13 Statistical Analysis

Results are depicted as raw data points showing the mean with standard error. Statistical analysis and data visualisation has been performed in Prism 9.2.0. Data were tested for normality with the Shapiro-Wilk test. For comparisons of data between multiple treated sets and one untreated set One-Way-ANOVA has been performed with Dunnett's correction for multiple testing. To compare only two sets an unpaired *t*-test has been performed. Statistically significant differences are shown with asterisks. *ns = not significant*, *$p < 0.05$, **$p < 0.01$, ***$p < 0.001$ and ****$p < 0.0001$.

3.14 Phylogenetic Analysis

Dscam protein sequences were retrieved using a Standard Protein Blast (blastp) search with the putative NvDscam (isoform 1) against the Reference Proteins (refseq_protein) database on the NCBI website. Retrieved sequences are shown in **table 1**. Dscam sequences should contain 9-10 Immunoglobulin (IG) domains and 5-6 Fibronection Type III (FNIII) domains in their extracellular part. One IG domain must be located between the fourth and fifth FNIII domain. Sequences were aligned with MAFFT 7 (Katoh et al., 2019) using default values except: *Iterative Refinement Methods* was set to G-INS-I, as less than 200 sequences with global homology were used and the *Unalignlevel* was set to 0.4. The resulting multiple sequence alignment was uploaded to the IQ-TREE webserver (CIBIV, Austria) (Nguyen et al., 2015), which conducts a phylogenetic analysis based on maximum likelihood. Default settings remained unchanged except that the *Number of Bootstrap Alignments* was set to 1500, *Maximum Iterations* 1500 and *Approximate Bayes* test was enabled. The tree was visualised on the iTOL website and adapted in Adobe Illustrator.

Table 1: List of sequences used for phylogenetic analysis.

Species name	**Protein**	**NCBI accessoion number**
Acanthaster planci	Dscam	XP_022093108.1
Acropora millepora	Dscam	XP_029186295.1
Actinia tenebrosa	Dscam	XP_031567656.1
Anneissia japonica	Dscam	XP_033114431.1
Asterias rubens	Dscam	XP_033641222.1
Centruroides sculpturatus	Dscam	XP_023221162.1
Danio rerio	Dscam	XP_009289749.1
Danio rerio	Dscam-like	XP_005157552.1
Daphnia magna	Dscam	XP_032784992.1
Dendronephthya gigantea	Dscam	XP_028412683.1
Drosophila melanogaster	Dscam-1	NP_724543.1
Drosophila melanogaster	Dscam-2	NP_729225.2
Drosophila melanogaster	Dscam-3	NP_996226.2
Drosophila melanogaster	Dscam-4	NP_001261571.1
Exaiptasia diaphana	Dscam	XP_020908773.1
Gigantopelta aegis	Dscam	XP_041373248.1
Homarus americanus	Dscam	XP_042239237.1
Homo sapiens	Dscam-1	XP_016883770.1
Homo sapiens	Dscam-2	AAM09558.1
Homo sapiens	Dscam-like-1	AAL57166.1
Homo sapiens	Dscam-like-1a	AAN32613.1
Homo sapiens	Dscam-like-1b	AAN32614.1
Homo sapiens	Neogenin	AAC51287.1
Hydra vulgaris	Dscam	XP_012558399.1
Lingula anatina	Dscam	XP_013381258.1
Lytechinus variegatus	Dscam	XP_041470659.1
Mus musculus	Dscam	XP_006522949.1
Mus musculus	Dscam-like	XP_006510010.1
Mus musculus	Neogenin	AAH54540.1
Nematostella vectensis	Dscam	XP_001626157.2
Nematostella vectensis	Neogenin	AIZ68366.1
Octopus sinensis	Dscam	XP_036359196.1
Orbicella faveolata	Dscam	XP_020603326.1
Parasteatoda tepidariorum	Dscam	XP_015921055.1
Patiria miniata	Dscam	XP_038065481.1
Pecten maximus	Dscam	XP_033758204.1
Pocillopora damicornis	Dscam	XP_027048594.1
Strongylocentrotus purpuratus	Dscam	XP_030832964.1
Xenopus tropicalis	Dscam	XP_031751619.1
Xenopus tropicalis	Dscam-like	XP_004916122.1

4. Results

The aim of this study was to characterise the potential NvNetrin receptors *NvDscam* and *NvNeogenin* by analysing their expression pattern during embryonic development as well as in context with two neuronal markers, *NvSoxB(2)* and *NvElav1*::mOrange. Furthermore, the establishment of transgenic reporter constructs, mutant lines and RNA interference knock downs serves as a basis for future morphological and functional analysis.

4.1 NvNetrin receptors in *Nematostella vectensis*

Using Blastp, Dscam sequences based on *Mus musculus* Dscam (NCBI Accession number EDL03664) were used to search for homologs in the *Nematostella vectensis* genome (Putnam et al., 2007). Criteria for being considered a potential Dscam were the possession of 9 to 10 IG domains, 5 to 6 FNIII domains and one of the IG domains being located between the 4th and 5th FNIII domains. The search resulted in two isoforms X1 and X2 of *NvDscam* (NCBI accession numbers XP_001626157 and XP_032229627, respectively). Isoform X1 contained an additional alanine at position 790. To retrieve the genomic DNA sequence of *NvDscam,* the two candidate sequences were blasted against the *N. vectensis* genome in the Vienna Genome Browser using the BLAT tool; the gene *Nve10272* was identified to encode for *NvDscam*.

The online tool SMART (Letunic et al., 2021; Letunic & Bork, 2018) allows domain predictions based on amino acid sequences. NvDscam was revealed to have a signal peptide at the N-terminus, 9 immunoglobulin (IG) domains, 5 fibronectin type III (FNIII) domains and 1 transmembrane (TM) domain. The intracellular part of the receptor did not contain a predicted domain (**Figure 4.1A**).

For comparison, the *Mus musculus* Dscam also had an N-terminal signal peptide, a TM domain, and 10 IG and 6 FNIII domains. No domains were predicted in the intracellular part (**Figure 4.1A**).

NvNeogenin (*Nve23574*) and *NvUnc-5* (*Nve8320*) were already previously described in *N.vectensis* by *in situ* hybridisation and/or phylogenetic analysis (Leclère & Rentzsch, 2014; Leclère & Rentzsch, 2012).

NvNeogenin had an N-terminal signal peptide, 4 IG and 6 FNIII domains, 1 TM domain, and an intracellular part. Similarly, the *Mus musculus* Neogenin was predicted to contain a signal peptide, 4 IG and 6 FNIII domains, 1 TM domain and an intracellular part, not assigned to any domains (**Figure 4.1B**). Additionally, if allowing SMART to search for domains using the PFAM database, it showed a Neogenin C-terminal domain in the intracellular part (not shown in **Figure 4.1B**).

NvUnc-5 was a potential candidate as a repulsive NvNetrin receptor. However, its domain prediction showed that it does not contain an N-terminal signal peptide, extracellular IGs or Thrombospondin (TSP) domains. The TM domain and 2 of the three known intracellular domains were predicted (Zona

Occludens and Death domain) (**Figure 4.1C**). If allowed to search within the Pfam database SMART predicted the UPA/Dcc binding domain between the Zona Occludens and Death domain (not shown in **Figure 4.1C**). The mouse orthologue showed a signal peptide, 1 IG domain, 2 TSP domains, 1 TM domain and 1 of the three intracellular domains, the DEATH domain (**Figure 4.1C**). Additionally, if allowing SMART to search for domains using the PFAM database, it showed a Zona Occludens-5 and an UPA/Dcc-binding domain (not shown in **Figure 4.1C**).

Taken together, putative sequences for the NvNetrin receptors *NvDscam*, *NvNeogenin* and *NvUnc-5* were found in the genome of *Nematostella vectensis*. Protein prediction revealed an almost identical domain composition in NvDscam and a similar one in NvNeogenin in comparison to the murine proteins. NvUnc-5 did not appear to have a conserved extracellular part.

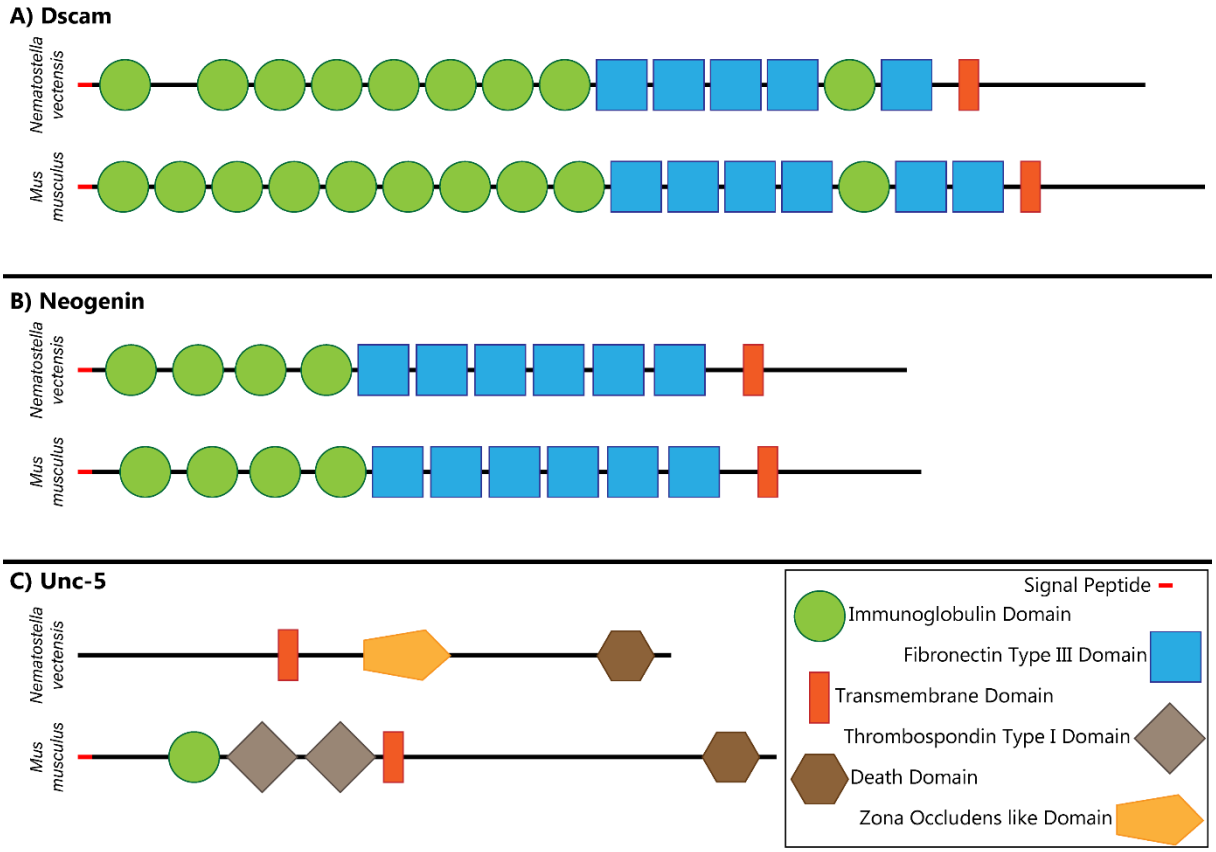

Figure 4.1: Conserved domain composition of Dscam and Neogenin in *Nematostella vectensis* and *Mus musculus*. A) NvDscam showed an N terminal signal peptide, 9 IG and 5 FNIII domains, as well as 1 TM domain. MmDscam contained an N-terminal signal peptide 10 IG and 6 FNIII domains and 1 TM domain. **B)** NvNeogenin and MmNeogenin both showed a signal peptide on the N terminus, 4 IG and 6 FNIII domains and 1 TM domain. **C)** NvUnc-5 did neither contain a signal peptide nor extracellular domains. It had a TM domain and intracellularly 1 ZU5 domain and 1 DEATH domain. MmUnc-5 contained a N-terminal signal peptide, 1 IG domain, 2 TSP domains, 1 TM domain and 1 DEATH domain.

4.2 Phylogenetic analysis revealed the presence of a *NvDscam* orthologue in *N. vectensis*

To determine whether *NvDscam* found in *N. vectensis* is a Dscam orthologue we conducted a phylogenetic analysis. Therefore, a NCBI blast search was performed using the NvDscam protein sequence as the query. Resulting sequences were selected according to the presence of 9 to 10 Immunoglobulin (IG) and 5 to 6 Fibronectin Type III (FNIII) domains. One of the IG domains should be located between the fourth and fifth FNIII domain. The full-length protein sequences were aligned with MAFFT-7 (Katoh et al., 2019) and Maximum likelihood (ML) phylogenetic analysis was performed with IQ-TREE (Nguyen et al., 2015). The resulting tree is depicted in **Figure 4.2**. Neogenin was chosen as the outgroup of the phylogenetic tree since it has a similar domain composition as Dscam, as it contains IG and FNIII domains (**Figure 4.1A & B**). Bootstrap values (0-100%) are estimates for confidence in the tree topology and indicate the support of internal branches. Values above 70% are considered significant (Hillis & Bull, 1993).

Dscam protein sequences were found to be present in Bilateria and Cnidaria. No Dscam protein sequences were found in Ctenophora, Porifera and other unicellular organisms. Within Cnidaria, Dscam was found to be present in Anthozoa and in the hydrozoan *Hydra vulgaris*. For the data available, no other hydrozoans or medusozoas were found to contain Dscam. The tree showed Cnidaria (orange) as the sister group to Bilateria with a confidence of 100%. The Bilateria were split into the four big subgroups: Vertebrata (blue), Echinodermata (green), Lophotrochozoa (violet) and Arthropoda (red).

From our resulting tree, we saw that *NvDscam* found in *N. vectensis* is a Dscam orthologue containing a conserved domain composition. *NvDscam* was found in the clade Cnidaria and the Dscam sequences were well separated from the Neogenin outgroup. The split into Cnidaria and the four bilaterian clades Vertebrata, Echinodermata, Lophotrochozoa and Arthropoda supported the tree model. However, the tree showed that Echinodermata were not a sister group to Vertebrata as would be expected. In this phylogeny, they showed a closer relation to Protostomia than to their deuterostome, vertebrate, neighbours. Furthermore, it could be inferred that gene duplications occurred in the vertebrate and insect lineages. *Danio rerio*, *Xenopus tropicalis* and *Mus musculus* contained two paralogues, Dscam and Dscam-like-1, while *Homo sapiens* showed five Dscam paralogues: Dscam-1, -2, -like-1, -like-1a and -like-1b. This suggested that the last common ancestor of Vertebrata had one *Dscam* and one *Dscam-like* gene. *Drosophila melanogaster* has four paralogues: Dscam-1 to -4. Interestingly, this tree suggested a closer relationship of DmDscam with DmagDscam (*Daphnia magna*) and DmDscam-4 with HaDscam (*Homarus americanus*) than the four DmDscam themselves.

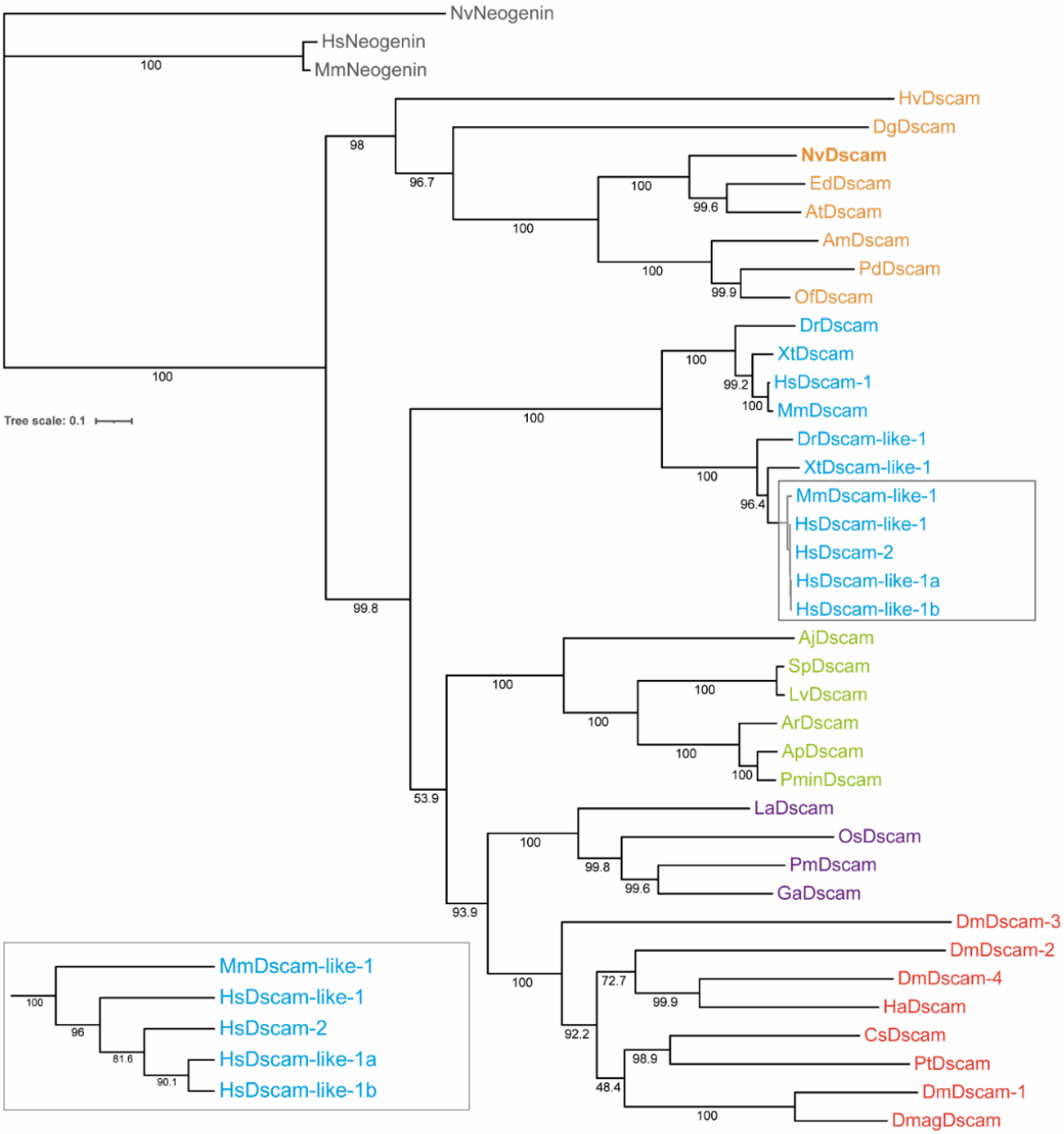

Figure 4.2: Phylogenetic analysis revealed that *NvDscam* in *Nematostella vectensis* is indeed a Dscam orthologue. The phylogeny was based on a maximum likelihood analysis of Dscam full-length amino-acid sequences. 40 sequences were used retrieved from NCBI. Bootstrap values are depicted on the branches. The Tree scale indicates substitutions per site. The box on the lower left shows the clade marked in the tree for an easier visualisation. Branch lengths in the box are random and are not to compare with the actual phylogenetic tree. Colour code: Orange: Cnidaria, blue: Vertebrata, green: Echinodermata, violet: Lophotrochozoa, red: Arthropoda. *Aj … Anneissia japonica, Am … Acropora millepora, Ap … Acanthaster planci, Ar … Asterias rubens, At … Actinia tenebrosa, Cs … Centruroides sculpturatus, Dg … Dendronephthya gigantea, Dm … Drosophila melanogaster, Dmag … Daphnia magna, Dr … Danio rerio, Ed … Exaiptasia diaphana, Ga … Gigantopelta aegis, Ha … Homarus americanus, Hs … Homo sapiens, Hv … Hydra vulgaris, La … Lingula anatine, Lv … Lytechinus variegatus, Mm … Mus musculus, Nv … Nematostella vectensis, Of … Orbicella faveolata, Os … Octopus sinensis, Pd … Pocillopora damicornis, Pm … Pecten maximus, Pmin … Patiria miniate, Pt … Parasteatoda tepidariorum, Sp … Strongylocentrotus purpuratus, Xt … Xenopus tropicalis*.

Taken together, the phylogenetic tree generated in this study showed that the predicted sequence of NvDscam was well grouped within the Cnidaria, suggesting a well-preserved sequence homology at the protein level as the Dscam sequences separated from the Neogenin sequences. Thus, the presence of a *NvDscam* orthologue in *N. vectensis* was confirmed. The tree clearly separated the five taxa Cnidaria, Vertebrata, Echinodermata, Lophotrochozoa and Arthropoda, which supported the

reliability. It also showed Cnidaria as the sister group to Bilateria. However, the position of Echinodermata in this tree not as a sister group to Vertebrata was inconsistent with their phylogenetic position (Dunn et al., 2014; Telford et al., 2015). Low bootstrap values within the Arthropoda showed some uncertainties in the separation, which may be caused by poorly aligned sequences or poor sequence conservation.

4.3 *NvDscam* and *NvNeogenin* were upregulated in *NvElav1*::mOrange and *NvSoxB(2)*::mOrange positive cells

To obtain first insights into the expression profiles of putative NvNetrin receptors, we analysed RNA-sequencing data from four transgenic reporter lines, which was already available. The reporter lines contained mOrange whose expression is under control of promoters which are specific for progenitor cells (*NvSoxB(2)::mOrange*), ganglion cells and sensory neurons (*NvElav1::mOrange*), sensory neurons (*NvFoxQ2d::mOrange*), and cnidocytes (*NvNcol3::mOrange*) (Busengdal & Rentzsch, 2017; Nakanishi et al., 2012; Richards & Rentzsch, 2014; Sunagar et al., 2018). This data was generated by dissociating primary polyps, then sorting the dissociated cells with fluorescence-activated cell sorting (FACS) into mOrange-positive and -negative cells, followed by sequencing the bulk-RNA (Kouzel, Gahan and Rentzsch, unpublished data).

Using this previously generated data, we saw that *NvDscam* and *NvNeogenin* were differentially expressed in *NvElav1*::mOrange and *NvSoxB(2)*::mOrange positive cells (**Table 2**). *NvDscam* was expressed almost 14-fold higher in *NvElav1*::mOrange and almost 7-fold higher in *NvSoxB(2)*::mOrange positive cells compared to the respective mOrange-negative cells. *NvNeogenin*-expression was elevated circa 3-fold in *NvElav1*::mOrange and 2.4-fold in *NvSoxB(2)*::mOrange positive cells. The genes did not seem to be differentially expressed in *NvFoxQ2d*::mOrange and *NvNcol3*::mOrange positive cells. No differential expression could be found for *NvUnc-5* in the dataset.

		Gene		
		NvDscam	***NvNeogenin***	***NvUnc-5***
Cell type	***NvElav1***	13.64	2.83	-
	NvSoxB(2)	7.16	2.39	-
	NvFoxQ2d	-	-	-
	NvNcol3	-	-	-

Table 2: Differential expression of *NvDscam* and *NvNeogenin* in *NvElav1*::mOrange and *NvSoxB(2)*::mOrange postive neurons. Values are depicted as the fold change compared to the cells negative for the respective transgenes and are based on bulk RNA sequencing data generated by Kouzel, Gahan and Rentzsch, unpublished data.

Next, the expression patterns of *NvDscam, NvNeogenin* and *NvUnc-5* were determined using colorimetric and fluorescence *in-situ* hybridisation (ISH and FISH, respectively).

4.4 *NvDscam* was expressed in scattered cells during gastrulation and in tentacles later during development

Figure 4.3 shows the expression pattern of *NvDscam* at multiple developmental stages. *NvDscam* was not detected in blastula stage (**Figure 4.3A – A'**). However, a broad staining was present at early gastrula stage, but also in scattered cells within the ectoderm, in the pharynx and in the invaginating endoderm (black arrowheads, **Figure 4.3B – B'**). Similarly, at late gastrula, expression was also seen in scattered cells throughout the ectoderm and in the pharynx (**Figure 4.3C – C')**. In early planula, *NvDscam* was expressed in scattered ectodermal cells in the oral half of the animal (black arrowheads **Figure 4.3D – D'**). By late planula, *NvDscam* expression was confined to the oral pole (**Figure 4.3E – E')** and became more orally restricted at later stages where it was seen at the tip of the developing tentacles of tentacle bud (**Figure 4.3F – F')** and primary polyp stage (**Figure 4.3G – G')**.

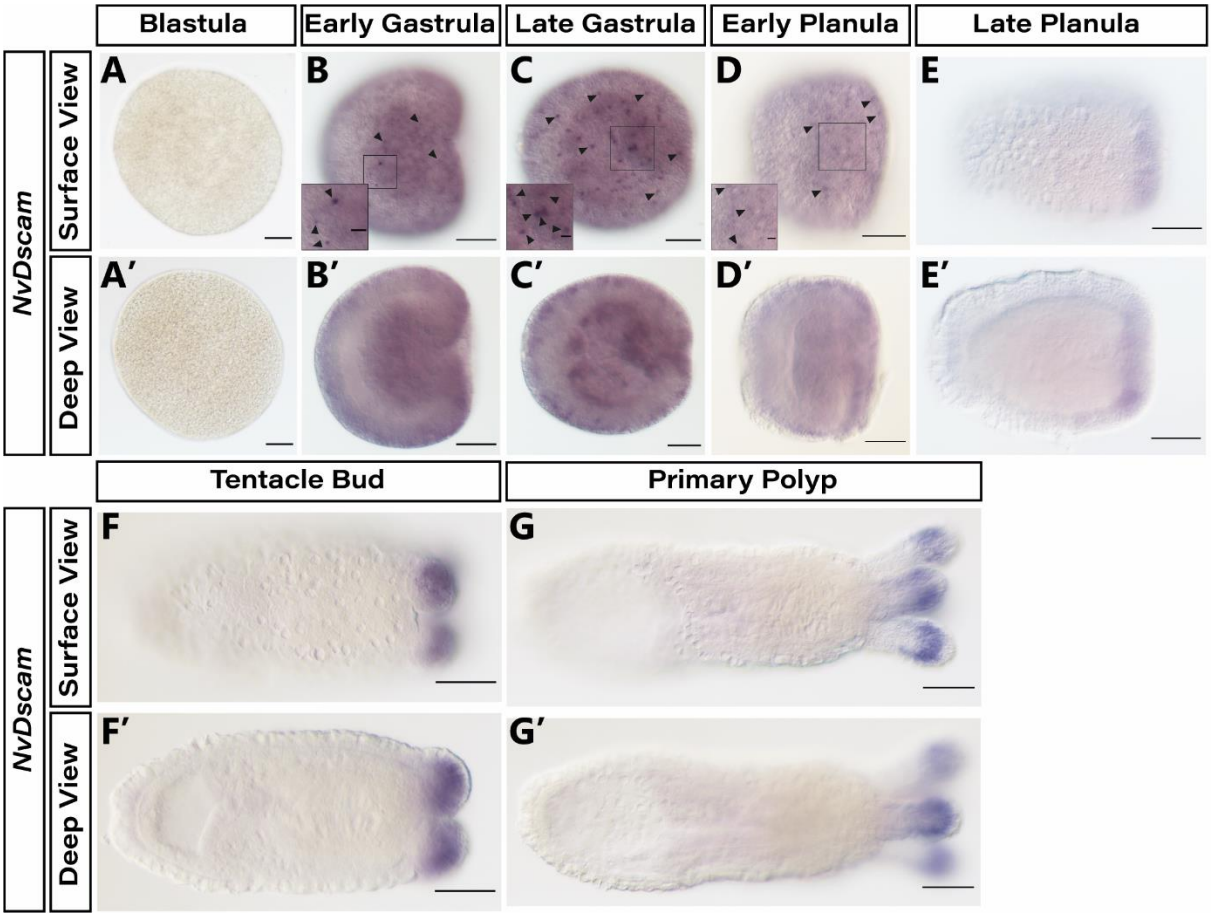

Figure 4.3: *NvDscam* was expressed in scattered ectodermal cells and tentacle tips. Here, representative images of an *in-situ* hybridisation of *NvDscam* is shown. Developmental stages (blastula to primary polyp) are indicated on top, gene name and focus planes on the left. Lateral View shows the surface of the animals; in Deep View the middle of the embryo is in focus. Animals are oriented with the oral side to the right. No *NvDscam* expression could be found at blastula stage (**A – A'**). At early (**B – B'**) and late Gastrula (**C – C'**), it was shown to be strongly expressed in scattered cells in the ectoderm (black arrowheads) and pharynx, but also weakly in the whole embryo. At early planula on (**D – D'**), expression got confined to the oral side and a few cells can be distinguished (black arrowheads). At late planula, expression could be found at the oral pole (**E – E'**). Finally staining was seen in the tentacle tips in tentacle bud (**F – F'**) and primary polyp stage (**G – G'**). **A – E** *n=3*, **F – G** *n=2;* **A – G** 30-50 were used animals per stage; Scale bars represent 50 µm.

4.5 *NvDscam* was co-expressed with *NvSoxB(2)* during gastrulation

The fluorescence *in-situ* hybridisation (FISH) of *NvSoxB(2)* showed that the gene was expressed in scattered ectodermal cells in **figure 4.4B**, **E**, **H**, **K** and this expression pattern matched what was previously described by (Richards & Rentzsch, 2014). Next, a double FISH (dFISH) was performed to determine if *NvDscam* and *NvSoxB(2)* are co-expressed in the same cells (**Figures 4.4**). In early gastrula, *NvDscam* positive cells could be seen in the ectoderm and the majority of these cells co-express *NvSoxB(2)* (**Figure 4.4A – C'**). It was observed that there are more *NvSoxB(2)*$^{+}$ cells not expressing *NvDscam* than vice versa. However, the abundance of co-expressing ectodermal cells seemed to lessen later in gastrulation (**Figure 4.4D – F''**) and in mid planula (**Figure 4.4G – I'**). The representative pictures of the gastrula stages were in oral view, where it cannot be determined if expression is seen at the aboral pole (**Figure 4A – F**). Also at mid planula, *NvDscam* was expressed in single cells in the endoderm with localisations to the oral and aboral endoderm, however we could not detect co-expression with *NvSoxB(2)* (**Supplementary Figure 1A - white arrowheads**).

We next aimed to better characterise the cells expressing *NvDscam*. For this, the *NvElav1::NTR-Cerulean* line was used to perform an immunostaining for Cerulean and a FISH to detect *NvDscam* in tentacle bud stage (**Supplementary Figure 2**). In the *NvElav1::NTR-Cerulean* line, the cytosolic fluorescent protein Cerulean is linked to the protein NTR (Nitroreductase) and labels *NvElav1*::NTR-Cerulean^{+} cells. In contrast to the ISH, the FISH for *NvDscam* showed a broad expression in the whole animal (**Supplementary Figure 2A**). Single cells could be detected at the aboral pole and tentacle tips as well as in the ecto- and endoderm, which are difficult to distinguish from the overall staining. The labelling of *NvElav1*::NTR-Cerulean brought forth the nerve net generated by Cerulean^{+} cells in the endoderm (**Supplementary Figure 2B**). Merging the two signals, one could see that some distinguishable *NvDscam*$^{+}$ cells are also expressing *NvElav1*::NTR-Cerulean (**Supplementary Figure 2C & A' – C'**). Overall, it was difficult to conclude a clear co-staining in this experiment. It suggested, that *NvElav1*::NTR-Cerulean^{+} cells express *NvDscam* in the endoderm, however, this should be confirmed by repeating the experiment with adapted settings.

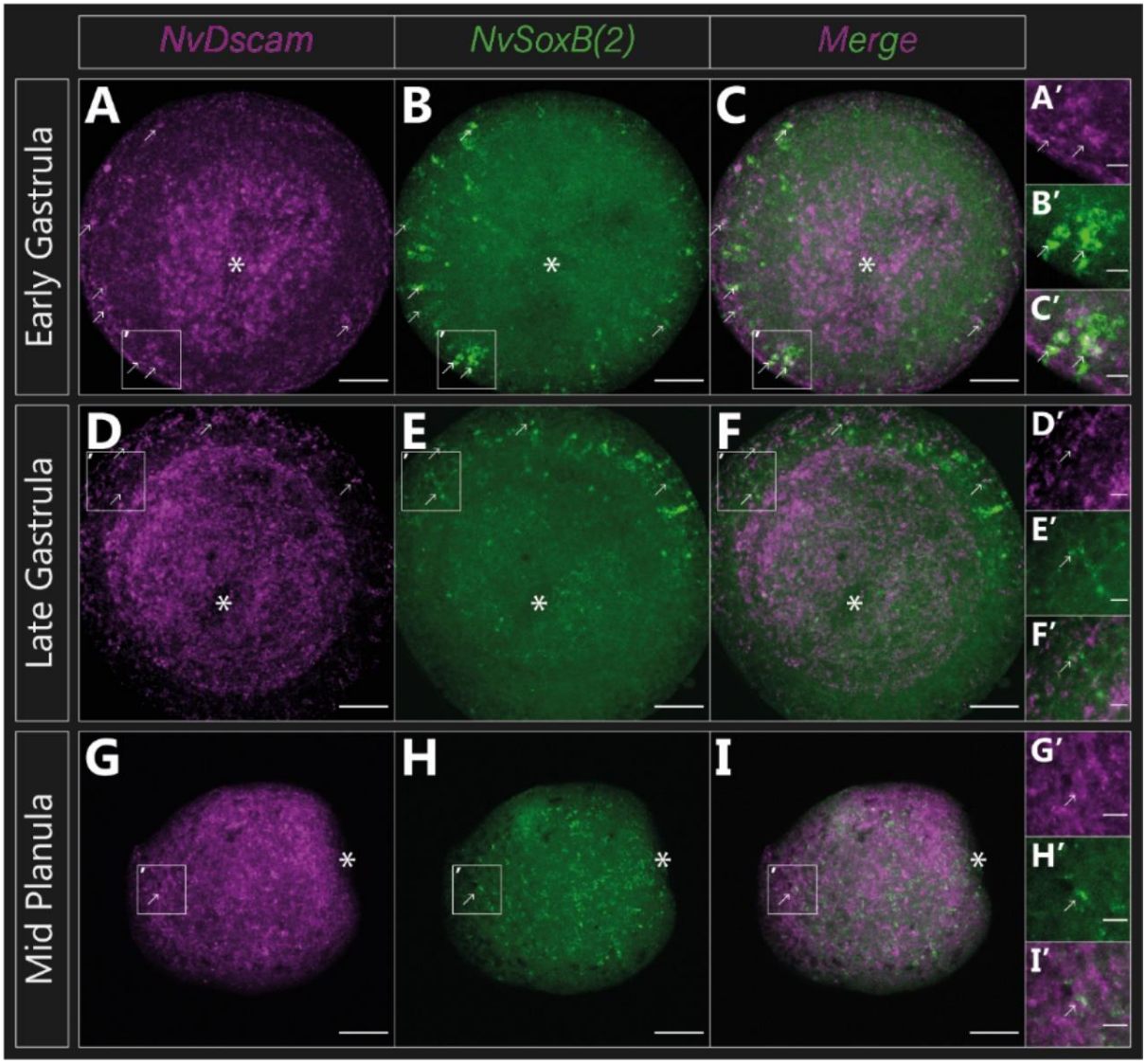

Figure 4.4: *NvDscam* was co-expressed with *NvSoxB(2)* during gastrulation. This graph shows a double fluorescence *in-situ* hybridisation of *NvDscam* (**A, D, G**) and the neural progenitor marker *NvSoxB(2)* (**B, E, H**), which is indicated by panels on the top. Panels to the left show developmental stages. Panels to the right marked with ' are enlargements of the region marked by the box (**A' – I'**). **A)** *NvDscam* was expressed in the whole animal in Early Gastrula. Cells could be seen in the ectoderm and endodermal plate. Panel **B** shows *NvSoxB(2)* expression in scattered cells in the ectoderm. The merge of the signals in **C** showed colocalization of *NvDscam* and *NvSoxB(2)* in the ectodermal cells (white arrows, **A' – C'**). In Late Gastrula *NvDscam* was broadly expressed in the endoderm and in single cells in the ectoderm (**D**). The scattered *NvSoxB(2)*$^{+}$ cells in the ectoderm were also present (**E**). The merge (**F**) revealed colocalization of *NvDscam* with *NvSoxB(2)* in some cells (white arrows, **D' – F'**). *NvDscam* was detected broadly on the surface of Mid Planula (**G**) as well as *NvSoxB(2)* (**H**); single cells could be detected in both, however co-expression was scarce (white arrows, **G' – I'**). Representative images show one confocal section, except **J – L** which are stacks of eight sections. Asterisks indicate the oral opening. Scale bars: 50 µm (**A – L**), 10 µm (**A' – I''**). *n=2*, 30-50 animals per stage

4.6 *NvNeogenin* was predominantly expressed in the endoderm

In **figure 4.5** the expression pattern of *NvNeogenin* is depicted. Expression could not be detected at blastula stage (**Figure 4.5A – A'**). In early gastrula the gene was shown in scattered ectodermal cells and in the invaginating endoderm (**Figure 4.5B – B'**). The staining in scattered cells was no longer visible in late gastrula. However, expression could be found on the oral side, in the pharynx, endoderm and aboral pole (**Figure 4.5C – C'**). A similar pattern was shown in early planula with a strong expression in the endoderm, pharynx and aboral pole (**Figure 4.5D – D'**). In the ectoderm more *NvNeogenin*

expressing cells could be detected from the aboral pole to the middle of the embryo (black arrowheads, **Figure 4.5D'**). In mid-planula expression was decreasing and single cells could be detected in the endoderm, but not in the ectoderm (**Figure 4.5E – E'**). Those endodermal single cells remained in late planula, with stronger staining in the aboral and oral endoderm (black arrowheads, **Figure 4.5F – F'**). In tentacle bud stage *NvNeogenin* seemed to be more broadly expressed in the endoderm, showing single cells and stronger signals in aboral and oral endoderm (black arrowheads, **Figure 4.5G – G'**). In addition, long neurites could be found in the endoderm that seem to be located along the mesenteries (white arrowheads, **Figure 4.5G'**).

Overall, expression started at gastrulation with a broad pattern in ectodermal cells and in the developing endoderm (later forming pharynx and endoderm), also the aboral pole. Then, it became more and more restricted to scattered cells in the endoderm.

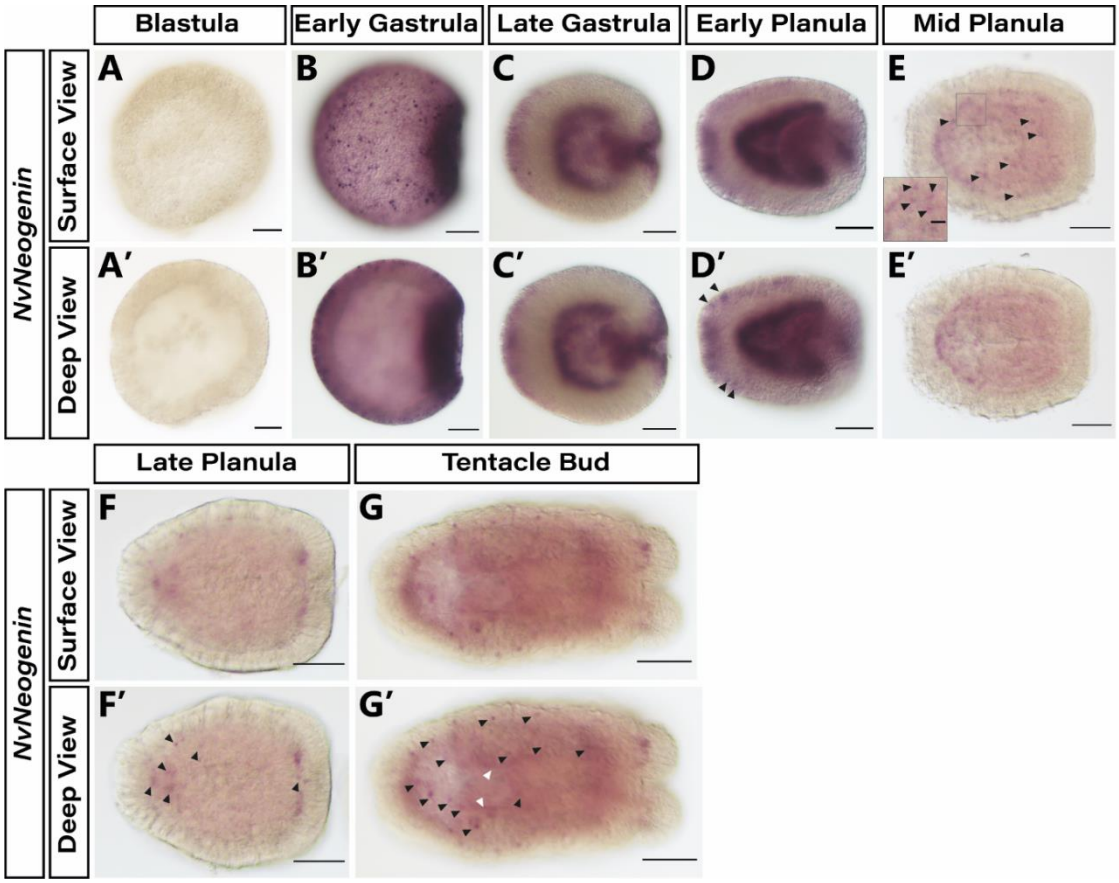

Figure 4.5: *NvNeogenin* was expressed in the endoderm throughout development. An *in-situ* hybridsiation of *NvNeogenin* is shown. Developmental stages (blastula to tentacle bud) are indicated on top, the gene name and focus planes on the left. Lateral View shows the surface of the animals; in Deep View the middle of the embryo is in focus. Animals are oriented with the oral side to the right. No *NvNeogenin* expression was found in blastula stage (**A – A'**), however, from early gastrula on in scattered ectodermal cells and in the endodermal plate (**B – B'**). In late gastrula *NvNeogenin* could be detected on the oral side, in the pharynx, endoderm and the aboral pole (**C – C'**), which was also seen in early planula (**D – D'**) but having more ectodermal cells closer to the aboral side (black arrowheads, **D'**). From mid planula on expression faded and could be detected in scattered endodermal cells (black arrowheads, **E – E'**). In late planula staining was stronger in the aboral and oral endoderm and scattered cells remain in the endoderm (black arrowheads, **F – F'**). At tentacle bud stage an overall endodermal staining could be seen, and single cells were detected in the endoderm and ectoderm (black arrowheads, **G – G'**). Also, longitudinal neurites were visible at tentacle bud stage, which went along the mesenteries (white arowheads, **G'**). **A – E** *n=3*, **F – G** *n=2;* **A – G** 30-50 were used animals per stage; Scale bars represent 50 µm.

4.7 *NvNeogenin* was partially co-expressed with the progenitor marker *NvSoxB(2)*

Again, to characterise the identity of *NvNeogenin*-positive cells a dFISH with *NvSoxB(2)* had been performed as well as a FISH and a co-staining of *NvElav1*::NTR-Cerulean.

In early gastrula, all cells seemed to express *NvNeogenin* (**Figure 4.6A**). Cells that could be distinguished with a stronger staining were termed *NvNeogenin*-high cells. *NvNeogenin*-high cells in the endoderm co-expressed *NvSoxB(2)* (**Figure 4.6A – C'**). Moreover, co-expression could be found in ectodermal cells as well (**Figure 4.6A' – C'**). In late gastrula, few cells could be found that co-express *NvNeogenin* and *NvSoxB(2)* (**Figure 4.6D – F**), for instance, one cell in the ectoderm and two in the endoderm (**Figure 4.6D' – F'**). Interestingly, in mid planula *NvNeogenin* positive cells in the aboral ectoderm co-expressed *NvSoxB(2)* (**Figure 4.6G – H'**). Overall, *NvNeogenin*-high cells were co-expressing *NvSoxB(2)* during gastrulation, which can hint to a progenitor-like identity. Since there were also *NvNeogenin*-positive cells that were not co-labelled with *NvSoxB(2)*, they might have originated from other progenitors or the cells start expressing *NvNeogenin* after *NvSoxB(2)* expression stopped.

FISH of *NvNeogenin* at tentacle bud stage showed that the gene was widely expressed throughout the ectoderm and endoderm, as well as in the aboral pole and developing tentacle buds (**Supplementary Figure 3A**). Single cells could not be discerned in the overall staining. Labelling of *NvElav1*::NTR-Cerulean revealed the nerve net made up by Cerulean^{+} neurons (**Supplementary Figure 3B**). In the merge of *NvNeogenin* and *NvElav1*::NTR-Cerulean overlapping signals of Cerulean^{+} neurons and the broad *NvNeogenin* staining could be found (**Supplementary Figure 3C & A' – C'**). However, a clear distinction of *NvNeogenin*$^{+}$ cells could not be made. Also, it could not be excluded that *NvNeogenin* was expressed by *NvElav1*::NTR-Cerulean^{+} neurons. To sum up, *NvNeogenin* showed an overall expression in the animal at tentacle bud stage, and it suggested that the whole endodermal tissue including *NvElav1*::NTR-Cerulean^{+} neurons expressed *NvNeogenin*. Repetitions of the experiment could elucidate a more distinct *NvNeogenin* signal and show the co-expression more clearly.

4.8 *NvUnc-5* showed no clear expression pattern

We also performed an *in-situ* hybridisation for *NvUnc-5* (**Supplementary Figure 4**). Staining was not detected at early and late gastrula (**Supplementary Figure 4A-B'''**). In early planula there was faint expression in the pharynx, regardless of how long specimens were stained (**Supplementary Figure 4C-C'''**). Also, in the specimen shown a scattered cell pattern in the ectoderm could be observed (**Supplementary Figure 4C-C'''**). However, the staining in pharynx and scattered cells was not consistent amongst different specimens. So, it is possible that the scattered-cell pattern could be the result of unspecific staining. Repeating the experiment with adapted conditions, like a new anti-*NvUnc-5* ISH-probe could already improve the staining.

Since we saw that *NvUnc-5* had an incomplete domain composition (**Figure 4.1C**), no differential expression was detected in the bulk-RNA-sequencing data (**Table 2**) and an unclear *in-situ* signal (**Supplementary Figure 4**), *NvUnc-5* was not subject to further experiments.

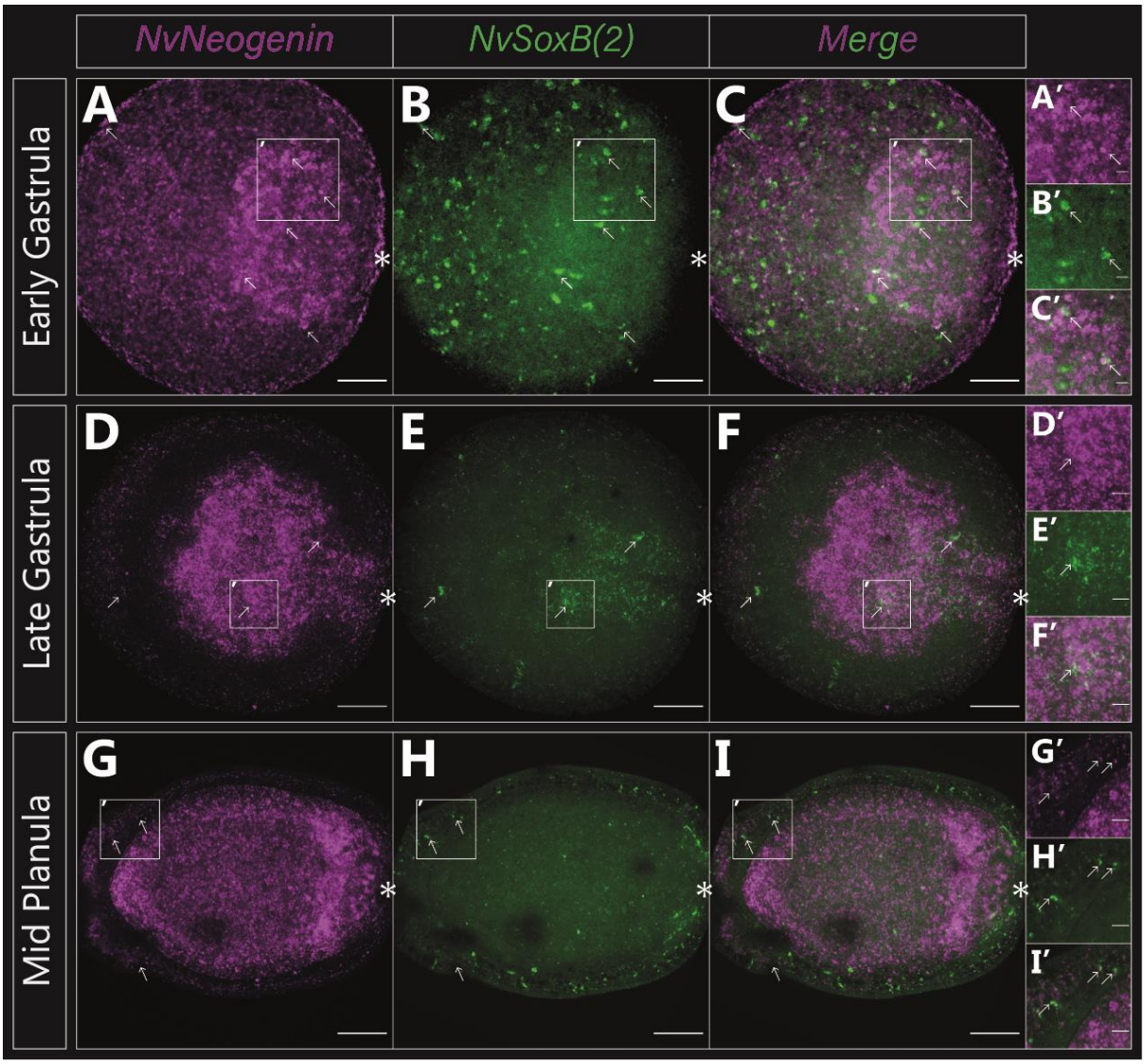

Figure 4.6: *NvNeogenin* was mainly expressed in the endoderm, pharynx and aboral ectoderm, and colocalised with the neural progenitor marker *NvSoxB(2)*. This graph shows a double fluorescence *in-situ* hybridisation of *NvNeogenin* (**A, D, G**) and *NvSoxB(2)* (**B, E, H**), which is indicated by panels on the top. Panels to the left show developmental stages. Panels to the right marked with ' are enlargement of the region marked by the box (**A' – I'**). **A)** In Early Gastrula *NvNeogenin* was expressed in the invaginating endoderm, as well in distal part of cells in the ectoderm. **B)** Pattern of scattered *NvSoxB(2)* expression. The merge (**C**) shows that *NvNeogenin* and *NvSoxB(2)* were co-expressed in the endoderm and in few ectodermal cells (white arrows, **C – C'**). In Late Gastrula *NvNeogenin* could be detected in the endoderm and pharynx (**D**) as well weakly in the ectoderm. **E)** *NvSoxB(2)* was weakly expressed in ectodermal cells and in the pharynx. An overlap between *NvNeogenin* and *NvSoxB(2)* could be found in cells in the ectoderm and endoderm (white arrows, **F – F'**). In Mid Planula *NvNeogenin* is expressed strongly in the oral and aboral endoderm, pharynx, as well as in the aboral ectoderm (**G**). **H)** *NvSoxB(2)* was detected in scattered cells in the whole ectoderm and pharynx region. Colocalization of *NvNeogenin* and *NvSoxB(2)* was detected in the aboral ectoderm (white arrows, **I – I'**). Representative images show one confocal section. Asterisks indicate the oral opening. Scale bars: 50 µm (**A – I**), 10 µm (**A' – I'**). *n=2*, 30-50 animals per stage

4.9 Generation of a *NvNeogenin::mGFP* transgenic reporter construct

To look closer into the morphology of cells expressing *NvDscam* and *NvNeogenin,* we attempted to establish transgenic reporter lines. In order to do this, we identified genomic regions in front of the first exon of the gene that had chromatin marks typical for promoters (Schwaiger et al., 2014). These regions were amplified from gDNA and cloned into a pUC II vector that carries a membrane targeted GFP (mGFP) flanked by I–SceI restriction enzyme sites (Renfer & Technau, 2017). Subseqently, constructs were injected into F0 zygotes. If the construct was incoorporated into the genome it was possible that mosaic expression of the transgene could occur. Signals could already be detected after 24 hpf in the majority of animals which was potentially the result of non-specific expression of the transgene that was present in high amounts. With time, the non-specific signal faded and after 7 dpf the signals that were still detectable are presumed to be expression of the transgene in the cells that actively expressed it because of the promoter. The goal was to have the transgene integrated into the genome of germline cells, thus it could be transmitted to the next generation. Additionally, if the transgene was integrated into other cell types, for example neurons, signals could be detected in F0 animals as well. *NvDscam::mGFP* injected animals did not show any signals after 7 dpf. However, few *NvNeogenin::mGFP* injected animals showed mosaic expression of the transgene after 7 dpf. mGFP signal could be detected along the mesenteries and neurons along the tracts (**Figure 4.7B**). Signal from the pharynx and tentacles were the result of autofluorescence in the animal. As a comparison, an *NvElav1::mOrange* animal is shown (**Figure 4.7A**) which also showed labelelling of neurons along the mesenteries. A closer analysis with the confocal microscope was not performed because the number of animals with a striking signal were low and we elected to keep these animals for breeding of an F1 generation.

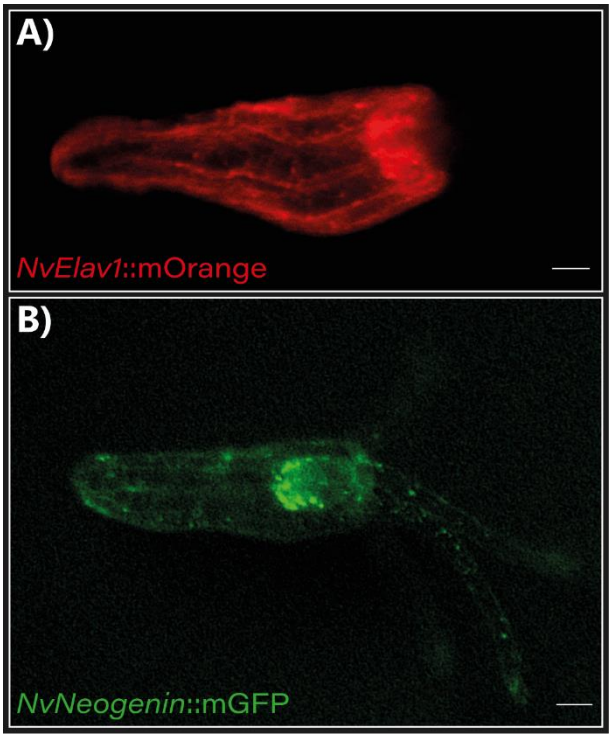

Figure 4.7: *N. vectensis* expressing a membrane targeted GFP under control of the *NvNeogenin* promoter shows expression in the mesenteries. This graph shows fluorescence pictures taken on a stereomicroscope. **A)** Visualisation of mOrange in the *NvElav1::mOrange* transgenic line showed the nerve net generated by *NvElav1*::mOrange^{+} neurons along the mesenteries in an F1 offspring. **B)** F0 animal injected with the *NvNeogenin::mGFP* transgene showed a mGFP signal along the mesenteries as well as single cells. Signals in the pharynx and tentacles derived from autofluorescence. Scale bars show 100 µm.

4.10 Melt curve analysis of F0 animals injected with sgRNAs allowed the identification of mutation-inducing sgRNAs directed against *NvDscam* and *NvNeogenin*

One of the ways to understand the function of a gene *in vivo* is to generate mutant animals using CRISPR/Cas9. After injection of Cas9 protein and the single guide RNAs (sgRNAs), the embryos were raised to 14 dpf and then genomic DNA (gDNA) from eight whole animals was isolated for melt curve analysis. Melt curves are generated after amplification of a PCR fragment of a ~100 bp region containing the sgRNA target site. Thus, it can be detected if changes to the DNA have been made, because point mutations can cause different binding affinities, insertions/deletions lead to longer/shorter amplicons (Samarut et al., 2016). As a control, eight un-injected WT animals from the same fertilisation day were used; for easier representation only two WT melt curves are shown. Melt curves derived from sgRNA injected animals are referred to as sgRNA curves and are shown in orange, WT curves in green.

Figure 4.8A shows the target sites for two *NvDscam*-sgRNAs. The first one was directed against *exon 7* which encodes the seventh IG domain that binds Netrin-1 in other organisms (Ly et al., 2008). The second one was directed against *exon 21* which encodes for the large intracellular domain and is supposed to mediate intracellular responses. **Figure 4.8B** shows the melt curves of eight F0 animals injected with sgRNA-*NvDscam-exon7* and of two WT animals. Seven melt curves of injected animals showed the same single peak as the two WT curves and thus these animals were not mutants. On the other hand, one injected animal showed a shoulder to the left at the beginning of the slope, which suggests an induced mutation (black arrowhead, black curve, **Figure 4.8B**). **Figure 4.8C** shows the melt curves of eight F0 animals injected with sgRNA-*NvDscam*-e*xon21* and of two WT animals. Five out of eight injected animals showed no change in their melt curves, whereas three were distinguishably different. Two of the three had a shoulder at the beginning of the peak and one showed a general shift of the peak.

In **Figure 4.8D** the target sites of four *NvNeogenin*-sgRNAs are depicted. Two were directed against the start of *exon 1* to disrupt the start codon or the signal peptide. One was directed against *exon 11* that encodes for the fourth FNIII domain which binds Netrin-1 in other organisms (Geisbrecht et al., 2003). One other sgRNA targeted *exon 15* which encodes for the transmembrane domain (TMD). Two melt curves of animals injected with sgRNA-1-*NvNeogenin-exon1* showed shoulders, however, six were having the same shape as the WT curves (**Figure 4.8E**). For sgRNA-2-*NvNeogenin-exon1* only one melt curve showed a different slope than the other seven (**Figure 4.8F**). Five melt curves of sgRNA-*NvNeogenin*-e*xon11* injected animals showed peculiar different shapes than the WT curves (**Figure 4.8G**). Strikingly, all animals injected with sgRNA-*NvNeogenin-exon15* showed different melt curves than the WT animals (**Figure 4.8H**).

Overall, sgRNAs targeted against *NvDscam*-exon21, *NvNeogenin*-exon11 and -exon15 were working most efficiently. All injected lines were kept and raised until adulthood to generate F1 offspring.

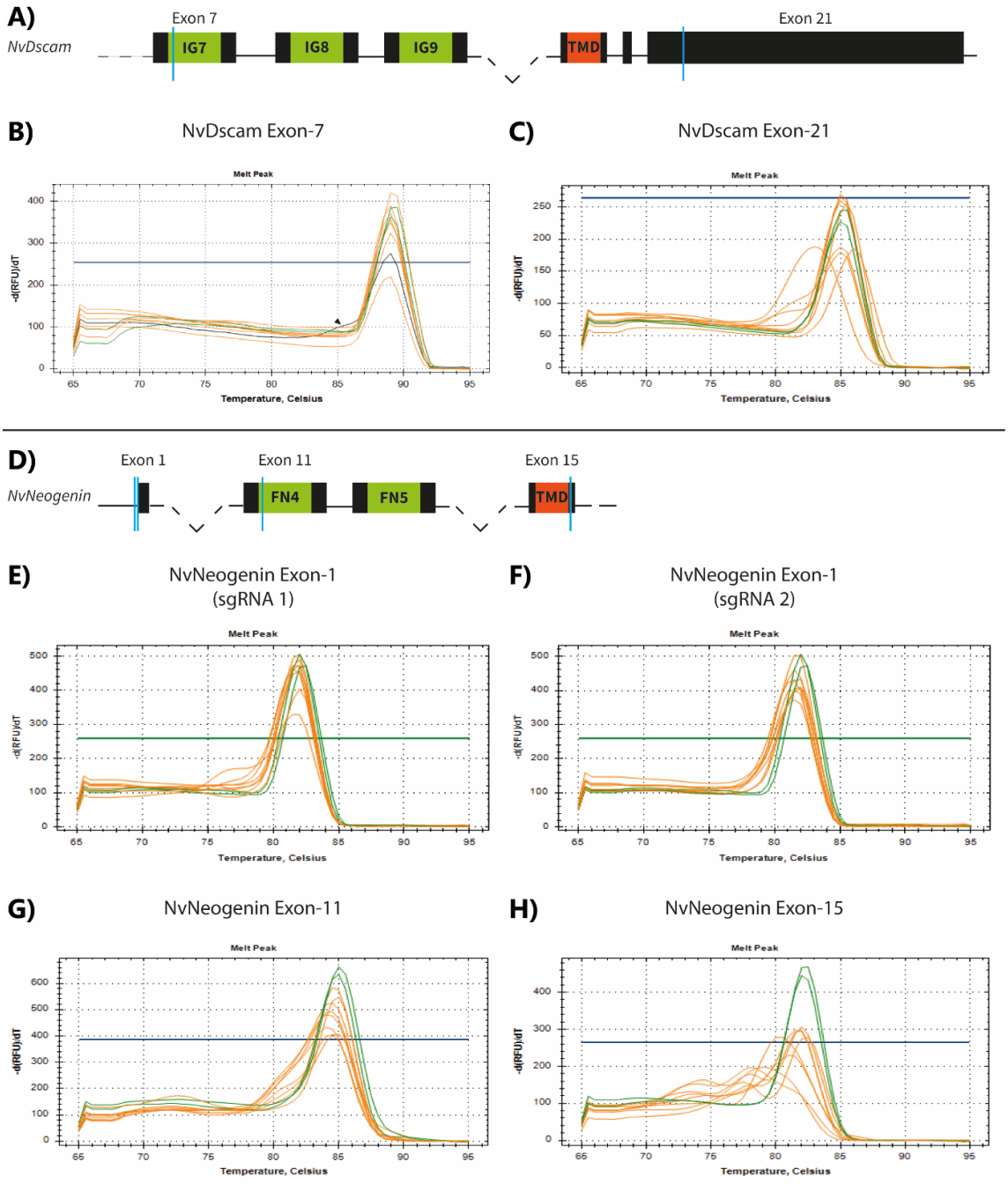

Figure 4.8: Melt curve analysis of F0 animals injected with sgRNAs. A) *NvDscam* gene map that shows target sites of the two sgRNAs targeted against e*xon-7* (seventh IG domain) and e*xon-21* (intracellular domain). **B)** Melt curve analysis of eight sgRNA-*NvDscam-exon-7* injected animals revealed one mutant, shown by the shoulder at the peak-beginning. **C)** Melt curve analysis of eight sgRNA-*NvDscam-exon-21* injected animals revealed three mutant animals, as seen by two having a shoulder and one having a shift of the peak. **D)** *NvNeogenin* gene map showing target sites of the four sgRNAs targeted against *exon-1* (start codon, signal peptide), *exon-11* (fourth FNIII domain) and *exon-15* (TMD domain). **E)** Melt curve analysis of eight sgRNA-1-*NvNeogenin-exon-1* injected animals revealed two mutants having a shoulder at the beginning of the peak. **F)** Melt curve analysis of eight sgRNA-2-*NvNeogenin-exon1* injected animals showed one different sgRNA curve. **G)** Melt curve analysis of eight sgRNA-*NvNeogenin-exon11* injected animals showed five sgRNA curves with a distinct shoulder. **H)** Melt curve analysis of eight sgRNA-*NvNeogenin-exon15* injected animals revealed that all injected animals are mutants.
As a control eight WT animals were used and two of them are shown for an easier overview. Melt curves are plotted as the derivative of the change of fluorescence as a function of temperature against the temperature. The peak describes the temperature at which 50% of double stranded molecules are separated.

4.11 Generation of mutant lines using the CRISPR/Cas9 system

The F0 animals injected with sgRNA-*NvDscam*-exon21 and sgRNA-*NvNeogenin*-exon15 were raised to sexual maturity, and females and males were identified. Male F0 animals were crossed to WT females then eight F1 animals were used for melt curve analysis and sequencing.

4.11.1 sgRNA-*NvDscam-exon21* caused a frameshift mutation and a truncated intracellular domain

Two male F0 individuals (IX and VII) injected with sgRNA-*NvDscam-exon21* produced mutant offspring. Melt curve analysis of eight offspring from each F0 animal suggested that four of each had mutations, as indicated by the extra peak in the curves (**Figure 4.9**, orange curves). PCR fragments with an approximate size of 400-500 bp including the sgRNA target site were sequenced. Sequencing results were analysed using CRISP-ID and are depicted below the melt curves in **Figure 4.9**. The sgRNA target site is underlined. Offspring of individual IX showed three point mutations and a two-base-pair-deletion, as marked in red (**Figure 4.9A**, **mutation D1.1**). The three point mutations led to exchange of amino acids from serine to arginine, asparagine to histidine and threonine to proline. Furthermore, the two-base-pair-deletion led to a frameshift mutation, thus, the following amino acids sequence was different to the WT. More importantly, an early stop-codon was introduced 72 bp downstream of the deletion, which led to a truncation of a large part of the NvDscam intracellular domain. Offspring of

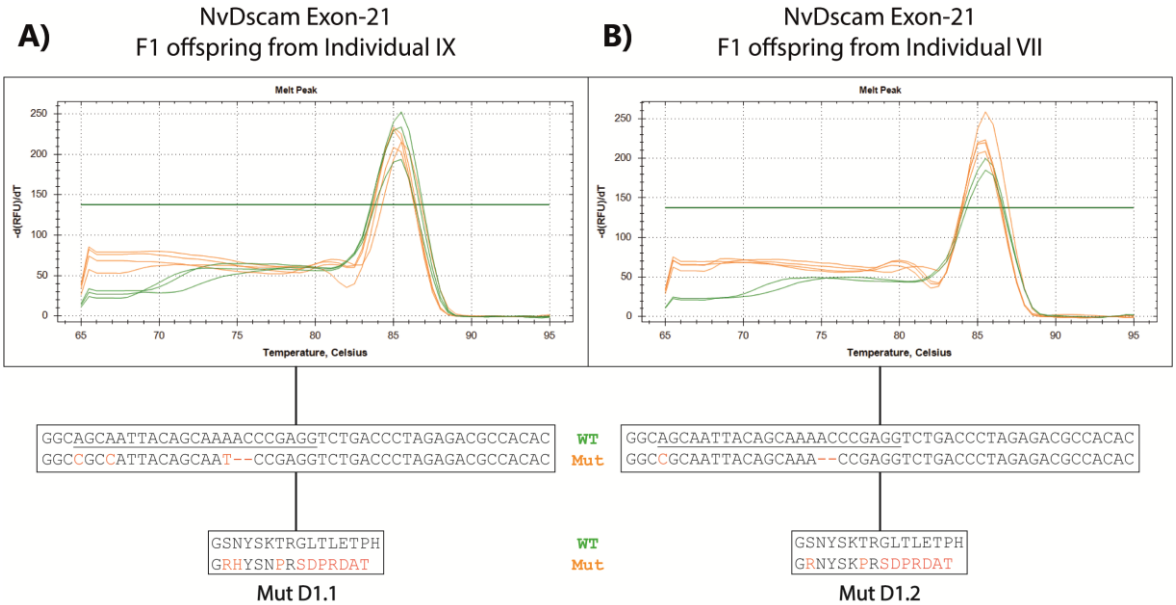

Figure 4.9: Generation of heterozygous F1 mutant lines using the sgRNA-*NvDscam-exon21*. Two F0 animals (Individuals IX and VII) were identified to produce heterozygous F1 offspring. Melt curve analysis of eight F1 offspring per F0 individual revealed that four of each have an extra peak in the curves. For easier depiction only the four double-peak sgRNA curves (orange) and three WT curves (green) are shown. The sgRNA target sequence is underlined. Resulting mutated sequences are shown in red. **A)** Sequence analysis revealed that individual IX produces offspring with three one-base-pair-conversions and one two-base-pair-deletion, which caused a frameshift mutation and an early stop codon 72 bp downstream of the deletion (Mutant D1.1). **B)** Individual VII produced offspring with one one-base-pair-conversion and a two-base-pair-deletion causing a frameshift and an early stop codon at the same position (Mutant D1.2). The mutant D1.1 amino acid sequence showed three exchanges from serine to arginine, asparagine to histidine and threonine to proline. Whereas the mutant D1.2 only showed amino acid changes from serine to arginine and threonine to proline. In both mutations, the frameshift induced a different amino acid sequence.

individual VII showed one point mutation which results in an amino acid change from serine to arginine (**Figure 4.9B**, **mutation D1.2**). The two-base-pair-deletion could also be found here at the same location as in offspring from individual IX, which led to an early stop codon as well 72 bp downstream. Thus, these two mutated sequences were only differing by two additional point mutations in mutant D1.1. However, they shared the two-base-pair-deletion which causes a truncated intracellular domain. To sum up, sgRNA-*NvDscam-exon21* worked well to introduce a frameshift mutation. Two carriers could be identified and a heterozygous F1 line could be generated.

4.11.2 sgRNA-*NvNeogenin-Exon15* caused four different mutations

Two male F0 individuals (X and IV) were crossed to WT females and eight of their offspring each were subject to melt curve analysis and sequencing. The eight F1 animals from individual X could be classified into two melt curve classes (**Figure 4.10A**), one with a double peak and one with a peak shift. Two F1 animals of each were sent for sequencing. The sgRNA target site is underlined. The double-peak animals showed a point mutation from T to A and a three-base-pair-deletion, causing a threonine instead of a serine and the loss of valine (**Figure 4.10A**, **mutation N1**). The peak-shift animals revealed a three-base-pair-insertion (ACG) and 15-base-pair-deletion, causing the change from valine and leucine to aspartate and alanine (**Figure 4.10A**, **mutation N2**). The two sequences were also subject to secondary structure analysis with Jpred4, which revealed no changes (data not shown). Although the last three amino acids of the TMD are lost, the TMD itself persists.

Next, eight F1 animals from individual IV were analysed (**Figure 4.10B**). Their melt curves could also be divided into two classes, though, both were showing double peaks. The first class showed a six-base-pair-deletion causing the loss of two amino acids and the change from serine to asparagine (**Figure 4.10B, mutation N3**). Nevertheless, this mutation also did not influence the secondary structure (data not shown). However, the second class revealed an eight-base-pair-insertion (AAGCAAGA) and a T to G point mutation, which led to a change in the amino acid sequence and a frameshift leading to a stop codon within *exon16* (**Figure 4.10B, mutation N4**).

To sum up, four mutations were detected for *NvNeogenin*. Three of them showed no changes to the reading frame or secondary structure and therefore might have no influence on the protein function. One mutation (**Mutation N4**) carried a frameshift mutation and thereby the protein contained a truncated intracellular domain.

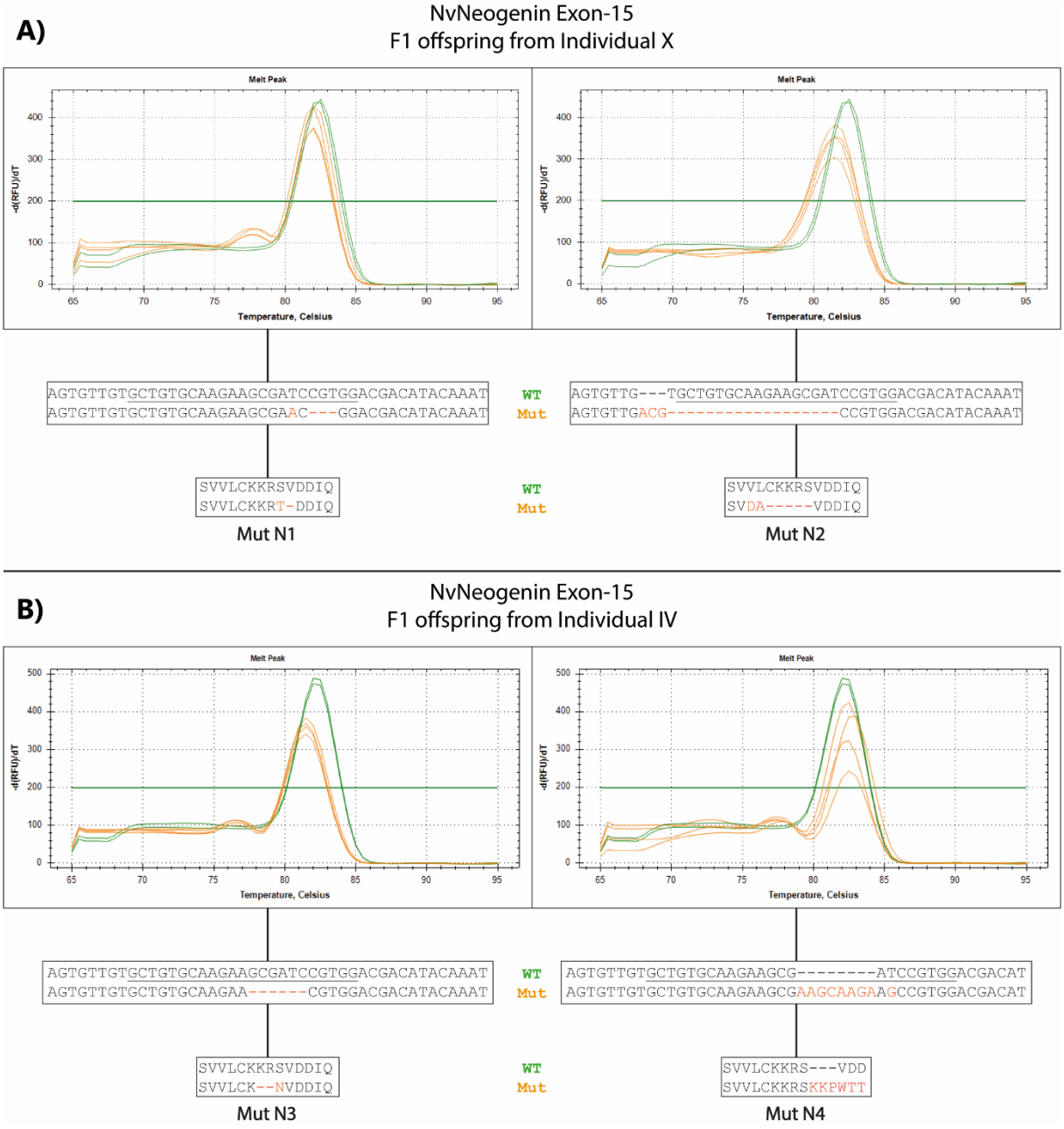

Figure 4.10: Generation of heterozygous F1 mutant lines using the sgRNA-*NvDscam-Exon21*. Two F0 animals (Individuals X and IV) were identified to produce heterozygous F1 offspring. **A)** Melt curve analysis of eight F1 offspring of F0 individual X revealed two mutation classes. One double peak and one peak shift. For easier depiction only two WT curves (green) are shown. The sgRNA target sequence is underlined. Resulting mutated sequences are shown in red. Sequence analysis revealed a T-to-A conversion and a three-base-pair deletion in the double-peak-mutant, causing only a serine-to-threonine change and the loss of one amino acid (**Mutation N1**). The peak-shift-mutant had a three-base-pair-insertion (AGC) and 15-base-pair-deletion, causing the conversion of valine and leucine to aspartate and alanine and the loss of five amino acids (**Mutation N2**). **B)** Melt curve analysis of eight F1 offspring of F0 individual IV revealed two double-peak classes. For easier depiction only two WT curves (green) are shown. The sgRNA target sequence is underlined. Resulting mutated sequences are shown in red. The first double-peak class showed a six-base-pair-deletion causing the loss of three amino acids and the change from serine to asparagine (**Mutation N3**). The second double-peak class revealed an eight-base-pair-insertion and a T-to-G conversion, causing a frameshift mutation and an early stop codon in *exon16* (**Mutation N4**).

4.12 Establishment of shRNA knock downs for *NvDscam* and *NvNeogenin*

shRNAs are small RNA molecules containing a hairpin. They are designed to bind to a specific mRNA and lead to its subsequent degradation, also called RNA interference. In this study three shRNAs targeted against *NvDscam* and two against *NvNeogenin* were designed. To determine their efficiency, they were injected into *Nematostella vectensis* zygotes and at 24 hpf total RNA was isolated and used for quantitative real-time PCR. Results derived from three independent injections are depicted in **Figure 4.11A** and **B**. All three shRNAs against *NvDscam* caused a significant reduction of expression. Expression levels were reduced to 51% after injection of shDscam-1 ($p = 0.0016$), 56% after shDscam-2-injection ($p = 0.0032$) and 37% after shDscam-3-injection ($p = 0.0003$) (**Figure 4.11A**). *NvNeogenin* expression was reduced to 21% after injection of either shNeogenin-1 or shNeogenin-2 shRNAs ($p < 0.0001$) (**Figure 4.11B**). Thus, the shRNAs shDscam-3 and shNeogenin-1 and -2 appeared as good candidates for further functional analysis. For example, downstream targets of *NvDscam* or *NvNeogenin* can be identified using qRT-PCR.

Previously, it has been discovered that the intracellular domains (ICDs) of Dscam and Neogenin in human and murine cell lines can be cleaved off and induce transcription of target genes (Goldschneider et al., 2008; Sachse et al., 2019). The Dscam-ICD was found to induce expression of genes involved in neuronal wiring (Sachse et al., 2019), however if genes involved in neurodevelopment were regulated by the Neogenin-ICD was not assessed (Goldschneider et al., 2008).

With this context, we next aimed to analyse if a *NvDscam* knock-down (KD) impacts *NvNeogenin* expression and *vice versa*. shNeogenin-2 injection led to a decrease of *NvDscam* expression to 53%, however this was found to be not statistically significant ($p = 0.0640$) (**Figure 4.11C**). Injection of shDscam-3 caused a reduction of *NvNeogenin* expression to 86% (**Figure 4.11D**), also lacked statistical significance ($p = 0.3057$). We furthermore investigated if *NvDscam*- or *NvNeogenin*-KD affected *NvNetrin* expression. *NvNetrin* expression levels were reduced to 73% with shDscam-3 and 48% with shNeogenin-2 (**Figure 4.11E**). However, these differences again showed no statistical significance ($p = 0.3250$ and $p = 0.0586$, respectively).

To sum up, a significant interaction between the receptors *NvNeogenin* and *NvDscam* on mRNA level could not be found even though there was reduction in the expression of *NvDscam* after shNeogenin-2 injection. In addition, *NvNetrin* expression showed a trend to reduced expression after shDscam-3 and shNeogenin-2 injection.

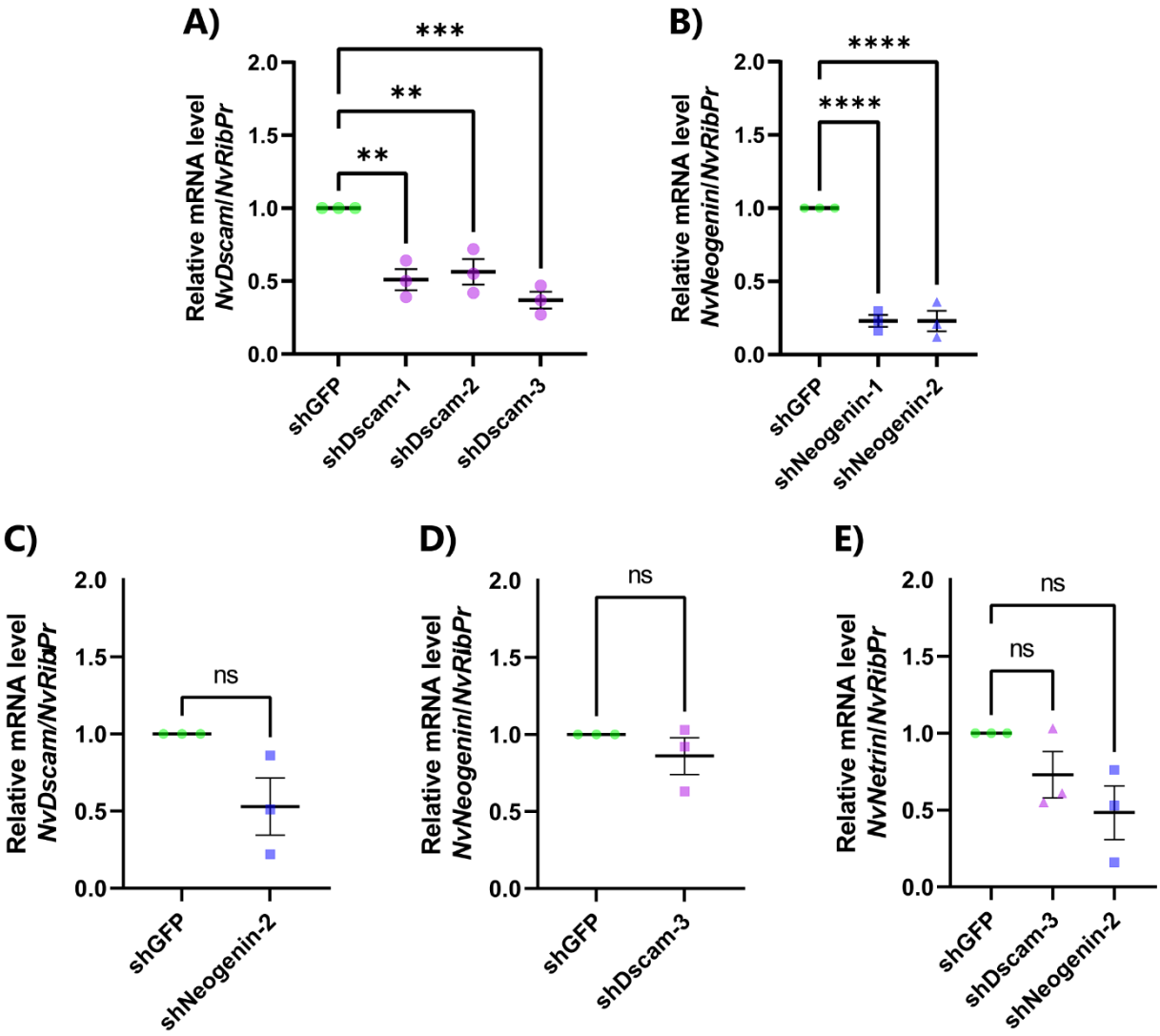

Figure 4.11: shRNA mediated knockdown of *NvDscam* and *NvNeogenin*. A) Relative mRNA levels of *NvDscam* at 1 dpf after knock-down using shDscam-1, shDscam-2 and shDscam-3. Injection of shDscam-1 led to a 0.51-fold, shDscam-2 to a 0.56-fold and shDscam-3 to a 0.37-fold decrease of *NvDscam* expression. **B)** Relative mRNA levels of *NvNeogenin* at 1 dpf after knock-down using shNeogenin-1 and shNeogenin-2. Injection of shNeogenin-1 and shNeogenin-2 led to 0.23-fold decrease of *NvNeogenin* expression. **C)** Relative mRNA levels of *NvDscam* at 1 dpf after shNeogenin-2 injection showed a 0.53-fold reduction. **D)** Relative mRNA levels of *NvNeogenin* at 1 dpf after shDscam-3 injection showed a 0.86-fold decrease in expression. **E)** shDscam-3 injection led to a 0.73-fold and shNeogenin-2 led to a 0.48-fold reduction in *NvNetrin* expression. shGFP was used as a scramble shRNA and served as the injection control. Expression data was normalised to *NvRiboprotein* expression. Individual values are shown with median and SEM. **A**, **B**, **E** One-Way-Anova with Dunnett's Multiple Comparison. **C**, **D** unpaired *t*-test. *n* = 3 injections; significant differences are indicated with asterisks (*ns* = not significant, * = $p < 0.05$, ** = $p < 0.01$, *** = $p < 0.001$, **** = $p < 0.0001$).

5. Discussion

This study describes the characterisation of the possible neurite guidance receptors *NvDscam* and *NvNeogenin* in the sea anemone *Nematostella vectensis*. The phylogenetic analysis confirms that *NvDscam* is a Dscam orthologue, and its domain architecture is conserved amongst Cnidaria and Bilateria (**Figure 4.2**). Furthermore, the expression pattern of *NvDscam* and *NvNeogenin* was assessed during several early development stages and suggested a neuronal-like expression during gastrulation (**Figure 4.3 & 4.5**). A subset of cells expressing aforementioned receptors were also identified as cells co-expressing *NvSoxB(2)* (**Figures 4.4 & 4.6**). A transgenic reporter construct was established (*NvNeogenin::mGFP*) and injected successfully to describe the morphology of cells expressing mGFP under control of the *NvNeogenin* promoter (**Figure 4.7**). Moreover, tools for functional analysis were developed. Specifically, stable mutant lines for *NvDscam* and *NvNeogenin* using the CRIPSR/Cas9 system were generated, carrying a mutation leading to truncated intracellular domains (ICDs) (**Figures 4.8**, **4.9 & 4.10**. Also, effective shRNAs for RNA-interference experiments were designed leading to a knock-down (KD) of *NvDscam* and *NvNeogenin* gene expression.

Overall, tools to study possible roles of *NvDscam* and *NvNeogenin* in neurite guidance in *Nematostella vectensis* were established during this master thesis. This will allow future investigations into the generation of the nervous system in this sea anemone and if the mechanisms leading to the establishment of a neural network are conserved between Cnidaria and Bilateria.

5.1 Orthologues of NvNetrin receptors are present in *Nematostella vectensis*

It was found that the domain compositions of NvDscam and NvNeogenin resemble vertebrate orthologues (**Figure 4.1**) and that *NvDscam* is indeed a Dscam orthologue based on phylogenetic analysis (**Figure 4.2**). A previous study described the phylogeny of Neogenin and the presence of an orthologue in *Nematostella vectensis* was confirmed (Leclère & Rentzsch, 2012). Interestingly, domain predictions showed that NvDscam has 1 immunoglobulin (IG) and 1 Fibronectin type III (FNIII) domain and NvNeogenin 1 FNIII domain less than their vertebrate orthologues (**Figure 4.1**). Between the 1st and 2nd IG domain in NvDscam, a long sequence could be found that was not assigned an IG domain (**Figure 4.1A**). It is possible that the domain prediction tool SMART does not predict an IG domain correctly since it also did not predict all domains for the murine Unc-5 (**Figure 4.1C**). It is questionable that this long sequence in *N. vectensis* is subject to alternative splicing. It was shown that the first 4 IG domains of Dscam can bind to the repulsive guidance cue Slit (Dascenco et al., 2015), which is involved in Slit-Robo mediated repulsion in axon guidance (Tong et al., 2019). It is possible that alternative splicing of the long region in *NvDscam* could regulate the interaction with NvSlit proteins. However, alternative splicing has not yet been studied and Slit proteins have not been identified in *N. vectensis*.

In *Drosophila*, Dscam is subject to alternative splicing of exons 4, 6, 9 and 17 generating a vast diversity of 38.016 isoforms of Dscam. This contributes to a role in neuron identity and dendritic self-avoidance (Schmucker et al., 2000). In vertebrates, protocadherins have a comparable role to establish neuron identity. Here, different protocadherin repertoires are achieved by regulation of alternative promoters, not by alternative splicing (Jin & Li, 2019; Pancho et al., 2020). Alternative splicing for *NvDscam* cannot be excluded as it has not yet been studied. Different splice variants could be detected using mRNA-sequencing (Wang et al., 2008).

5.2 *NvDscam* and *NvNeogenin* show a neuron-like expression pattern

Using colorimetric *in-situ* hybridisation (ISH) it was found that expression of *NvDscam* started during gastrulation in the developing endoderm and scattered cells in the ectoderm (**Figure 4.3**). At late planula stages, the staining was seen at the oral pole, and in the developing tentacles of the tentacle bud and primary polyp. Based on their position, the expressing cells seen in the tentacle tips at later stages could be cnidocytes. However, the RNA-sequencing suggested no differential expression of *NvDscam* in *NvNcol3*::mOrange-positive cells (**Table 2**), which are specific for cnidocytes (David et al., 2008). A basic expression of *NvDscam* in cnidocytes cannot be excluded, still this needs to be determined by further experiments, for example co-staining of *NvDscam* with fluorescent *in-situ* hybridisation (FISH) and *NvNcol3*::mOrange with immunostaining.

The sequencing data showed an elevated expression of *NvDscam* in *NvSoxB(2)*::mOrange-positive cells. The scattered cells in gastrula stages nicely reflected a staining also seen with *NvAth-like*, *NvAshA* and *NvSoxB(2)*, which are genes known to be involved in neurogenesis in other organisms (Richards & Rentzsch, 2015). In *N. vectensis*, *NvSoxB(2)* is a marker for progenitor cells, giving rise to various neural populations (Richards & Rentzsch, 2014) but also to non-neural gland/secretory cells (Tournière et al., n.d.). Furthermore, double FISH (dFISH) at early gastrula showed that almost all *NvSoxB(2)*-positive cells co-express *NvDscam* (**Figure 4.4A – C**). At late gastrula, less cells co-express *NvSoxB(2)* and *NvDscam* (**Figure 4.4D – F**), and later at mid planula very few cells could be found co-expressing those two genes. This suggested that *NvDscam*-positive cells arise from *NvSoxB(2)*-positive progenitors during gastrulation. However, since there was a reduction in detectable co-expression during development, it is possible that *NvDscam*-positive cells are derived from other progenitors and that *NvDscam* plays a role in specialised cells in later developmental stages. To elucidate whether *NvDscam* is expressed by progenitors or differentiated cells an EdU labelling can be performed in combination with a FISH of *NvDscam*. Here, proliferating cells in S-phase are marked and thus progenitor cells can be detected. Further experiments to decipher the origin of *NvDscam* expressing cells could involve dFISH with *NvSoxB(2)* or *NvAth-like* at earlier timepoints between blastula and early gastrula. As well, dFISH can be performed with immunostaining of mOrange in the *NvSoxB(2)::mOrange* transgenic

reporter line. Crossing a transgenic reporter line in which mGFP is regulated by *NvDscam* regulatory regions to the *NvSoxB(2)::mOrange* transgenic reporter line also helps to study the origin of *NvDscam*::mGFP^{+} cells.

Putting ISH and dFISH into comparison, the *NvDscam*-expression patterns detected with ISH resembled the pattern seen in FISH at gastrulation (**Figure 4.3, 4.4A & D**). The signal in FISH seemed clearer since only one confocal plane is depicted, while in ISH the images are taken with more focal planes. Interestingly, the *NvDscam*-FISH in mid planula showed an overall staining in the ectoderm (**Figure 4.4G**) while in the endoderm single cells could be detected, which were located along the mesenteries (**Supplementary figure 1 – white arrows)** and co-expression with *NvSoxB(2)* could not be found. The *NvDscam*-ISH at late planula stage showed only staining at the oral pole. Thus, the question arises, does the endodermal expression decrease during planula development? It is possible that the ISH method is not as sensitive. Here, a transgenic reporter line could provide further insights. Unfortunately, due to time limits in this study the F1 offspring of the *NvDscam::mGFP* line could not be analysed, and expression of the reporter plasmid in F0 injected animals could not be seen.

Expression of *NvNeogenin* could be first detected at early gastrula with a strong staining in the developing endoderm and in ectodermal cells (**Figure 4.5**). Again, the scattered cells in the ectoderm resembled the staining seen with putative neural progenitor genes (Richards & Rentzsch, 2015). Bulk-RNA-sequencing data showed a moderately elevated expression of *NvNeogenin* in *NvSoxB(2)*::mOrange-positive cells (**Table 2**). dFISH experiments at early gastrula revealed that a subset of *NvSoxB(2)*-positive cells co-expressed *NvNeogenin* in the ecto- and endoderm (**Figure 4.6A – C**). However, a majority of *NvNeogenin*-positive cells were not positive for *NvSoxB(2)* in the endoderm, which suggests either an origin from a different progenitor cell population, or *NvNeogenin*-positive cells arise earlier between blastula and early gastrula from *NvSoxB(2)*-progenitors. To find out if the co-expression with *NvSoxB(2)* means that *NvNeogenin*-high cells are indeed progenitor cells, one could perform EdU-labelling. Also, dFISH at earlier timepoints could be carried out or crossing of the newly generated transgenic reporter line *NvNeogenin::mGFP* to the *NvSoxB(2)::mOrange* transgenic reporter line could provide more insights. It is also possible to perform a FISH of *NvNeogenin* together with an immunostaining of mOrange in the *NvSoxB(2)::mOrange* transgenic reporter line.

At mid and late planula stages the *NvNeogenin* expression patterns confined to the oral and aboral endoderm (**Figure 4.5**) which could also be seen at mid-planula in the FISH (**Figure 4.6G**). Recently, it was found that sensory-like cells expressing the neuropeptide NvRPamide are detected at the aboral pole at planula stage and form an aboral nerve net, close to the apical tuft. At early planula NvRPamide-positive cells extend their neurites to the aboral pole (Zang & Nakanishi, 2020). *NvNetrin* is also detected in the apical tuft at early planula stage (Matus et al., 2006), which could indicate guidance of

NvRPamide-neurites towards the aboral pole. Also, *NvNeogenin* transcripts could be detected at the aboral pole at mid planula (**Figure 4.6G**). Possibly, further dFISH experiments with *NvRPamide* and *NvNeogenin* could reveal co-expression. FISH of *NvRPamide* on a *NvNetrin* or *NvNeogenin* knock out could indicate a possible role of NvNetrin signalling in the guidance of *NvRPamide* neurons.

In addition, elevated expression of *NvDscam* and *NvNeogenin* in cell populations labelled by *NvElav1*::mOrange was found by RNA-sequencing (**Table 4.1**), which can indicate a role in *NvElav1*::mOrange neurons. In *N. vectensis* the *NvElav1::mOrange* transgenic reporter line describes a subpopulation of sensory and ganglion cells in the ecto- and endoderm (Nakanishi et al., 2012). In this work, a FISH of *NvDscam* or *NvNeogenin* was performed at tentacle bud stage in combination with an immunostaining of *NvElav1*::NTR-Cerulean-positive cells (**Supplementary figures 2 & 3**). The nerve net formed by *NvElav1*::NTR-Cerulean-positive neurons was nicely stained, however, the FISH for *NvDscam* and *NvNeogenin* showed a broad staining and single cells could barely be identified expressing *NvDscam* (**Supplementary figure 2A** - white arrows). Here, it was difficult to distinguish a real signal from eventual background staining. Moreover, the ISH for *NvDscam* at tentacle bud showed only staining in the tentacle tips (**Figure 4.3**), which could be seen slightly in the FISH as well (**Supplementary figure 2A**). Also, single cells in the ectoderm could be seen slightly (white arrows). Nevertheless, repeating this experiment with for example a lower concentration *in-situ*-probe can already improve the staining. Thus, it could not be excluded that *NvElav1*::NTR-Cerulean-positive cells were present that also express *NvDscam* (**Supplementary figure 2 – white arrows**). In the *NvNeogenin* FISH single cells could not be detected (**Supplementary figure 3A**), although the ISH staining showed single cells at tentacle bud stage (**Figure 4.5**).

5.3 Repulsive axon guidance in *N. vectensis*

In other organisms Dscam and Neogenin alone were shown to be involved in attraction of neurites in response to Netrin (Ly et al., 2008; Wilson & Key, 2006). In this study, only *NvDscam* and *NvNeogenin* were described. In contrast, Unc-5 is the major mediator of repulsive axon guidance in other organisms (Culotti & Merz, 1998). In *N. vectensis* the extracellular domains of *NvUnc-5* were not predicted (**Figure 4.1C**) and the ISH did not show a clear staining (**Supplementary Figure 4**). Previously, it was shown that Unc-5 can mediate repulsion in response to Netrin even without extracellular domains, merely the interaction of its intracellular UPA/Dcc binding domain with the P1 domain of Dcc is required (Hong et al., 1999). Thus, the absence of a conserved extracellular part does not necessarily mean that *NvUnc-5* cannot mediate repulsion. Regarding the ISH signal, it is possible, that the antisense RNA probe for *NvUnc-5* did not work well. Synthesis of new anti-*NvUnc-5* RNA probes and repeating the ISH could possibly reveal a more informative *in-situ* pattern.

Recently, it has been found that Neogenin interacts with Rgm (Repulsive guidance molecule) (Isaksen et al., 2020; Wilson & Key, 2006) suggesting that Rgm could also be part of the Netrin signalling system. The interaction with Neogenin results in a suppression of neurite outgrowth (Isaksen et al., 2020). In *N. vectensis*, *NvRgm* shows an interesting, asymmetric ISH pattern at late gastrula and planula stages in the endoderm like *NvNetrin* (Leclère & Rentzsch, 2014; Matus et al., 2006), with the difference that *NvNetrin* is expressed in the apical tuft and *NvRgm* is seen in a ring surrounding the apical tuft. In the endoderm, *NvNetrin* is expressed on the opposite side of *NvRgm* (Leclère & Rentzsch, 2014). At late gastrula and planula stages *NvNeogenin* was also found in the endoderm, pharynx and aboral pole (**Figure 4.5C & D**). This suggests possible roles of *NvNeogenin* interacting with *NvRgm* and *NvNetrin*, for example, in establishing transversal neurite outgrowth due to repulsion of *NvNeogenin*$^{+}$ neurites by *NvRgm* and attraction by *NvNetrin*. Here the *NvElav1::mOrange* transgenic reporter line can be used, since transversal neurite outgrowth can be observed (Nakanishi et al., 2012) and *NvNeogenin* was overexpressed in *NvElav1::mOrange*$^{+}$ cells (**Table 2**). Future experiments can involve the establishment of mutant lines for *NvNetrin* and *NvRgm* and crossing them to a *NvElav1::mOrange/ NvNeogenin::mGFP* double transgenic reporter line.

5.4 Establishment of tools for morphological and functional analysis

Here, two novel transgenes were synthesised with a membrane associated GFP (mGFP) under control of the *NvDscam* or *NvNeogenin* promoter. After injection into F0 WT zygotes expression of the transgene could be observed in early stages, likely because the high concentration of the transgene construct. This gave a first hint that the transgene can be expressed. During development, the likely unspecific expression ceased and if the transgene was transmitted to some cells that actively expressed *NvDscam* or *NvNeogenin*, the signal could be detected after the primary polyp stage. A signal in the *NvDscam::mGFP* was not detected in F0 juveniles, which could be caused by the lack of key regulatory information. Analysis of the *NvDscam::mGFP* F1s would give more insights. However, few *NvNeogenin::mGFP* animals showed a GFP signal which is visible in cells and neurites that were located along the mesenteries (**Figure 4.7B**). Thus, *NvNeogenin*::mGFP^{+} neurons had long neurites and contribute to the overall morphology of the nerve net. Those long neurites could also be seen in *NvElav1*::mOrange^{+} cells (**Figure 4.7A**). If the *NvNeogenin::mGFP* or *NvDscam::mGFP* transgene will be transmitted to the next generation, carriers of the transgene can be identified. The lines can be used to study the morphology of cells expressing *NvNeogenin* or *NvDscam*. They will be compared to the obtained ISH- and FISH-signals to investigate if mRNA- and fluorescent protein-expression patterns resemble each other. In addition, the transgenic reporter lines can be further characterised by crossing to already existing transgenic reporter lines, as well as to existing mutant lines. For example, to investigate if *NvSoxB(2)* progenitors give rise to *NvDscam*- or *NvNeogenin* cells, the transgenic reporter lines of the latter two can be crossed to *NvSoxB(2)*-mutant lines (Tournière and Rentzsch, unpublished

data). If they derive from *NvSoxB(2)*-progenitors then a fluorescent signal might not be detected. Also, crossing the *NvNeogenin::mGFP* to the *NvSoxB(2)::mOrange* transgenic reporter line can show if *NvNeogenin*::mGFP cells derive from *NvSoxB(2)*::mOrange cells.

Furthermore, mutant lines for *NvDscam* and *NvNeogenin* were generated using the CRISPR/Cas9 system (**Figures 4.9 & 4.10**). For both genes two mutant lines were established containing a frameshift mutation induced downstream of the transmembrane domain (TMD). Either a truncated protein without the intracellular domain will be expressed, or it will be degraded due to malfunction. In Vertebrata, the intracellular domains (ICDs) of Neogenin and Dscam mediate signalling to the cytoskeleton (Isaksen et al., 2020; Schmucker et al., 2000). In Bilateria, the ICDs of Dscam and Neogenin can be cleaved by γ-secretase and translocate to the nucleus (Goldschneider et al., 2008; Sachse et al., 2019) to activate expression of genes involved in neuronal wiring, like *Robo-2*, *Unc-5A* and *Netrin-4* (Sachse et al., 2019). Yet it is not known if signalling to the cytoskeleton or activation of transcription mediated by NvDscam and NvNeogenin is conserved in *N. vectensis*. In this case, the mutants generated in this work could give further insights into the downstream targets of NvDscam and NvNeogenin. Already, the RNA-interference experiments show that knock-down of *NvNeogenin* reduced mRNA levels of *NvDscam* (**Figure 4.11C**) and *NvNetrin* (**Figure 4.11E**) expression, though statistical significance could not be reached. Also, knock-down of *NvDscam* showed a minor reduction of *NvNeogenin*- (**Figure 4.11C**) and *NvNetrin*-mRNA levels (**Figure 4.11E**). Aside from transcriptional regulation, lower mRNA levels could also be explained by the presence of fewer cells in the animal expressing *NvDscam* or *NvNeogenin*, causing a lower amount of the genes' transcript.

After raising the heterozygous CRISPR-induced mutant lines to maturity and crossing them to each other, homozygous mutants can be obtained. Then, their phenotype can be described. It can be examined if a knock-out of *NvDscam* or *NvNeogenin* influences the establishment of the nerve net. For instance, crossing them to *NvElav1::mOrange* animals can reveal an effect on the neurite outgrowth.

5.5 Summary

In a whole, this study characterised the putative NvNetrin receptors *NvDscam* and *NvNeogenin* in the sea anemone *Nematostella vectensis*. The tools generated in this work provide a fundament and starting point to study the roles of *NvDscam* and *NvNeogenin* in neurite guidance in *N. vectensis*. It can be investigated if those mechanisms responsible for neurite guidance like neurite outgrowth or Netrin-mediated signalling that are found in Bilateria are evolutionary conserved in Cnidaria and are also involved in the same or similar pathways. Various future experiments can help to characterise *NvDscam* and *NvNeogenin* more, for example dFISH of *NvDscam* or *NvNeogenin* with other interesting genes, crosses of the transgenic reporter lines to other transgenic reporter lines and mutant lines.

5.6 Future perspectives

This study has contributed to establish the possibility to study genes thought to be involved in neurite guidance. Various possible future experiments have been mentioned before, as working more with the *NvElav1::mOrange* line, dFISH of *NvDscam* or *NvNeogenin* with genes like *NvNetrin*, *NvRgm* and *NvRPamide*. Also, in the genome of *N. vectensis* other receptors like *NvRobo* and *NvPlexin* are found, that are known to be involved in neurite guidance in Vertebrata (Chédotal, 2019). In Vertebrata, a vast diversity of guidance molecules plus their receptors contribute to a complex centralised nervous system (Chédotal, 2019). For example, as reviewed by Chédotal, 2019, Wnt and Bmp signalling contribute to neurite guidance in mouse. NvWnt and NvBmp molecules can also be found in *N. vectensis* where they are involved in patterning of the oral-aboral and directive axis, respectively (Genikhovich & Technau, 2017). Their implications in neurite guidance in *N. vectensis* have not been studied yet. Overall, there are more molecules which could be interesting to investigate in relation to neurite guidance. In comparison to Cnidaria, Bilateria may seem to have complex nervous systems. It will be interesting to find out whether basic mechanisms required for the establishment of such more complex nervous systems are present and evolutionary conserved in animals which possess a comparably “simple” nervous system such as *Nematostella vectensis*.

6. References

Abe, K., Katow, T., Ooka, S., & Katow, H. (2013). Unc-5/netrin-mediated axonal projection during larval serotonergic nervous system formation in the sea urchin, Hemicentrotus pulcherrimus. *The International Journal of Developmental Biology*, *57*(5), 415–425. https://doi.org/10.1387/ijdb.120256hk

Ahmed, G., Shinmyo, Y., Ohta, K., Islam, S. M., Hossain, M., Naser, I. B., Riyadh, M. A., Su, Y., Zhang, S., Tessier-Lavigne, M., & Tanaka, H. (2011). Draxin Inhibits Axonal Outgrowth through the Netrin Receptor DCC. *Journal of Neuroscience*, *31*(39), 14018–14023. https://doi.org/10.1523/JNEUROSCI.0943-11.2011

Bode, H. R., Heimfeld, S., Chow, M. A., & Huang, L. W. (1987). Gland cells arise by differentiation from interstitial cells in Hydra attenuata. *Developmental Biology*, *122*(2), 577–585. https://doi.org/10.1016/0012-1606(87)90321-6

Botman, D., Jansson, F., Röttinger, E., Martindale, M. Q., de Jong, J., & Kaandorp, J. A. (2015). Analysis of a spatial gene expression database for sea anemone Nematostella vectensis during early development. *BMC Systems Biology*, *9*(1), 63. https://doi.org/10.1186/s12918-015-0209-4

Brignani, S., Raj, D. D. A., Schmidt, E. R. E., Düdükcü, Ö., Adolfs, Y., de Ruiter, A. A., Rybiczka-Tesulov, M., Verhagen, M. G., van der Meer, C., Broekhoven, M. H., Moreno-Bravo, J. A., Grossouw, L. M., Dumontier, E., Cloutier, J.-F., Chédotal, A., & Pasterkamp, R. J. (2020). Remotely Produced and Axon-Derived Netrin-1 Instructs GABAergic Neuron Migration and Dopaminergic Substantia Nigra Development. *Neuron*, *107*(4), 684-702.e9. https://doi.org/10.1016/j.neuron.2020.05.037

Busengdal, H., & Rentzsch, F. (2017). Unipotent progenitors contribute to the generation of sensory cell types in the nervous system of the cnidarian Nematostella vectensis. *Developmental Biology*, *431*(1), 59–68. https://doi.org/10.1016/j.ydbio.2017.08.021

Chédotal, A. (2019). Roles of axon guidance molecules in neuronal wiring in the developing spinal cord. In *Nature Reviews Neuroscience* (Vol. 20, Issue 7, pp. 380–396). Nature Publishing Group. https://doi.org/10.1038/s41583-019-0168-7

Chisholm, A. D., Hutter, H., Jin, Y., & Wadsworth, W. G. (2016). The Genetics of Axon Guidance and Axon Regeneration in *Caenorhabditis elegans*. *Genetics*, *204*(3), 849–882. https://doi.org/10.1534/genetics.115.186262

Culotti, J. G., & Merz, D. C. (1998). DCC and netrins. *Current Opinion in Cell Biology*, *10*(5), 609–613. https://doi.org/10.1016/S0955-0674(98)80036-7

Dascenco, D., Erfurth, M.-L., Izadifar, A., Song, M., Sachse, S., Bortnick, R., Urwyler, O., Petrovic, M., Ayaz, D., He, H., Kise, Y., Thomas, F., Kidd, T., & Schmucker, D. (2015). Slit and Receptor Tyrosine Phosphatase 69D Confer Spatial Specificity to Axon Branching via Dscam1. *Cell*, *162*(5), 1140–1154. https://doi.org/10.1016/j.cell.2015.08.003

David, C. N. (2012). Interstitial stem cells in Hydra: multipotency and decision-making. *The International Journal of Developmental Biology*, *56*(6-7–8), 489–497. https://doi.org/10.1387/ijdb.113476cd

David, C. N., Özbek, S., Adamczyk, P., Meier, S., Pauly, B., Chapman, J., Hwang, J. S., Gojobori, T., & Holstein, T. W. (2008). Evolution of complex structures: minicollagens shape the cnidarian nematocyst. *Trends in Genetics*, *24*(9), 431–438. https://doi.org/10.1016/j.tig.2008.07.001

Denker, E., Manuel, M., Leclère, L., le Guyader, H., & Rabet, N. (2008). Ordered progression of nematogenesis from stem cells through differentiation stages in the tentacle bulb of Clytia hemisphaerica (Hydrozoa, Cnidaria). *Developmental Biology*, *315*(1), 99–113. https://doi.org/10.1016/j.ydbio.2007.12.023

Dunn, C. W., Giribet, G., Edgecombe, G. D., & Hejnol, A. (2014). Animal Phylogeny and Its Evolutionary Implications. *Annual Review of Ecology, Evolution, and Systematics*, *45*(1), 371–395. https://doi.org/10.1146/annurev-ecolsys-120213-091627

Fazeli, A., Dickinson, S. L., Hermiston, M. L., Tighe, R. v., Steen, R. G., Small, C. G., Stoeckli, E. T., Keino-Masu, K., Masu, M., Rayburn, H., Simons, J., Bronson, R. T., Gordon, J. I., Tessier-Lavigne, M., & Weinberg, R. A. (1997). Phenotype of mice lacking functional Deleted in colorectal cancer (Dcc) gene. *Nature*, *386*(6627). https://doi.org/10.1038/386796a0

Gahan, J. M., Bradshaw, B., Flici, H., & Frank, U. (2016). The interstitial stem cells in Hydractinia and their role in regeneration. *Current Opinion in Genetics & Development*, *40*, 65–73. https://doi.org/10.1016/j.gde.2016.06.006

Galliot, B., Quiquand, M., Ghila, L., de Rosa, R., Miljkovic-Licina, M., & Chera, S. (2009). Origins of neurogenesis, a cnidarian view. *Developmental Biology*, *332*(1), 2–24. https://doi.org/10.1016/j.ydbio.2009.05.563

Geisbrecht, B. v., Dowd, K. A., Barfield, R. W., Longo, P. A., & Leahy, D. J. (2003). Netrin Binds Discrete Subdomains of DCC and UNC5 and Mediates Interactions between DCC and Heparin. *Journal of Biological Chemistry*, *278*(35). https://doi.org/10.1074/jbc.M302943200

Genikhovich, G., & Technau, U. (2017). On the evolution of bilaterality. *Development (Cambridge)*, *144*(19), 3392–3404. https://doi.org/10.1242/dev.141507

Gibson, D. G., Young, L., Chuang, R.-Y., Venter, J. C., Hutchison, C. A., & Smith, H. O. (2009). Enzymatic assembly of DNA molecules up to several hundred kilobases. *Nature Methods*, *6*(5), 343–345. https://doi.org/10.1038/nmeth.1318

Goldschneider, D., Rama, N., Guix, C., & Mehlen, P. (2008). The Neogenin Intracellular Domain Regulates Gene Transcription via Nuclear Translocation. *Molecular and Cellular Biology*, *28*(12). https://doi.org/10.1128/MCB.02114-07

Hand, C., & Uhlinger, K. R. (1992). The Culture, Sexual and Asexual Reproduction, and Growth of the Sea Anemone Nematostella vectensis. In *Bulletin* (Vol. 182, Issue 2).

Hillis, D. M., & Bull, J. J. (1993). An Empirical Test of Bootstrapping as a Method for Assessing Confidence in Phylogenetic Analysis. *Systematic Biology*, *42*(2), 182–192. https://doi.org/10.1093/sysbio/42.2.182

Hong, K., Hinck, L., Nishiyama, M., Poo, M., Tessier-Lavigne, M., & Stein, E. (1999). A Ligand-Gated Association between Cytoplasmic Domains of UNC5 and DCC Family Receptors Converts Netrin-Induced Growth Cone Attraction to Repulsion. *Cell*, *97*(7), 927–941. https://doi.org/10.1016/S0092-8674(00)80804-1

Howard, L. J., Brown, H. E., Wadsworth, B. C., & Evans, T. A. (2019). Midline axon guidance in the Drosophila embryonic central nervous system. *Seminars in Cell & Developmental Biology*, *85*, 13–25. https://doi.org/10.1016/j.semcdb.2017.11.029

Hutter, H. (2019). Formation of longitudinal axon pathways in Caenorhabditis elegans. *Seminars in Cell & Developmental Biology*, *85*, 60–70. https://doi.org/10.1016/j.semcdb.2017.11.015

Isaksen, T. J., Fujita, Y., & Yamashita, T. (2020). Repulsive Guidance Molecule A Suppresses Adult Neurogenesis. *Stem Cell Reports*, *14*(4), 677–691. https://doi.org/10.1016/j.stemcr.2020.03.003

Jin, Y., & Li, H. (2019). Revisiting Dscam diversity: lessons from clustered protocadherins. *Cellular and Molecular Life Sciences*, *76*(4), 667–680. https://doi.org/10.1007/s00018-018-2951-4

Katoh, K., Rozewicki, J., & Yamada, K. D. (2019). MAFFT online service: multiple sequence alignment, interactive sequence choice and visualization. *Briefings in Bioinformatics*, *20*(4), 1160–1166. https://doi.org/10.1093/bib/bbx108

Kayal, E., Bentlage, B., Sabrina Pankey, M., Ohdera, A. H., Medina, M., Plachetzki, D. C., Collins, A. G., & Ryan, J. F. (2018). Phylogenomics provides a robust topology of the major cnidarian lineages and insights on the origins of key organismal traits. *BMC Evolutionary Biology*, *18*(1), 68. https://doi.org/10.1186/s12862-018-1142-0

Kee, N., Wilson, N., Key, B., & Cooper, H. M. (2013). Netrin-1 is required for efficient neural tube closure. *Developmental Neurobiology*, *73*(2), 176–187. https://doi.org/10.1002/dneu.22051

Keino-Masu, K., Masu, M., Hinck, L., Leonardo, E. D., Chan, S. S.-Y., Culotti, J. G., & Tessier-Lavigne, M. (1996). Deleted in Colorectal Cancer (DCC) Encodes a Netrin Receptor. *Cell*, *87*(2), 175–185. https://doi.org/10.1016/S0092-8674(00)81336-7

Layden, M. J., Johnston, H., Amiel, A. R., Havrilak, J., Steinworth, B., Chock, T., Röttinger, E., & Martindale, M. Q. (2016). MAPK signaling is necessary for neurogenesis in Nematostella vectensis. *BMC Biology*, *14*(1). https://doi.org/10.1186/s12915-016-0282-1

Leclère, L., & Rentzsch, F. (2012). Repeated evolution of identical domain architecture in metazoan netrin domain-containing proteins. *Genome Biology and Evolution*, *4*(9), 883–899. https://doi.org/10.1093/gbe/evs061

Leclère, L., & Rentzsch, F. (2014). RGM Regulates BMP-Mediated Secondary Axis Formation in the Sea Anemone Nematostella vectensis. *Cell Reports*, *9*(5), 1921–1930. https://doi.org/10.1016/j.celrep.2014.11.009

Letunic, I., & Bork, P. (2018). 20 years of the SMART protein domain annotation resource. *Nucleic Acids Research*, *46*(D1), D493–D496. https://doi.org/10.1093/nar/gkx922

Letunic, I., Khedkar, S., & Bork, P. (2021). SMART: recent updates, new developments and status in 2020. *Nucleic Acids Research*, *49*(D1), D458–D460. https://doi.org/10.1093/nar/gkaa937

Liu, Y., Stein, E., Oliver, T., Li, Y., Brunken, W. J., Koch, M., Tessier-Lavigne, M., & Hogan, B. L. M. (2004). Novel Role for Netrins in Regulating Epithelial Behavior during Lung Branching Morphogenesis. *Current Biology*, *14*(10), 897–905. https://doi.org/10.1016/j.cub.2004.05.020

Livak, K. J., & Schmittgen, T. D. (2001). Analysis of relative gene expression data using real-time quantitative PCR and the 2-ΔΔCT method. *Methods*, *25*(4). https://doi.org/10.1006/meth.2001.1262

Ly, A., Nikolaev, A., Suresh, G., Zheng, Y., Tessier-Lavigne, M., & Stein, E. (2008). DSCAM Is a Netrin Receptor that Collaborates with DCC in Mediating Turning Responses to Netrin-1. *Cell*, *133*(7), 1241–1254. https://doi.org/10.1016/j.cell.2008.05.030

Matus, D. Q., Pang, K., Marlow, H., Dunn, C. W., Thomsen, G. H., & Martindale, M. Q. (2006). *Molecular evidence for deep evolutionary roots of bilaterality in animal development*. www.pnas.orgcgidoi10.1073pnas.0601257103

Meijers, R., Smock, R. G., Zhang, Y., & Wang, J. H. (2020). Netrin Synergizes Signaling and Adhesion through DCC. In *Trends in Biochemical Sciences* (Vol. 45, Issue 1, pp. 6–12). Elsevier Ltd. https://doi.org/10.1016/j.tibs.2019.10.005

Montgomery, K. L., Iyer, S. M., Christensen, A. J., Deisseroth, K., & Delp, S. L. (2016). Beyond the brain: Optogenetic control in the spinal cord and peripheral nervous system. *Science Translational Medicine*, *8*(337). https://doi.org/10.1126/scitranslmed.aad7577

Nakanishi, N., Renfer, E., Technau, U., & Rentzsch, F. (2012). Nervous systems of the sea anemone Nematostella vectensis are generated by ectoderm and endoderm and shaped by distinct mechanisms. *Development*, *139*(2), 347–357. https://doi.org/10.1242/dev.071902

Negishi, M., Oinuma, I., & Katoh, H. (2005). Plexins: axon guidance and signal transduction. *Cellular and Molecular Life Sciences*, *62*(12), 1363–1371. https://doi.org/10.1007/s00018-005-5018-2

Nguyen, L.-T., Schmidt, H. A., von Haeseler, A., & Minh, B. Q. (2015). IQ-TREE: A Fast and Effective Stochastic Algorithm for Estimating Maximum-Likelihood Phylogenies. *Molecular Biology and Evolution*, *32*(1), 268–274. https://doi.org/10.1093/molbev/msu300

Palmesino, E., Haddick, P. C. G., Tessier-Lavigne, M., & Kania, A. (2012). Genetic Analysis of DSCAM's Role as a Netrin-1 Receptor in Vertebrates. *Journal of Neuroscience*, *32*(2), 411–416. https://doi.org/10.1523/JNEUROSCI.3563-11.2012

Pancho, A., Aerts, T., Mitsogiannis, M. D., & Seuntjens, E. (2020). Protocadherins at the Crossroad of Signaling Pathways. *Frontiers in Molecular Neuroscience*, *13*. https://doi.org/10.3389/fnmol.2020.00117

Pourchet, O., Morel, M.-P., Welniarz, Q., Sarrazin, N., Marti, F., Heck, N., Galléa, C., Doulazmi, M., Roig Puiggros, S., Moreno-Bravo, J. A., Vidailhet, M., Trembleau, A., Faure, P., Chédotal, A., Roze, E., & Dusart, I. (2021). Loss of floor plate Netrin-1 impairs midline crossing of corticospinal axons and leads to mirror movements. *Cell Reports*, *34*(3), 108654. https://doi.org/10.1016/j.celrep.2020.108654

Purohit, A. A., Li, W., Qu, C., Dwyer, T., Shao, Q., Guan, K.-L., & Liu, G. (2012). Down Syndrome Cell Adhesion Molecule (DSCAM) Associates with Uncoordinated-5C (UNC5C) in Netrin-1-mediated Growth Cone Collapse. *Journal of Biological Chemistry*, *287*(32), 27126–27138. https://doi.org/10.1074/jbc.M112.340174

Putnam, N. H., Srivastava, M., Hellsten, U., Dirks, B., Chapman, J., Salamov, A., Terry, A., Shapiro, H., Lindquist, E., Kapitonov, V. v., Jurka, J., Genikhovich, G., Grigoriev, I. v., Lucas, S. M., Steele, R. E., Finnerty, J. R., Technau, U., Martindale, M. Q., & Rokhsar, D. S. (2007). Sea Anemone Genome Reveals Ancestral Eumetazoan Gene Repertoire and Genomic Organization. *Science*, *317*(5834), 86–94. https://doi.org/10.1126/science.1139158

Renfer, E., & Technau, U. (2017). Meganuclease-assisted generation of stable transgenics in the sea anemone Nematostella vectensis. *Nature Protocols*, *12*(9), 1844–1854. https://doi.org/10.1038/nprot.2017.075

Rentzsch, F., Layden, M., & Manuel, M. (2017). The cellular and molecular basis of cnidarian neurogenesis. *Wiley Interdisciplinary Reviews: Developmental Biology*, *6*(1), e257. https://doi.org/10.1002/wdev.257

Richards, G. S., & Rentzsch, F. (2014). Transgenic analysis of a SoxB gene reveals neural progenitor cells in the cnidarian Nematostella vectensis. *Development (Cambridge)*, *141*(24), 4681–4689. https://doi.org/10.1242/dev.112029

Richards, G. S., & Rentzsch, F. (2015). Regulation of Nematostella neural progenitors by SoxB, Notch and bHLH genes. *Development (Cambridge)*, *142*(19), 3332–3342. https://doi.org/10.1242/dev.123745

Rye, C., Wise, R., Jurukovski, V., DeSaix, J., Choi, J. C., & Avissar, Y. (2016). *Biology*. https://openstax.org/books/biology/pages/35-1-neurons-and-glial-cells

Sachse, S. M., Lievens, S., Ribeiro, L. F., Dascenco, D., Masschaele, D., Horré, K., Misbaer, A., Vanderroost, N., de Smet, A. S., Salta, E., Erfurth, M., Kise, Y., Nebel, S., van Delm, W., Plaisance, S., Tavernier, J., de Strooper, B., de Wit, J., & Schmucker, D. (2019). Nuclear import of the DSCAM -cytoplasmic domain drives signaling capable of inhibiting synapse formation . *The EMBO Journal*, *38*(6). https://doi.org/10.15252/embj.201899669

Samarut, É., Lissouba, A., & Drapeau, P. (2016). A simplified method for identifying early CRISPR-induced indels in zebrafish embryos using High Resolution Melting analysis. *BMC Genomics*, *17*(1), 547. https://doi.org/10.1186/s12864-016-2881-1

Schindelin, J., Arganda-Carreras, I., Frise, E., Kaynig, V., Longair, M., Pietzsch, T., Preibisch, S., Rueden, C., Saalfeld, S., Schmid, B., Tinevez, J. Y., White, D. J., Hartenstein, V., Eliceiri, K., Tomancak, P., & Cardona, A. (2012). Fiji: An open-source platform for biological-image analysis. In *Nature Methods* (Vol. 9, Issue 7, pp. 676–682). https://doi.org/10.1038/nmeth.2019

Schmucker, D., Clemens, J. C., Shu, H., Worby, C. A., Xiao, J., Muda, M., & Dixon, J. E. (2000). Drosophila Dscam Is an Axon Guidance Receptor Exhibiting Extraordinary Molecular Diversity modified by neuronal activity (reviewed by Albright et al., 2000). Extraordinary progress has been made in identifying. In *Cell* (Vol. 101). Guthrie.

Schwaiger, M., Schönauer, A., Rendeiro, A. F., Pribitzer, C., Schauer, A., Gilles, A. F., Schinko, J. B., Renfer, E., Fredman, D., & Technau, U. (2014). Evolutionary conservation of the eumetazoan gene regulatory landscape. *Genome Research*, *24*(4), 639–650. https://doi.org/10.1101/gr.162529.113

Srinivasan, K., Strickland, P., Valdes, A., Shin, G. C., & Hinck, L. (2003). Netrin-1/Neogenin Interaction Stabilizes Multipotent Progenitor Cap Cells during Mammary Gland Morphogenesis. *Developmental Cell*, *4*(3), 371–382. https://doi.org/10.1016/S1534-5807(03)00054-6

Stoeckli, E. T. (2018). Understanding axon guidance: are we nearly there yet? *Development*, *145*(10). https://doi.org/10.1242/dev.151415

Stone, M. C., Kothe, G. O., Rolls, M. M., & Jegla, T. (2020). Cytoskeletal and synaptic polarity of LWamide-like+ ganglion neurons in the sea anemone Nematostella vectensis. *Journal of Experimental Biology*, *223*(21). https://doi.org/10.1242/jeb.233197

Sun, K. L. W., Correia, J. P., & Kennedy, T. E. (2011). Netrins: Versatile extracellular cues with diverse functions. *Development*, *138*(11), 2153–2169. https://doi.org/10.1242/dev.044529

Sunagar, K., Columbus-Shenkar, Y. Y., Fridrich, A., Gutkovich, N., Aharoni, R., & Moran, Y. (2018). Cell type-specific expression profiling unravels the development and evolution of stinging cells in sea anemone. *BMC Biology*, *16*(1). https://doi.org/10.1186/s12915-018-0578-4

Telford, M. J., Budd, G. E., & Philippe, H. (2015). Phylogenomic Insights into Animal Evolution. *Current Biology*, *25*(19), R876–R887. https://doi.org/10.1016/j.cub.2015.07.060

Tong, M., Jun, T., Nie, Y., Hao, J., & Fan, D. (2019). The Role of the Slit/Robo Signaling Pathway. *Journal of Cancer*, *10*(12), 2694–2705. https://doi.org/10.7150/jca.31877

Tournière, O., Busengdal, H., Gahan, J. M., & Rentzsch, F. (n.d.). *Insm1-expressing neurons and secretory cells develop from a common pool of progenitors in the sea anemone Nematostella vectensis*. https://doi.org/10.1101/2021.04.09.439178

Varadarajan, S. G., Kong, J. H., Phan, K. D., Kao, T. J., Panaitof, S. C., Cardin, J., Eltzschig, H., Kania, A., Novitch, B. G., & Butler, S. J. (2017). Netrin1 Produced by Neural Progenitors, Not Floor Plate Cells, Is Required for Axon Guidance in the Spinal Cord. *Neuron*, *94*(4), 790-799.e3. https://doi.org/10.1016/j.neuron.2017.03.007

Wang, E. T., Sandberg, R., Luo, S., Khrebtukova, I., Zhang, L., Mayr, C., Kingsmore, S. F., Schroth, G. P., & Burge, C. B. (2008). Alternative isoform regulation in human tissue transcriptomes. *Nature*, *456*(7221), 470–476. https://doi.org/10.1038/nature07509

Williams, S. E., Mann, F., Erskine, L., Sakurai, T., Wei, S., Rossi, D. J., Gale, N. W., Holt, C. E., Mason, C. A., & Henkemeyer, M. (2003). Ephrin-B2 and EphB1 Mediate Retinal Axon Divergence at the Optic Chiasm. *Neuron*, *39*(6), 919–935. https://doi.org/10.1016/j.neuron.2003.08.017

Wilson, N. H., & Key, B. (2006). Neogenin interacts with RGMa and Netrin-1 to guide axons within the embryonic vertebrate forebrain. *Developmental Biology*, *296*(2). https://doi.org/10.1016/j.ydbio.2006.06.018

Wilson, N. H., & Key, B. (2007). Neogenin: One receptor, many functions. *The International Journal of Biochemistry & Cell Biology*, *39*(5), 874–878. https://doi.org/10.1016/j.biocel.2006.10.023

Yebra, M., Montgomery, A. M. P., Diaferia, G. R., Kaido, T., Silletti, S., Perez, B., Just, M. L., Hildbrand, S., Hurford, R., Florkiewicz, E., Tessier-Lavigne, M., & Cirulli, V. (2003). Recognition of the Neural Chemoattractant Netrin-1 by Integrins α6β4 and α3β1 Regulates Epithelial Cell Adhesion and Migration. *Developmental Cell*, *5*(5), 695–707. https://doi.org/10.1016/S1534-5807(03)00330-7

Zang, H., & Nakanishi, N. (2020). Expression Analysis of Cnidarian-Specific Neuropeptides in a Sea Anemone Unveils an Apical-Organ-Associated Nerve Net That Disintegrates at Metamorphosis. *Frontiers in Endocrinology*, *11*. https://doi.org/10.3389/fendo.2020.00063

Zelina, P., Blockus, H., Zagar, Y., Péres, A., Friocourt, F., Wu, Z., Rama, N., Fouquet, C., Hohenester, E., Tessier-Lavigne, M., Schweitzer, J., Crollius, H. R., & Chédotal, A. (2014). Signaling Switch of the Axon Guidance Receptor Robo3 during Vertebrate Evolution. *Neuron*, *84*(6), 1258–1272. https://doi.org/10.1016/j.neuron.2014.11.004

7. Supplementary Material

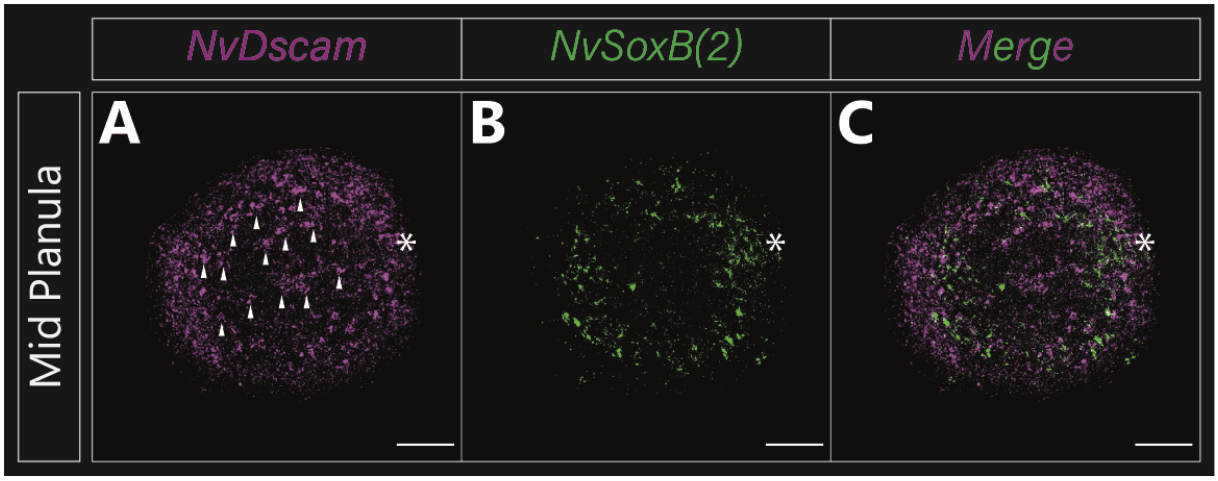

Supplementary Figure 1: *NvDscam* and *NvSoxB(2)* at mid planula are not co-expressed in the endoderm. This graph shows a double fluorescence *in-situ* hybridisation at mid planula stage of *NvDscam* (**A**) and the neural progenitor marker *NvSoxB(2)* (**B**), which is indicated by panels on the top. Panels to the left shows the developmental stage. Co-expression in the endoderm cannot be found (**C**). Despite, single cells expressing *NvDscam* can be found at the oral and aboral endoderm and in between, which suggests that *NvDscam* is expressed along the developing mesenteries (white arrowheads **A**). All images are stacks of eight confocal sections. Asterisks indicate the oral pole. *n=2*, 30-50 animals per stage, scale bars: 50 µm

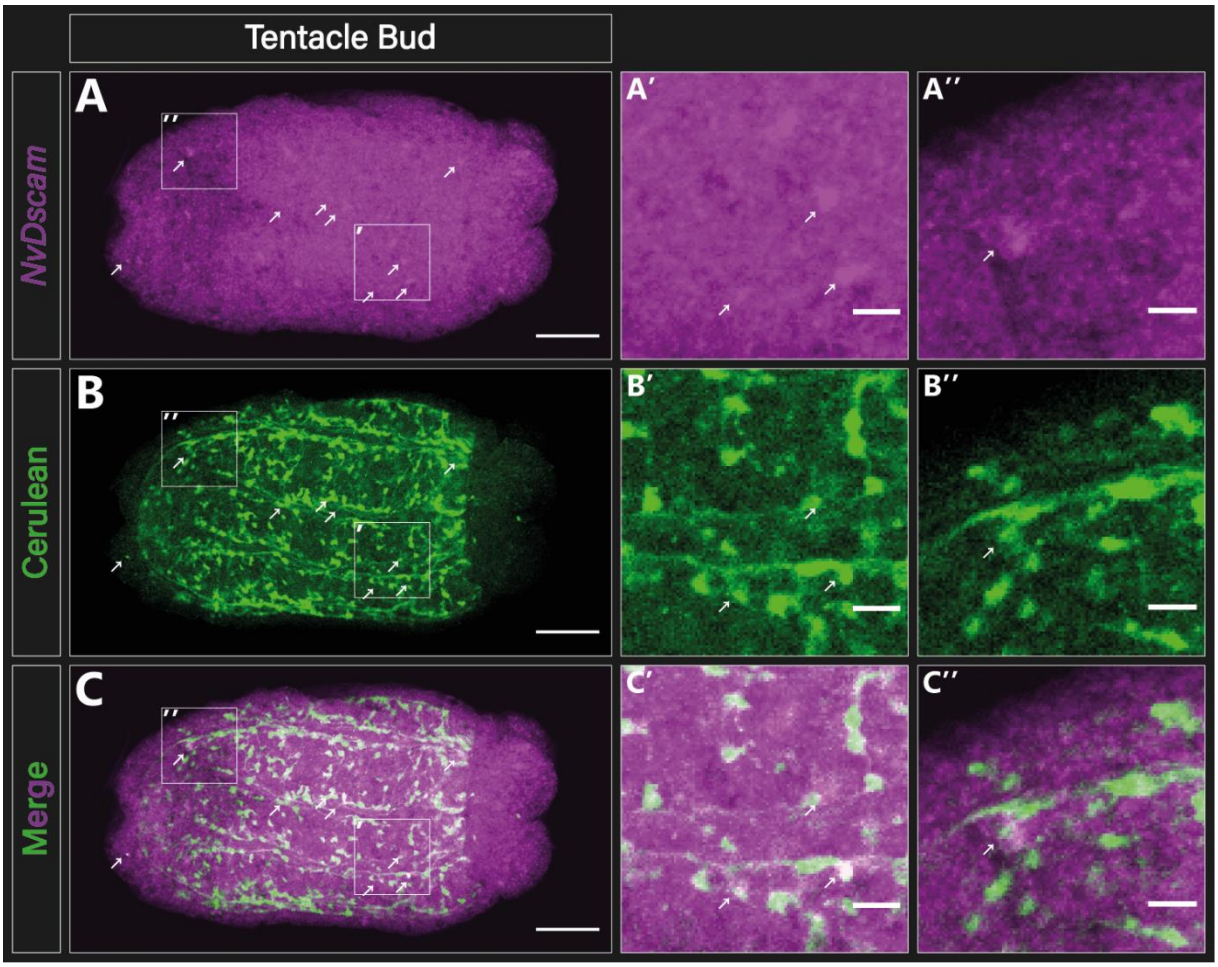

Supplementary Figure 2: *NvDscam* is widely expressed at tentacle bud stage and it is expressed by *NvElav1*::NTR-Cerulean⁺ cells in the endoderm. This graph shows a fluorescene *in-situ* hybridisation of *NvDscam* combined with immunohistochemistry of *NvElav1*::NTR-Cerulean. Animals are oriented with their oral pole to the right. **A' – C'** and **A'' – C''** depict magnifications of the areas marked ' and '' in the images **A – C**, respectively. **A)** Fluorescene in-situ hybridisation of *NvDscam* shows a rather ubiquitous expression with some single cells having a stronger distinguished signal in the endoderm and developing tentacle buds. **B)** Immunohistochemistry of Cerulean shows *NvElav1*::NTR-Cerulean positive cells, and the nerve net they built up. **C)** The merge of *NvDscam* and Cerulean signals should give more insights into colocalization of *NvDscam* and *NvElav1*::NTR-Cerulean⁺ cells. Enlargements in **A' – C''** visualise that some Cerulean⁺ cells express *NvDscam*. Most of the *NvDscam*⁺ cells are Cerulean⁺ as well. All images show one confocal section. *n=1*, 30-50 animals per stage, scale bars: 50 µm (**A – C**), 10 µm (**A' – C''**).

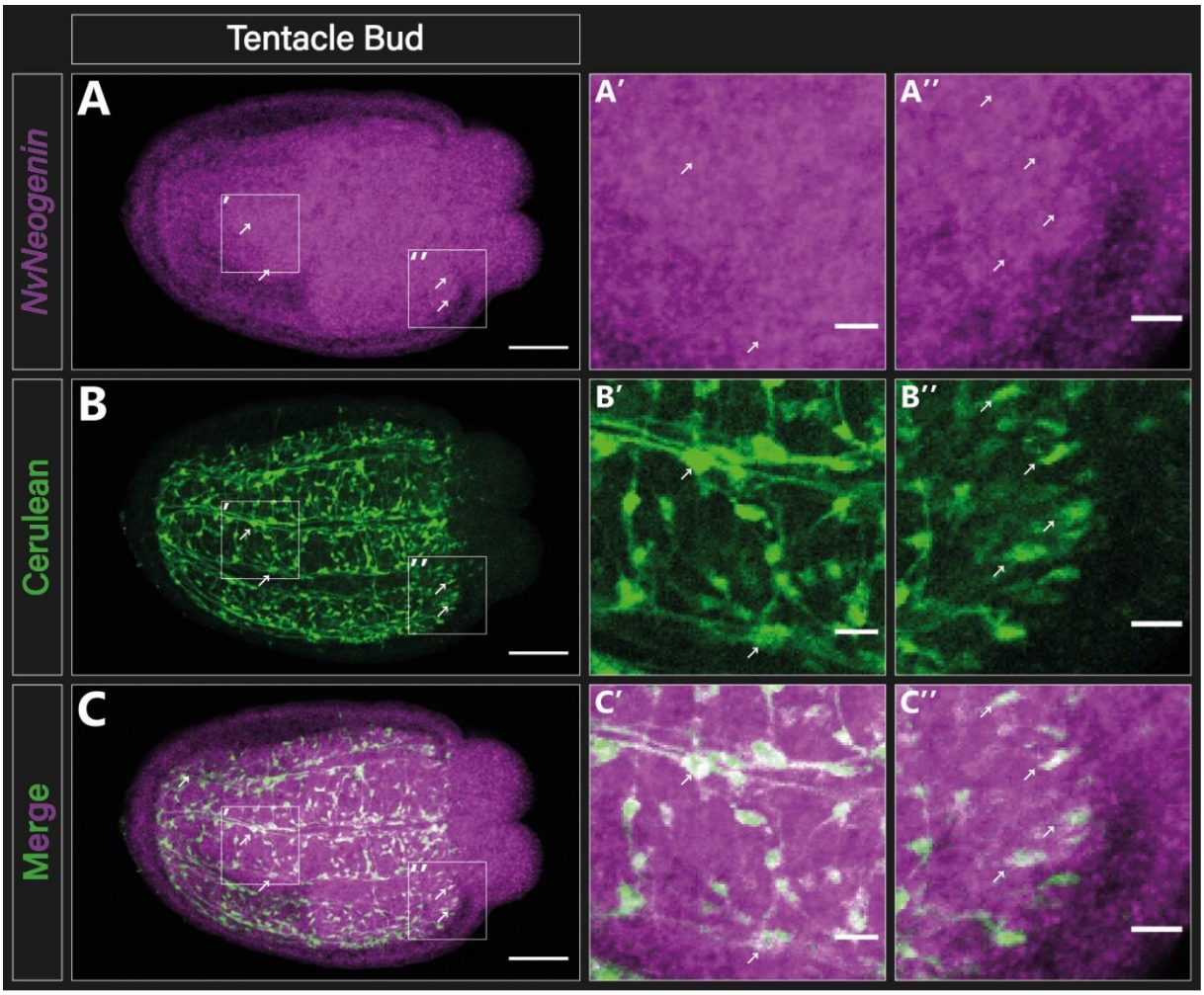

Supplementary Figure 3: *NvNeogenin* is expressed throughout the ectoderm, tentacle bud region and endoderm, and it colocalises with the Cerulean⁺ cells in the endoderm. This graph shows a fluorescene *in-situ* hybridisation of *NvNeogenin* combined with immunohistochemistry of *NvElav1*::NTR-Cerulean in Late Planula stage. Animals are oriented with their oral pole to the right. A' – C' and A'' – C'' depict magnifications of the areas marked ' and '' in the images A – C, respectively. **A)** Fluorescene *in-situ* hybridisation of *NvNeogenin* visualises its expression in the whole ectoderm, also in the aboral pole. It is present ubiquitously in the endoderm and developing tentacle buds. However, single cells cannot be distinguished. **B)** Immunohistochemistry of Cerulean shows *NvElav1*::NTR-Cerulean positive cells, and the nerve net they built up.**C)** The merge of *NvNeogenin* and Cerulean signals should give more insights into colocalization of *NvNeogenin* and Cerulean⁺ cells. Due to the overall expression of *NvNeogenin* it cannot be excluded that the whole endodermal tissue including Cerulean⁺ neurons express the gene. Enlargements in **A' – C''** visualise that Cerulean⁺ cells are positive for *NvNeogenin* in the endoderm. All images show one confocal section. *n=1*, 30-50 animals per stage, scale bars: 50 µm (**A – C**), 10 µm (**A' – C''**).

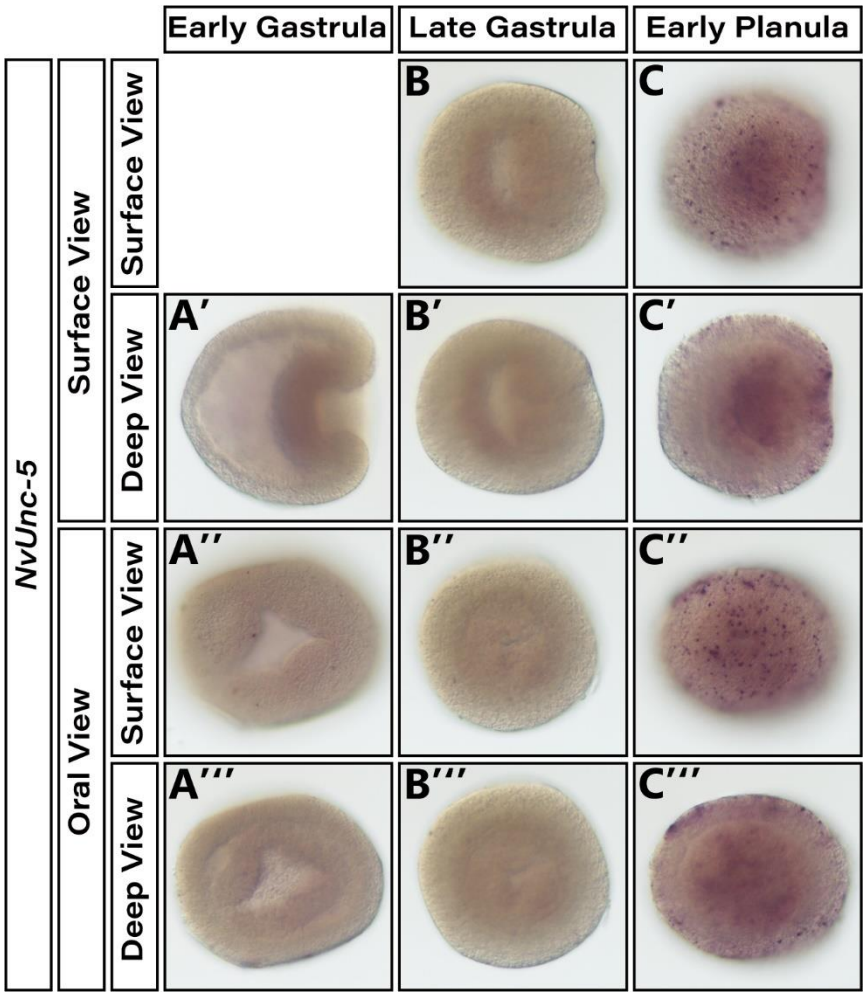

Supplementary Figure 4: *NvUnc-5* shows no clear expression pattern. Colorimetric *in-situ* hybridisation of *NvUnc-5*. Developmental stages (early gastrula to early planula) are indicated on top, gene name and focus planes on the left. Surface View shows the surface of the animals; in Deep View the middle of the embryo is in focus. Animals in Lateral View are oriented with the oral side to the right. Expression of *NvUnc-5* cannot be detected at early and late gastrula. At early planula some staining in the pharynx and endoderm can be seen. The salt and pepper pattern in the ectoderm is seen on the surface and is difficult to attribute to single cells. *n=3*, 30-50 animals per stage